# DRMY1 promotes robust morphogenesis by sustaining translation of a hormone signaling protein

Shuyao Kong,[1,2,†] Mingyuan Zhu,[1,2,3,†] M. Regina Scarpin,[4] David Pan,[1,2] Longfei Jia,[5] Ryan E. Martinez,[4] Simon Alamos,[6,7,8] Batthula Vijaya Lakshmi Vadde,[1,2] Hernan G. Garcia,[9,10,11,12,13] Shu-Bing Qian,[5] Jacob O. Brunkard,[4] Adrienne H. K. Roeder [1,2,14,*]

[1] Weill Institute for Cell and Molecular Biology, Cornell University, Ithaca, NY 14853, USA
[2] Section of Plant Biology, School of Integrative Plant Science, Cornell University, Ithaca, NY 14853, USA
[3] Present address: Department of Biology, Duke University, Durham, NC 27708, USA
[4] Laboratory of Genetics, University of Wisconsin, Madison, WI 53706, USA
[5] Division of Nutritional Sciences, Cornell University, Ithaca, NY 14853, USA
[6] Environmental Genomics and Systems Biology Division, Lawrence Berkeley National Laboratory, Berkeley, CA 94720, USA
[7] Feedstocks Division, Joint BioEnergy Institute, Emeryville, CA 94608, USA
[8] Department of Plant and Microbial Biology, University of California at Berkeley, Berkeley, CA 94720, USA
[9] Biophysics Graduate Group, University of California at Berkeley, Berkeley, CA 94720, USA
[10] Department of Physics, University of California at Berkeley, Berkeley, CA 94720, USA
[11] Institute for Quantitative Biosciences-QB3, University of California at Berkeley, Berkeley, CA 94720, USA
[12] Department of Molecular and Cell Biology, University of California at Berkeley, Berkeley, CA 94720, USA
[13] Chan Zuckerberg Biohub-San Francisco, San Francisco, CA 94158, USA
[14] Lead Contact
[†] These authors contributed equally
[*] Correspondence: ahr75@cornell.edu

## SUMMARY

Robustness is the invariant development of phenotype despite environmental changes and genetic perturbations. In the Arabidopsis flower bud, four sepals initiate at robust positions and times and grow to equal size to enclose and protect the inner floral organs. We previously characterized the mutant *development related myb-like1* (*drmy1*), where 3-5 sepals initiate at irregular positions and variable times and grow to different sizes, compromising their protective function. The molecular mechanism underlying this loss of robustness was unclear. Here, we show that *drmy1* has reduced TARGET OF RAPAMYCIN (TOR) activity, ribosomal content, and translation. Translation reduction decreases the protein level of ARABIDOPSIS RESPONSE REGULATOR7 (ARR7), a rapidly synthesized and degraded cytokinin signaling inhibitor. The resultant upregulation of cytokinin signaling disrupts the robust positioning of auxin signaling, causing variable sepal initiation. Our work shows that the homeostasis of translation, a ubiquitous cellular process, is crucial for the robust spatiotemporal patterning of organogenesis.

Keywords: Robustness, TOR, translation, cytokinin, auxin, ARR, ribosomopathy, Arabidopsis, sepal, morphogenesis

## INTRODUCTION

Robustness, or canalization, is the invariant, reproducible development of phenotype, unchanged by environmental fluctuations, genetic perturbations, or gene expression noise[1–4]. Commonly, within an individual, a given number of organs develop at well-defined positions to a robust final size and shape, which is crucial for fitness under stabilizing selection[2]. For example, transplanted eyes, limbs, and kidneys in mammals grow to a mature size similar to their donor, irrespective of the mature size of the same type of organ in the recipient[5–7]. The pairs of wings and halteres in Drosophila develop to robust, precisely coordinated final size and shape, which are required for flight[8–11]. The characteristic cruciform flower in *Brassicaceae* consists of four petals[12], a trait that can contribute to pollinator attraction[13]. The robust positioning of leaves around the shoot apical meristem in plants, or phyllotaxis, ensures optimal light capture[14–16]. While these examples of developmental robustness have been documented for a long time, the underlying molecular mechanisms have just begun to be unveiled.

Earlier studies looking for genes involved in maintaining robustness have found *HEAT SHOCK PROTEIN 90* (*HSP90*). Mutations of *HSP90* cause a diverse array of phenotypic changes in plants, fruit fly, zebrafish, worm, and humans[4,17,18]. Notably, the display and severity of these changes vary between individuals and even between different parts of the same individual, indicating that developmental robustness is disrupted[17,18]. *HSP90* encodes a protein chaperone which has clients from nearly all developmental and signaling pathways[4]. *HSP90*, therefore, is a hub gene that affects numerous other genes within the gene network[2]. Disruption of such a hub gene would therefore trigger many defects in numerous developmental processes. Similarly, genes involved in central cellular processes such as chromatin remodelling[19–21], transcription[19,20], translation[22,23], and protein degradation[24,25] are also hub genes, and they have been found to be important for developmental robustness in various systems including fungi, animals, and plants. How these broadly acting hub genes contribute to the robustness of tissue-specific developmental phenotypes is still largely unclear.

We have developed the *Arabidopsis* sepal as a system to elucidate the mechanisms maintaining robustness in organ size and shape[26–28]. Sepals are the outermost floral organs whose function is to enclose buds and protect the developing inner organs, i.e. petals, stamens, and carpels, before the flower blooms. To fulfill this protective function, each flower robustly develops four sepals of equal length, allowing them to close at the top (Figure 1A, middle left); these four sepals are of equal width and positioned 90° from each other, leaving no gap on the sides (Figure 1A, top left). This robustness in sepal size and shape stems from the robust initiation of the four sepal primordia from the floral meristem with precisely coordinated spatiotemporal patterns[26] (Figure 1A, bottom left). The initiated sepal primordia attain robust final size and shape by spatiotemporal averaging of cellular growth variability during sepal elongation, and synchronous progression of a whole-flower growth termination signal from tip to base[27]. In addition, noise in gene expression must be kept low to ensure sepal size robustness[29]. We previously characterized a mutant in *DEVELOPMENT RELATED MYB-LIKE 1* (*DRMY1*) that

develops flowers where the inner organs are exposed due to gaps between sepals[26]. The gaps are caused by variability in sepal development. Specifically, some sepals are shorter than others, leaving gaps on the top (Figure 1A, middle right); the arrangement of sepals around the flower deviate from the canonical form such that parts of the flower are not covered by a sepal, leaving gaps on the side (Figure 1A, top right). This variability in the size, number, and position of the mature sepal originates from the earliest stages of floral development where the initiation of sepal primordia is variable in spatiotemporal patterns (Figure 1A, bottom right). Variability in sepal initiation, in turn, is driven by the loss of robust patterning of auxin and cytokinin[26], two plant hormones critical for organ initiation and morphogenesis[30–32], in the floral meristem before sepal initiation. However, the molecular mechanism through which DRMY1 maintains robust hormone patterning is still unknown.

In this study, we elucidate a mechanism through which DRMY1 maintains robust hormone patterning and thus robust sepal initiation. Specifically, we find that DRMY1 maintains proper activity of TARGET OF RAPAMYCIN (TOR), a crucial regulator of ribosome biogenesis and protein translation[33,34], and thereby sustains translation *in vivo*. When *DRMY1* is mutated, the protein level of ARABIDOPSIS RESPONSE REGULATOR7 (ARR7), a rapidly synthesized and degraded cytokinin signaling inhibitor, is reduced in the floral meristem. Consequently, cytokinin signaling uniformly increases in the meristem periphery, causing variability in auxin patterning and sepal initiation. We further propose that the increase in cytokinin signaling may be a survival mechanism to alleviate the translation rate reduction when ribosomal content is limited. In summary, our work shows that the hub processes of TOR signaling and translation, which occur in every cell, have very specific roles in robust organ primordium initiation by sustaining the rapid synthesis of a hormone signaling protein.

## RESULTS

### The *drmy1* mutant has reduced TOR activity, ribosome content, and translation rate

*DRMY1* encodes a MYB/SANT domain protein which may exert transcriptional regulation[26]. To look for differentially expressed genes in *drmy1* which may be candidates underlying variable sepal initiation, we performed RNA-sequencing (RNA-seq) in *drmy1* and wild type (WT) of *apetala1* (*ap1) cauliflower (cal) AP1-GR* background[35,36]. The *ap1 cal AP1-GR* inflorescence produces numerous tightly packed ball-shaped meristems, which, upon induction of AP1-GR with dexamethasone, synchronously initiate sepal primordia, allowing us to collect large quantities of floral meristems with sepal primordia initiating (Stage 3)[37] (Figure S1A). We crossed *drmy1* into *ap1 cal AP1-GR* and performed RNA-seq on induced inflorescences of WT and *drmy1* in this background. We detected transcripts from a total of 21,496 genes, of which 1,042 (4.8%) were differentially expressed in *drmy1* (Figure S1B; Supplemental Dataset 1). We found that the 443 genes downregulated at the transcript level in *drmy1* were most enriched in the gene ontology (GO) term “Translation”, a fundamental and ubiquitous cellular process that

converts genetic information from transcript to protein. Within this term, genes encoding ribosomal components were most downregulated (Figure S1C). The 443 downregulated genes were also enriched in several other GO terms related to ribosome biogenesis and assembly (Figure 1B). We therefore hypothesized that ribosome abundance and translation rate are lower in *drmy1*, potentially altering the accumulation of proteins critical to developmental robustness.

To determine whether and how ribosome abundance and translation are affected in *drmy1*, we performed polysome profiling in induced inflorescences of WT and *drmy1* in *ap1 cal AP1-GR* background. Compared to WT, polysomal peaks are drastically reduced in *drmy1* (Figure 1D; Supplemental Dataset 2). To see whether this reduction in ribosomal content affected translation rate (*de novo* protein synthesis) *in vivo*, we performed puromycin labeling. Samples were incubated with puromycin, an amino acid-tRNA analog that is incorporated into nascent polypeptide chains and can be detected using an anti-puromycin antibody to infer global translation rate[38,39]. In both young seedlings and induced *ap1 cal AP1-GR* inflorescences, we found that the puromycin level detected in *drmy1* mutant samples was much reduced compared to WT (Figure 1E), indicating translation rate is reduced. We hypothesized that a reduction in protein translation should likely result in a decrease in protein level. For this, we looked at a ubiquitously expressed membrane marker *UBQ10::mCherry-RCI2A*, and found that it had a small (~25%) but significant decrease in fluorescence intensity in the inflorescence meristem and young floral buds of *drmy1* compared with WT. We also measured its fluorescence intensity in the ribosomal mutant *ul4y* (*rpl4d*)[40] and we found that the decrease in fluorescence intensity in *drmy1* is even greater than in *ul4y* (Figure S1G-J). These results validate our proteomics findings, and show that ribosome content and translation are indeed reduced in the *drmy1* mutant.

To test how the global repression of translation in *drmy1* impacts its proteome, we extracted total soluble protein from induced inflorescences of WT and *drmy1* in *ap1 cal AP-GR* background and performed mass spectrometry. We identified a total of 5,077 proteins, of which 548 (10.8%) were differentially accumulated in *drmy1* (Figure S1B; Supplemental Dataset 1). These differentially accumulated proteins were enriched in GO terms related to translation and ribosomal assembly (Figure 1C). Despite the overall reduction in ribosomes (Figure 1D), relative to other proteins, ribosomal components are more abundant in *drmy1* (Figure S1D; Supplemental Dataset 1). This is not true for all proteins involved in translation; poly-A binding proteins and tRNA synthetases, for example, are relatively less abundant in *drmy1* than in WT. Moreover, the 26S proteasome responsible for targeted protein degradation is much more abundant in *drmy1* than in WT (Supplemental Dataset 1). In concert, these results demonstrate that the machinery responsible for maintaining protein homeostasis is substantially dysregulated in *drmy1*.

A key signaling pathway that regulates protein homeostasis is TARGET OF RAPAMYCIN (TOR)[41,42]. TOR is a hub that integrates information from light, sugars, nutrient availability, etc., to promote growth-related processes, including ribosome biogenesis and translation, and to repress catabolic processes, including protein degradation by autophagy and the proteasome[33,34,43–45]. We therefore hypothesize that the decrease in ribosomal content and protein

translation in *drmy1* may reflect altered TOR signaling. To test for signatures of transcriptomic changes that have been well defined in seedlings under TOR inhibition[34,46,47], we performed RNA-seq on seedlings of WT, *drmy1*, WT treated with AZD-8055 (a potent TOR inhibitor), and mock-treated WT (Supplemental Dataset 3). We found that the *drmy1* mutation causes transcriptomic changes similar to TOR inhibition (Figure 1F). A significant portion of genes differentially expressed under TOR inhibition vs. mock were also differentially expressed in *drmy1* vs. WT (466/2044 = 22.8%; hypergeometric test, $p = 4.7x10^{-108}$). Not only were these 466 genes differentially expressed in both situations, but also most of them were coherently downregulated or upregulated (439/466 = 94.2%, Chi-square test, $p < 2.2x10^{-16}$; Figure S1E). Genes coherently downregulated in both situations were enriched in GO terms related to translation and ribosome biogenesis, and, most strikingly, a quarter of them were under the GO term “translation” (Figure 1F, S1F). These similar transcriptomic changes support our hypothesis that TOR activity is reduced in *drmy1*. To further test this hypothesis, we measured TOR activity in WT and *drmy1* by assaying the phosphorylation of its direct substrate, RIBOSOMAL PROTEIN eS6 KINASE (S6K)[48,49]. While the total protein level of S6K did not change in *drmy1*, we found that S6K phosphorylation decreased by half, demonstrating reduced TOR activity (Figure 1G, 1H). Overall, these results are consistent with the idea that *drmy1* has reduced TOR activity—a main pathway controlling ribosome biogenesis and translation—which causes reduced ribosomal content and translation rate.

**Defects in TOR activity, ribosome integrity, and translation disrupt robust sepal initiation**

We next asked whether defects in TOR activity, ribosome, or translation have any effects on robust sepal initiation like the *drmy1* mutation does (Figure 2A vs 2B; also see Zhu et al.[26]). In a WT bud, initiation is robust in that four sepal primordia of similar size form evenly spaced around the periphery of the floral meristem (Figure 2A, 2H). Angles between them vary little, i.e., they are all at around 90° angles from each other (Figure 2I, 2J). By contrast, in *drmy1* buds, three to five sepal primordia initiate and grow to different sizes (Figure 2B, 2H; also see Zhu et al.[26]). The *drmy1* sepal primordia are generally unevenly spaced, and angles between them have a high coefficient of variation (CV) (Figure 2I, 2J). To determine whether defects in ribosomes can cause the same sepal initiation defects, we imaged three ribosomal mutants, *ul4z* (*rpl4a*), *ul4y*, and *ul18z* (*rpl5a*)[40], each mutated in a gene encoding a ribosomal component that is also downregulated in *drmy1* at the transcript level (Figure S1C). The *ul4z* mutant bud shows reduced size of the inner sepal primordia relative to the outer sepal primordia (Figure 2C), and slightly more variable spatial distribution of sepal primordia (Figure 2J), although it always develops four sepal primordia (Figure 2H). This is a weaker phenotype than *drmy1* but has similar characteristics. The *ul4y* and *ul18z* mutants show great variability in the number and position of sepal primordia (Figure 2D, 2E, 2H, 2J), more similar to *drmy1*. We also crossed these ribosomal mutants with *drmy1* to study sepal variability in the double mutants (Figure S2A-H). In *drmy1 ul4z*, *drmy1 ul4y*, and *drmy1 ul18z/+*, on average, sepal initiation was as variable as in the *drmy1* single mutant (Figure S2I, SIJ). However, there were buds with no outgrowth in the adaxial or lateral regions of the bud periphery (Figure S2B, S2E, S2G), buds with six sepal primordia (Figure S2C, S2F, S2H), and

buds with two outer sepal primordia (Figure S2D, S2H), which were not seen in the single mutants. Note that we were unable to characterize the homozygous *drmy1 ul18z* double mutant because they were embryo-lethal (Figure S2K), further supporting the idea that ribosomal mutations enhance the phenotypic defects in *drmy1*.

We then imaged mutants with reduced TOR activity to determine whether sepal initiation is also less robust. *lst8-1-1* is a T-DNA insertional mutant of the TOR complex component LST8-1[50] and is weakly hypomorphic in TOR activity. We found that *lst8-1-1* shows variable sepal initiation in a small proportion of buds (4/41, 9.8%) (Figure 2F, 2H, 2J). The *spaghetti-1* mutant defective in TOR complex 1 (TORC1) assembly[51] showed a level of variability comparable to the *drmy1* mutant and the ribosomal mutants *ul4y* and *ul18z* (Figure 2G, 2H, 2J). Mutants with more severe disruption of TOR activity are embryo lethal and could not be analyzed[51,52]. These results show that reduction in TOR activity can cause variability in sepal initiation, similar to *drmy1*.

To corroborate these findings, we directly inhibited translation by *in vitro* culture of dissected WT inflorescences on 2 μM cycloheximide (CHX, a chemical inhibitor of translation) for 9-10 days. This is a low concentration that does not completely block translation, as inflorescences were still alive after 10 days in this condition. Compared with mock, CHX-treated inflorescences develop buds that have 2 to 6 sepal primordia of variable sizes that are unevenly spaced around the bud periphery (Figure 2K, 2M, 2N). These phenotypes are stronger than *drmy1*. Similarly, we directly inhibited TOR activity by continuous bi-daily application of 2 nmol Torin2 to the growing shoot apex for 15 days, and we observed variable sepal initiation (Figure 2L, 2M, 2N). Overall, data reported above show that inhibition of TOR activity and translation can disrupt the robustness of sepal initiation, in terms of sepal primordium number, position, and size.

We previously showed that the *drmy1* mutant bud develops sepals of different sizes because some sepal primordia initiate much later than others[26]. The late-initiating primordia remain smaller throughout development. They end up as smaller sepals relative to those that initiated earlier, leaving gaps that expose the developing inner floral organs[26]. We asked whether TOR or ribosomal defects disrupt the relative timing of sepal initiation just as the *drmy1* mutation does. We live imaged WT and *ul4y* every six hours during sepal initiation and quantified the amount of time the bud takes to initiate the inner and lateral sepals after it initiates the outer sepal. In WT, after the initiation of the outer sepal, most buds initiate the inner sepal within 6 hours and the lateral sepals within 12 hours (Figure 3A, 3C; also see Zhu et al.[26]). In *ul4y*, the initiation times of the inner and lateral sepals are more variable and delayed relative to the outer sepal, with 7.5% of the buds initiating the inner sepal 18 hours after the outer sepal, and 32.5% of the buds initiating the lateral sepals 18 hours after the outer sepal (Figure 3B, 3C). Similarly, we compared the relative timing of sepal initiation in Torin2 vs mock-treated WT buds. While in most mock-treated buds, the inner and lateral sepals initiate within 12 hours after the outer sepal (Figure 3D, 3F), in Torin2-treated buds they are much more variable and delayed (Figure 3E, 3F), to a similar extent as previously observed in *drmy1*[26]. In some cases, the inner and lateral sepals initiate more than

30 hours after the outer sepal. These results show that TOR and ribosomal defects can disrupt the precisely orchestrated initiation timing of sepal primordia.

Does the variability in initiation timing cause variable sizes and gaps in mature sepals, as in *drmy1* (Figure S3A,B,G,H; also see Zhu et al. [26])? We imaged the mature sepals of the ribosomal mutants *ul4z*, *ul4y*, *ul18z*, as well as the TOR component mutant *lst8-1-1*. Surprisingly, unlike *drmy1*, the sepals in *ul4z*, *ul4y*, *ul18z* enclose the inner floral organs perfectly, leaving no gaps, regardless of sepal number (Figure S3C-E). Small gaps still exist in buds of *lst8-1-1*, although sepal size differences appear greatly reduced (Figure S3F). Further dissection shows that in these mutants, sepals within the same flower are of similar sizes, although sepals from different flowers can be of vastly different sizes, most conspicuously for *lst8-1-1* (Figure S3I-N). This is unlike *drmy1*, where sepal size variability is equally high comparing sepals within the same flower or from different flowers (Figure S3H, S3M-N). Upon closer examination, while sepals initiating late in *drmy1* buds remain small, continuously leaving a gap in the sepal whorl (Figure S3O-P), those in *ul4y* were able to catch up with the other sepals and close the gap (Figure S3Q). Our results are consistent with the hypothesis that there exists a size-coordinating mechanism independent of TOR or ribosome function that allows sepals within the same bud to reach the same mature length, and that this mechanism is disrupted in *drmy1*. Such a mechanism requires further investigation in future studies.

**Inhibition of TOR activity and translation increase cytokinin signaling and disrupts the robust spatial pattern of auxin and cytokinin signaling**

Auxin and cytokinin are two important plant hormones critical to many aspects of plant development[30–32], and there is accumulating evidence that they act synergistically in the shoot apical meristem to promote lateral organ initiation[16,53,54]. We previously showed that, in a WT floral meristem prior to sepal initiation, auxin and cytokinin signaling are concentrated at the four incipient primordia, which is required for robust sepal initiation from these regions (Figure 4A, S4A; Zhu et al.[26]). In the *drmy1* mutant, cytokinin signaling becomes stronger and diffuse around the bud periphery (Figure 4A-B). Auxin signaling also becomes more diffuse, forming irregular auxin maxima that are less focused than those in WT, except at the incipient outer sepal where it remains robust (Figure 4A, S4B; Zhu et al.[26]). These changes in hormone signaling correlate with variable sepal initiation (Figure S4B)[26]. We wondered whether ribosomal mutations have similar effects on auxin and cytokinin signaling. To this end, we imaged the auxin signaling reporter *DR5::3xVENUS-N7* and the cytokinin signaling reporter *TCS::GFP* in floral meristems of the ribosomal mutant *ul4y*. Both reporters lose their robust spatial pattern except in the incipient outer sepal (Figure 4A, S4C). The hormone signaling patterns were quantified by circular histogram analysis (see Methods for details). For each of DR5 and TCS, WT buds showed four clear peaks ~90 degrees apart from each other, with very little signal in between, whereas in *drmy1* and *ul4y*, peaks were barely seen except at the incipient outer sepal (at 45 degrees), and there was greater noise and variation all around the bud (Figure 4C-D). Diffuse bands of auxin signaling that typically occurs in the adaxial or lateral periphery of *drmy1* and *ul4y* buds (Figure S4B and S4C, brackets)

can later resolve into several distinct auxin maxima of various intensity and at various positions, correlated with the initiation of sepal primordia of various sizes at these same positions (Figure S4B and S4C, red arrowheads).

We also tested whether drug treatments that inhibit TOR activity or translation can disrupt the robust hormone patterning. Buds treated *in vitro* with the translation inhibitor CHX (2 μM) for 3 days showed a 50% increase in cytokinin signaling, and both auxin and cytokinin signaling became diffuse around the bud periphery (Figure 4E-H). By day 6, cytokinin signaling was still diffuse all around, and increased to more than two-fold relative to mock (Figure 4I, 4J, 4L). Auxin signaling formed maxima of variable number at variable positions (Figure 4I arrowheads, 4K), correlated with the variable initiation of sepal outgrowth at these positions (Figure S4D-E). Similar changes occurred in buds treated *in vitro* with the TOR inhibitor AZD-8055 (2 μM) for 6 days (Figure 4I-L). For both CHX and AZD-8055, the disruptions of hormone signaling are similar to *drmy1*. *In vivo* treatment using another TOR inhibitor Torin2 for 15 days increased cytokinin signaling by 70%, although it did not make auxin and cytokinin signaling more diffuse (Figure S4F-I). Overall, these results show that defects in TOR activity and translation increase cytokinin signaling, and disrupt the precise spatial patterning of cytokinin and auxin signaling required for robust sepal initiation.

**An increase in cytokinin signaling is necessary and sufficient for variable auxin signaling and sepal initiation under translation inhibition**

Auxin is a critical hormone in organogenesis[55,56]. As shown above, variable patterning of auxin signaling correlates with variable sepal initiation during inhibition of TOR activity and translation. We wondered what caused auxin to lose its robust patterning under such conditions. It was previously reported that the ribosomal mutants *ul4y*, *ul18z*, and *el24y* have reduced protein levels of AUXIN RESPONSE FACTOR (ARF) 3, 5, and 7[57–59], key transcription factors that mediate the auxin signaling response[60]. The transcripts of these ARFs contain upstream open reading frames (uORFs), requiring translation reinitiation to translate their main open reading frames[61,62], a process defective in *ul4y*, *ul18z*, and *el24y*[57–59]. We therefore hypothesized that *drmy1* loses robust auxin signaling pattern because of reduced translation of uORF-containing transcripts, including those of certain ARFs. To begin, we utilized our transcriptomics and proteomics data, and considered that the protein-transcript ratio of a gene should reflect both its level of translation and stability. Therefore, following our hypothesis, genes containing uORFs should, in general, have a lower protein-transcript ratio in *drmy1* than in WT. We calculated the difference of this ratio between *drmy1* and WT for all 5,086 gene-protein pairs in our inflorescence dataset, and compared the ratio against the number of uORFs in each transcript (Figure S5A; uORF data from von Arnim et al.[62]). We found a small but significant decrease in the protein-transcript ratio in *drmy1* for the 724 genes containing at least 2 uORFs in their transcripts, supporting the hypothesis that *drmy1* has reduced translation reinitiation for uORF-containing transcripts, just like the ribosomal mutants *ul4y*, *ul18z*, and *el24y*[57–59]. Then, we examined whether the translation reinitiation of uORF-containing ARFs are indeed reduced in the *drmy1*

mutant. We selected *ARF3/ETTIN*, *ARF5/MONOPTEROS*, and *ARF6*, which have 2, 6, and 6 uORFs respectively, and as controls, *ARF8* and *ARF10* which do not contain uORFs. None of these *ARF*s were differentially expressed in *drmy1* at the transcript level, except *ARF10* which was slightly upregulated (Figure S5B). We utilized promoter-fluorescent protein fusion reporters (Figure S5C) which have the same uORFs in the promoter region as the corresponding ARF genes if the genes have them. These reporters reflect transcriptional and uORF-mediated translational regulation. *pARF3::N3xGFP*, *pARF5::ER-EYFP-HDEL*, and *pARF6::N3xGFP* contain uORFs and thus, following our hypothesis, are expected to drastically decrease in fluorescence intensity in *drmy1* compared to WT. *pARF8::N3xGFP* and *pARF10::N3xGFP* do not have uORFs and are thus expected to have comparable or higher fluorescence intensity in *drmy1*. Surprisingly, we saw no correlation between the presence of uORFs and decrease in fluorescent intensity in *drmy1* (Figure S5C). While it might arise from additional layers of regulation on these ARFs, this result suggests that the decrease in translation reinitiation of uORF-containing ARFs is not the main factor explaining the loss of robust auxin signaling pattern in *drmy1*.

It was previously reported that external application of cytokinin increases auxin biosynthesis in actively growing tissue including the shoot apex, young leaves, and roots[63], and cytokinin application also changes the expression and polarity of PIN-FORMED (PIN) polar auxin transport carriers[64,65]. We previously noticed that external application of 6-benzylaminopurine (BAP), a synthetic cytokinin, induced additional convergence points of PIN1 and increased variability in auxin signaling, causing variability in sepal initiation (Zhu et al.[26], in this reference see Fig. 4e, Extended Data Fig. 7e and 7f). Here, we confirmed this observation by circular histogram analysis (Figure 5A-D). While the mock-treated WT buds showed four clear peaks of DR5 signal with very little signal in between (Figure 5A-B), those treated with 5 μM BAP showed a less robust spatial pattern, with less distinguishable peaks and larger variation all around the bud (Figure 5C-D). Thus, excessive cytokinin is sufficient for the variable spatial pattern of auxin signaling.

We then wondered whether an increase in cytokinin signaling (Figure 4) is the cause of variable pattern of auxin signaling under translation-limited conditions such as *drmy1*. To test this hypothesis, we crossed *drmy1* containing the DR5 reporter with a triple mutant of *ARABIDOPSIS RESPONSE REGULATOR* (*ARR*) *1*, *10*, and *12*, the three most highly expressed B-type ARRs in our RNA-seq (Supplementary Dataset 1) which are crucial for the activation of cytokinin-responsive genes[66]. While buds of *arr1,10,12* did not show apparent phenotypic differences from WT, the quadruple mutant *drmy1 arr1,10,12* largely rescued the *drmy1* phenotype, with much less variability in sepal number and position (Figure 5E-G). While mature buds of *drmy1* have sepals of variable sizes, leaving gaps and exposing the inner floral organs (Figure S6D vs. S6A), those of *drmy1 arr1,10,12* have sepals of robust sizes that are able to close (Figure S6E). Likewise, mutation in a cytokinin receptor *WOODEN LEG* (*WOL*)/*ARABIDOPSIS HISTIDINE KINASE 4* (*AHK4*) showed a similar rescue of the *drmy1* sepal phenotype (Figure 5E-G, S6F). While the auxin signaling reporter DR5 was diffuse and variable in *drmy1* except in the incipient outer sepal (Figure 5H-I), in *drmy1 arr1,10,12*, it was focused in all the four incipient sepals that

were robustly positioned, although the signal intensity in the incipient outer sepal was much higher than others (Figure 5J-K). These results indicate that cytokinin signaling is required for the variability in auxin signaling pattern and sepal initiation in *drmy1*.

Furthermore, we wanted to test whether cytokinin signaling is required for variability in more general conditions where translation is inhibited. The translation inhibitor CHX disrupted robustness in auxin signaling and sepal initiation in WT (Figure 2K, 4E, 4I), and we tested whether these effects are still present in *arr1,10,12* and *wol* mutants. We found that, unlike WT, sepal initiation remained mostly robust in *arr1,10,12* and *wol* after ten days of 2 μM CHX treatment (Figure 5L-N). While DR5 in WT became diffuse and occurred in variable positions after three days of CHX treatment (Figure 5O-P, arrow), DR5 in *arr1,10,12* remained robust and concentrated at the four incipient sepal primordia (Figure 5Q-R). These results suggest that elevated cytokinin signaling level is the primary cause for variability in auxin patterning under translation-inhibited conditions. Thus, in WT, maintaining a low level and focused cytokinin signaling is crucial for robust auxin patterning and sepal initiation.

**Upregulation of cytokinin signaling is required to sustain translation and fitness in *drmy1***

Why does the plant upregulate cytokinin signaling at the cost of robust morphogenesis under translation-inhibited conditions? Early studies revealed that cytokinin signaling can stimulate translation[67–71], by increasing transcription or protein abundance of ribosomal components or biogenesis factors[72–74] and modification of initiation and elongation factors[75]. We therefore hypothesized that an increase in cytokinin signaling under translation-inhibited conditions such as in *drmy1* serves to sustain a survivable rate of translation in a feedback loop. We first validated that, under our growth conditions, an increase in cytokinin signaling (*arr1 35S::ARR1*) increases translation rate (Figure 6A; also see Karunadasa et al.[67]) in 14-day-old seedlings. We then tested whether cytokinin signaling is required to sustain translation, especially in *drmy1* (Figure 6B-C). The cytokinin receptor single mutant *wol* does not differ from WT in translation rate 8 days after germination but shows a reduced translation rate at day 14. Conversely, at day 8, *drmy1* seedlings showed a drastically reduced translation rate compared to WT, but by day 14, translation rate in *drmy1* increased and matched WT. In the *drmy1 wol* double mutant, however, translation rate was unable to recover at day 14 and remained lower than either single mutant. Our data suggests that cytokinin signaling is required to sustain translation in *drmy1*, despite reduced ribosomal content (Figure 1D).

We then examined whether removal of cytokinin signaling and consequent failure to sustain translation in *drmy1* affects plant vitality and reproduction. As expected, at day 14, the *drmy1 wol* double mutant plants were extremely small, with tiny and chlorotic cotyledons and true leaves (Figure 6D). These plants typically produced tiny rosettes and short inflorescences with a few chlorotic buds that develop into small, short siliques (Figure 6E, S6F). Similarly, the *drmy1 arr1,10,12* quadruple mutant plants are slightly chlorotic and accumulate anthocyanins in the rosette leaves (Figure 6F). They produced a tiny inflorescence composed of very few buds (Figure

6F, S6E) and, in the end, siliques in which all seeds had aborted (Figure 6G). Overall, these results show that the growth defects in *drmy1* are exaggerated by downregulation of cytokinin signaling. While it is possible that *drmy1* can be particularly sensitive to other defects caused by cytokinin downregulation, our results are consistent with the hypothesis that the upregulation of protein synthesis by increased cytokinin signaling promotes the survival of mutants with reduced ribosomal content such as *drmy1*.

**Translation inhibition decreases the level of ARR7, a cytokinin signaling inhibitor protein**

What causes cytokinin signaling to increase in plants with reduced TOR activity and translation (Figure 4)? It was previously known that *cis*-type cytokinins can be synthesized from tRNAs by the tRNA isopentenyltransferases (IPTs), IPT2 and IPT9[76]. We hypothesized that the decrease in translation rate may increase the availability of tRNAs as substrates for cytokinin biosynthesis, increasing the level of cytokinins. To test this idea, we extracted cytokinins from induced inflorescences of WT and *drmy1* in *ap1 cal AP1-GR* background (Figure S1A). We measured the level of three cytokinin bases, *trans*-Zeatin (tZ), *cis*-Zeatin (cZ), and isopentenyladenine (iP), and their corresponding nucleosides (tZR, cZR, and iPR), using liquid chromatography-mass spectrometry. Surprisingly, we found no significant difference in their levels between WT and *drmy1*, and notably, the amount of *cis*-Zeatin was barely detectable in all samples (Figure S7A). This suggests that the increase in *cis*-type cytokinin synthesis is not the mechanism underlying the increase in cytokinin signaling under our translation-inhibited conditions.

We then considered the effects that a decrease in translation rate might have on the protein components of the cytokinin signaling pathway. A-type ARR proteins are inhibitors of cytokinin signaling[77–79]. They are rapidly induced upon cytokinin application and serve to dampen cytokinin response in the tissue[80–82]. These proteins also have a fast turnover rate, being rapidly depleted upon blocking translation with a half-life ranging from 60 to 180 min[83]. The rapid synthesis and degradation of these proteins may be crucial for maintaining homeostasis of cytokinin signaling during developmental processes. We therefore hypothesized that, during sepal initiation, translation defects in *drmy1* cause reduced synthesis of A-type ARR proteins, decreasing them to a level insufficient to repress cytokinin signaling (Figure 7A).

We set out to test whether the level of A-type ARR proteins are reduced in *drmy1*. We were unable to detect fluorescence in the inflorescence of a published GFP-tagged A-type ARR line under the endogenous promoter (*pARR4::ARR4-GFP*)[84]. We reasoned that this was because A-type ARRs have low protein levels in the inflorescence (none was detected in our proteomics dataset) and fast turnover rates[83]. We therefore employed LlamaTagging, a recently developed method to visualize the abundance of nuclear-localized proteins with short half-lives[85]. Rapidly degraded proteins cannot be visualized through fusion with standard fluorescent proteins, because fluorescent proteins take time to fold and mature before they fluoresce, and the protein of interest is degraded before the maturation of the fluorescent protein. On the other hand, the

LlamaTag folds immediately. A LlamaTag with a high affinity for GFP can be encoded as a translational fusion with a nuclear-localized protein of interest. In this case, soon after translation, the fusion immediately binds GFP in the cytosol and translocates the GFP with the protein to the nucleus. Thus, increased GFP fluorescence in the nucleus indicates higher abundance of the protein of interest. We decided to focus on ARR7, the A-type ARR that is most highly expressed in our RNA-seq dataset and not differentially expressed in *drmy1* (Figure 7B; Supplemental Dataset 1). We designed a construct with ARR7 fused with GFP-specific LlamaTag by a short linker, driven by the ARR7 native promoter (*pARR7::ARR7-linker-llama-ARR7ter*; *ARR7-llama* for short). This construct was co-transformed with cytosol-localized GFP containing a nuclear exclusion signal (*pUBQ10::sfGFP-nes-UBQ3ter*; *GFP-nes* for short; Figure 7C). When ARR7-llama is produced in the cytosol, LlamaTag binds to cytosolic GFP. ARR7 then localizes to the nucleus, guided by its C-terminal nuclear localization signal[86,87], dragging GFP into the nucleus. Thus, when ARR7-llama is present at a low level, GFP is predominantly cytosol-localized; at an intermediate level, GFP may be nearly equally localized in the cytosol and nucleus; at a high level, most GFP are transported by ARR7-llama into the nucleus, and thus GFP signal is mainly seen in the nucleus (Figure 7D).

As a proof of concept, we treated this reporter in WT background with 200 μM BAP. We found that GFP signal became more nuclear-localized within 5 hours of the treatment (Figure S7B), agreeing with an increased expression and stability of A-type ARR proteins upon cytokinin application as previously reported[83,88].

We then compared the localization of GFP signal in floral meristems of WT and *drmy1* before sepal initiation. Following our hypothesis, if the increase in cytokinin signaling in *drmy1* is caused by reduced translation of A-type ARR proteins, there should be a decrease in ARR7 level, and thus an increase in cytosolic GFP signal, in *drmy1* vs WT. On the other hand, if the increase in cytokinin signaling in *drmy1* is caused by any other mechanism, we should see an increase in ARR7 level and nuclear GFP signal because cytokinin signaling increases the gene expression and protein stability of A-type ARRs[81,83,89]. We found that WT buds had slightly more nuclear-localized GFP signal than cytosol-localized GFP signal, with brighter spots corresponding to the nucleus surrounded by darker grooves in between corresponding to the cytosol (Figure 7E-F). In contrast, in the periphery of *drmy1* buds, GFP signal localizes more to the cytosol than to the nucleus, with darker spots surrounded by brighter grooves (Figure 7E-F). More nuclear GFP was present near the center of *drmy1* buds. This result indicates nuclear ARR7 protein concentration is reduced in the *drmy1* mutant, particularly in the zone where sepals initiate. To see whether this conclusion holds in other translation-inhibited conditions, we treated WT plants carrying the *ARR7-llama* and *GFP-nes* reporters with the translation inhibitor CHX and the TOR inhibitor AZD-8055. 2 μM CHX treatment for 24 hours drastically reduced the nuclear localization of the GFP signal and increased its cytosolic localization (Figure 7G). 2 μM AZD-8055 treatment for 72 hours had a milder but similar effect (Figure 7H). These treatments did not affect the localization of the GFP signal in plants without *ARR7-llama* (Figure S7C-D). These results show that conditions that decrease translation rate generally decrease the nuclear level of ARR7 protein. Further, these

results are consistent with our hypothesis that disruption of protein translation upregulates cytokinin signaling in the floral meristem due to depletion of A-type ARR proteins. This suggests that the rapid synthesis of A-type ARR proteins is crucial for maintaining homeostasis of cytokinin signaling during sepal initiation.

Given that the level of nuclear ARR7 was reduced in *drmy1*, we next asked whether increasing the level of ARR7 would restore robustness in *drmy1*. We found that while WT buds carrying the *ARR7-llama* and *GFP-nes* constructs do not phenotypically differ from WT without these constructs (Figure 7I-J, S7E-F), *drmy1* plants with these constructs show a partial restoration of sepal initiation robustness, particularly in terms of sepal primordium position (Figure 7K-N, S7G-H). In stage 9-12 buds, some buds have robustly sized sepals that are able to close properly, while others still have variably sized sepals that leave gaps just like in *drmy1* (Figure S7H). Thus, increasing ARR7 level by adding an extra functional transgene of *ARR7-llama* to the genome can partially restore robustness in both sepal initiation and mature sepal size in *drmy1*. This indicates that the decrease in ARR7 protein level in *drmy1* is at least partially responsible for its variability in these aspects.

We also considered other protein components of auxin and cytokinin signaling that are being rapidly synthesized and degraded during developmental processes, and therefore, may be depleted under translation defects. AUXIN/INDOLE-3-ACETIC ACID INDUCIBLE (Aux/IAA) proteins are auxin signaling inhibitors that are rapidly induced by auxin[90,91]. In the presence of auxin, they are rapidly degraded, mediated by the ubiquitin E3 ligase SKP1, CUL1, F-BOX PROTEIN (SCF) complex involving TRANSPORT INHIBITOR RESPONSE1/AUXIN SIGNALING F-BOX (TIR1/AFB)[92–95]. Degradation is dependent on the Short Linear Motif (SLiM) degron contained within Domain II (DII)[94–96]. We hypothesized that the level of DII-containing proteins including Aux/IAAs would be drastically decreased in *drmy1* because they are unable to be rapidly synthesized to keep up with their degradation. To test this, we used the R2D2 reporter[97], which contains a DII fused with 3xVENUS (*pUS7Y::DII-n3xVENUS*), and as a control, a mutated non-degraded DII fused with tdTomato (*pUS7Y::mDII-ntdTomato*). We compared this reporter in *drmy1* vs. WT. The ratio of *VENUS* to *tdTomato* was not reduced in *drmy1*, but instead slightly but significantly elevated (Figure S7I-J). In addition, *drmy1* has stochastic patches of DII-VENUS degradation, consistent with its often mislocalized auxin maxima (Figure 4A, S4B), unlike WT which had four patches of degradation corresponding to the four incipient sepal primordia where auxin maxima robustly form (Figure 4A, S4A). Overall, these results suggest that the level of DII-containing Aux/IAA proteins is not reduced in *drmy1*, despite the high requirement for synthesis due to their rapid turnover. They also indicate that not all proteins that are rapidly synthesized and depleted in response to hormone signaling are equally affected by translation inhibition, which may result in different changes in hormone signaling output under such condition.

## DISCUSSION

Robustness, the strikingly reproducible development of phenotype, has fascinated biologists for decades[2]. The Arabidopsis flower robustly develops four sepals of equal size. This stems from the robust initiation of four sepal primordia from the floral meristem, which is in turn dictated by the robust patterning of auxin and cytokinin controlled by DRMY1[26]. Here we elucidated how DRMY1 controls robust hormone patterning and thus robust sepal initiation. We show that DRMY1 sustains TOR activity, ribosomal content, and translation. We further show that inhibition of TOR activity or translation is sufficient to cause variability in the timing, position, and number of sepal primordia, mimicking the *drmy1* phenotype. Our findings are in concert with previous studies that have shown robustness is often maintained by genes involved in central cellular processes[2]. In our case, the rate of translation in wild type maintains a proper level of ARR7, which needs to be rapidly synthesized to dampen cytokinin signaling. ARR7 in turn ensures a normal level and spatial pattern of cytokinin signaling and indirectly auxin signaling, and thus robust sepal initiation (Figure 7O, top). In the *drmy1* mutant, the reduced TOR activity, ribosomal content, and translation rate causes inability to rapidly synthesize ARR7, which are short-lived proteins that are easily depleted[83]. Consequently, cytokinin signaling is elevated, disrupting the robust spatial distribution of both cytokinin and auxin, leading to variable sepal initiation (Figure 7O, bottom). Blocking cytokinin signaling in *drmy1* is sufficient to restore robust initiation of four sepal primordia, but has severe consequences on the overall fitness of the plant. Our results reveal how defects in hub cellular processes such as TOR signaling and translation can have very tissue-specific phenotypic effects.

It was discovered long ago that extrinsic cytokinin application to plant tissue or cell-free extracts can promote mRNA translation[68–71]. Recent studies further confirmed that the up-regulation of translation by cytokinin is at least in part mediated by the cytokinin signaling pathway[67,75]. Here, we show that cytokinin signaling in floral buds is upregulated in translation-inhibited conditions, such as *drmy1*, AZD-8055 treatment, or CHX treatment (Figure 4; also see Zhu et al.[26]), through reduced level of ARR7 (Figure 7). The enhanced cytokinin signaling maintains translation rate at a level necessary for the survival and reproduction of the plant (Figure 6). We propose that there is a homeostasis mechanism where plants leverage increased cytokinin signaling to rescue the translation rate reduction caused by deficient TOR activity and ribosomal content (Figure 7O, bottom). It remains to be tested how widely this mechanism is applicable to other mutants with ribosomal defects, or whether parallel mechanisms operate in other species across kingdoms.

While translation-inhibited plants likely upregulate cytokinin signaling to maintain protein synthesis, this upregulation negatively affects developmental robustness. We have previously shown that exogenous cytokinin application to the WT floral meristem increases variability in PIN1 convergence and auxin signaling patterns, and consequently, in sepal initiation. Mutation of a cytokinin signaling inhibitor *AHP6* causes similar variability in sepal initiation. These effects are more pronounced in the *drmy1* mutant, which by itself has increased and diffuse cytokinin signaling[26]. Here, we provide additional evidence that increased and diffuse cytokinin signaling is necessary for such variability. While *drmy1* and CHX-treated WT floral meristems are variable in

auxin signaling pattern and sepal initiation (Figure 2, 4), mutations in *wol* and *arr1,10,12*, which decreases cytokinin signaling, largely restore robustness (Figure 5). Robustness is also restored in the mature sepals of *drmy1 wol* and *drmy1 arr1,10,12*, enabling sepal closure (Figure S6). Similar effects in restoring robustness are seen when an extra functional transgene of *ARR7* (*pARR7::ARR7-llama*) is introduced to the *drmy1* mutant (Figure 7, S7). Our results suggest that cytokinin upregulation is necessary and sufficient for variability in auxin patterning and sepal initiation, indicating that the cytokinin signaling changes are primary defects in *drmy1*, and the auxin signaling changes are secondary. Our results suggest a mechanism different from that previously reported in *ul4y*, *ul18z*, and *el24y*, where ribosomal mutations affect auxin signaling through reduced translation reinitiation of uORF-containing mRNAs, including those of AUXIN RESPONSE FACTOR (ARF) 3, 5, and 7[57–59]. While we found that uORF-containing mRNAs generally have reduced protein-transcript ratio in *drmy1* suggestive of reduced translation, we did not see a consensus reduction in the level of uORF-containing promoter reporters of ARFs (Figure S5). This suggests that the variable auxin signaling pattern in *drmy1* is unlikely to result from changes in uORF-mediated translational regulation of ARFs. Overall, our results suggest that homeostasis in cytokinin signaling is crucial for maintaining robust patterns of auxin signaling and robust morphogenesis in the floral meristem.

Mutations affecting ribosome biogenesis or translation have long attracted interest due to the surprisingly tissue-specific phenotypes they cause[98]. In humans, these mutations have been associated with diseases collectively known as ribosomopathies, where patients show various abnormalities in blood, skeleton, hair, teeth, and pancreas, as well as intellectual disability and increased risk of cancer[99–104]. Ribosomal protein mutants have been characterized in numerous other species with similarly diverse impacts. They display a range of specific phenotypic changes, such as altered pigmentation and skeletal structure in mouse[105–107] and zebrafish[108], shorter bristles and notched wing margins in fruit fly[22,109], abnormal gonad development in worm[110], and pointed leaves and abnormal vascular patterning in Arabidopsis[57,58,111–113]. Here, we show that the Arabidopsis mutant *drmy1* has reduced TOR activity, ribosomal content, and translation rate, causing variable sepal initiation which phenocopies the ribosomal mutants *ul4y* and *ul18z* and the TORC1 assembly mutant *spaghetti-1* (Figure 2, 3). We therefore propose that *drmy1* is an Arabidopsis ribosomopathy mutant like those previously characterized[112].

Several mechanisms have been proposed to explain why ribosomopathies do not usually cause a general reduction in growth, but rather affect development in tissue-specific ways. These include extra-ribosomal functions of certain ribosomal proteins[114–118], altered translation behavior of ribosomal variants on certain mRNAs[119], different competitiveness of mRNAs for scarce ribosomes[57–59,120–123], and high translation rate requirement for certain proteins[124,125]. For example, neurotransmitter release in animals relies on constant synthesis of the synaptic vesicle protein Syt1[126]. A Drosophila *Minute* mutant, *uS15/+,* shows reduced synthesis of Syt1, which in turn reduces ecdysone secretion in 5-HT neurons, causing delayed larval-to-pupal transition[124]. Similarly, the human apoptosis inhibitor Mcl-1 has a half-life of ~30 min and thus requires a high translation rate to maintain its proper level. Under translation inhibition, Mcl-1 is rapidly degraded,

causing apoptosis[125]. Here, we show that the level of ARR7, another rapidly synthesized and degraded protein[83], is drastically reduced under translation inhibition, which underlies the upregulation of cytokinin signaling and loss of robustness in auxin signaling and morphogenesis (Figure 7). This mechanism parallels those previously found in animal systems[124,125], and highlights how defects in translation, which occurs in every cell, can have tissue-specific effects on how cells robustly arrange into organs. Outside the floral meristem, the *drmy1* mutant shows other phenotypic changes such as enlarged shoot apical meristem, reduced apical dominance, phyllotaxy defects, and reduced root system, all of which are related to altered cytokinin/auxin signaling activity[26].

In addition, we note that not all proteins that are rapidly synthesized and depleted in response to hormone signaling are equally affected under broad translation inhibition. Our data suggest that DII-containing proteins, including auxin signaling inhibitors Aux/IAAs, are not present at a lower level in *drmy1* (Figure S7H-I). Aux/IAAs are degraded by the proteasome in an auxin-dependent manner[96], while A-type ARRs can also be degraded by selective autophagy when phosphorylated, in addition to proteasomal degradation[84]. In addition, the transcription of *Aux/IAA* genes can be induced under translation inhibition, possibly as a feedback mechanism to maintain Aux/IAA protein homeostasis[90]. Therefore, distinct turnover mechanisms and/or transcriptional regulation may shape distinct effects of translational inhibition on the level of these hormone signaling proteins.

## ACKNOWLEDGEMENTS

We thank Bella Burda, Frances Clark, Byron Rusnak, Erich Schwarz, Avilash Yadav, and Maura Zimmermann for comments and suggestions on the manuscript. We thank Frank Wellmer for the *ap1 cal 35S::AP1-GR* (Ler) seeds. We thank Elliot Meyerowitz and Arnavaz Garda for the *DR5::3xVENUS-N7*/*PIN1::GFP* (Ler) seeds. We thank Teva Vernoux and Géraldine Brunoud for the *TCS::GFP* and *TCS-DR5* (Col) seeds. We thank Jan Smalle for the *arr1-1 35S::ARR1* seeds. We thank Joseph Kieber, Jamie Winshell, and Kwame Acheampong for the *pARR4::ARR4-GFP* seeds. We thank Thomas Greb and Min-Hao Chiang for the *pARF5::ER-ARF5-HDEL* seeds. We thank Georg Jander for advice and protocol for cytokinin extraction. We thank Brian Curtis and Frank Schroeder for help on mass spectrometry. We thank Sheng Zhang and Qin Fu for help on Xcalibur. We thank Richie Ragas, Yanã Rizzieri, and Ziqing Wei for assistance on experiments and data analysis. We thank Vicky Spencer and Minsung Kim for sharing the *in vivo* Torin2 treatment protocol. We thank Arabidopsis Biological Resource Center for providing seed stocks and plasmids used in this research. Research reported in this publication was supported by the National Institute of General Medical Sciences of the National Institutes of Health (NIH) under award numbers R01GM134037, DP5OD023072, and R01GM145814; Cornell Graduate School new student fellowship (S.K.); and in part by a Schmittau-Novak Grant from the School of Integrative Plant Science, Cornell University (M.Z.). H.G.G. was supported by NIH Director's New Innovator Award (DP2 OD024541-01) and NSF CAREER Award (1652236), NIH R01 Award (R01GM139913), and the Koret-UC Berkeley-Tel Aviv University Initiative in Computational

Biology and Bioinformatics. H.G.G. is also a Chan Zuckerberg Biohub Investigator. We thank the Biotechnology Resource Center (BRC) Genomics Facility (RRID:SCR_021727) of Cornell University for performing RNA-seq on *ap1 cal AP1-GR* inflorescence samples. We thank Novogene for performing seedling RNA-Seq library synthesis and sequencing. We thank the BRC Proteomics Facility (RRID:SCR_021743) of Cornell University for performing mass spectrometry on *ap1 cal AP1-GR* inflorescence samples, and NIH SIG Grant 1S10 OD017992-01 for supporting the Orbitrap Fusion mass spectrometer. The content is solely the responsibility of the authors and does not necessarily represent the official views of the National Institutes of Health.

## AUTHOR CONTRIBUTIONS

S.K.: Conceptualization, Investigation, Formal Analysis, Visualization, Writing - Original Draft, Writing - Review & Editing. M.Z.: Conceptualization, Investigation, Formal Analysis, Writing - Review & Editing. M.R.S: Investigation, Visualization. D.P.: Investigation, Formal Analysis, Visualization. L.J.: Investigation. R.E.M.: Investigation, Formal Analysis. S.A.: Methodology, Resources. B.V.L.V.: Methodology, Resources, Writing - Review & Editing. H.G.: Methodology, Resources, Writing - Review & Editing, Supervision. S.B.Q: Writing - Review & Editing, Supervision. J.O.B.: Resources, Writing - Review & Editing, Supervision. A.H.K.R: Conceptualization, Writing - Review & Editing, Supervision, Project administration, Funding acquisition.

## DECLARATION OF INTERESTS

The authors declare no competing interests.

## FIGURE TITLES AND LEGENDS

**Figure 1. *drmy1* has reduced ribosome abundance, translation rate, and TOR activity.**
**(A)** Top row, stage 12 buds of WT (left) and *drmy1* (right) viewed from the top. Arrowheads point to sepals. Note that the *drmy1* bud has 5 sepals of unequal size and unevenly spaced, exposing the stamens and carpels. Middle row, stage 12 buds of WT (left) and *drmy1* (right) viewed from the side. Asterisk shows the gap between sepals with petals and carpels exposed. Bottom row, stage 5 buds of WT (left) and *drmy1* (right) containing *35S::mCitrine-RCI2A* (plasma membrane marker). Arrowheads point to sepal primordia. Note that the *drmy1* bud has 5 sepal primordia of different sizes. Scale bars are 0.5 mm for stage 12 bud images and 25 µm for stage 5 bud images.
**(B-C)** Gene ontology (GO) enrichment of downregulated genes **(B)** and differentially accumulated proteins **(C)** in *drmy1* compared to WT, in the *ap1 cal AP1-GR* background. Shown are the top 8 GO terms and their enrichment p-values. A complete list can be found in Supplemental Dataset 1. Arrowheads highlight terms related to ribosome biogenesis or translation.
**(D)** Ribosome profiles of WT (blue) and *drmy1* (red) in the *ap1 cal AP1-GR* background, representative of 3 biological replicates each. Polysomal peaks are highlighted. All replicates can be found in Supplemental Dataset 2.
**(E)** Puromycin labeling of WT vs *drmy1*. Left, puromycin labeling in WT and *drmy1* seedlings. From left to right: WT pre-treated with CHX, two biological replicates of WT pre-treated with mock, and two biological replicates of *drmy1* pre-treated with mock. All groups were then treated with puromycin. For seedlings to match in size, WT seedlings were 8 days old and *drmy1* seedlings were 10 days old. Right, puromycin labeling in WT and *drmy1* inflorescences of induced *ap1 cal AP1-GR* background. From left to right: WT co-treated with puromycin and CHX, three biological replicates of WT treated with puromycin, and three biological replicates of *drmy1* treated with puromycin. In both experiments, RuBisCO large subunit on Ponceau S-stained membrane is shown as a loading control (bottom).
**(F)** Coherent alteration of gene expression by *drmy1* and AZD-8055 TOR inhibitor treatment. Shown here is a scatterplot of RNA log 2 fold change in *drmy1* vs WT (x-axis), and WT+AZD vs WT+Mock (y-axis), in 7-day-old seedlings. Genes are color-coded based on the following categories: genes in “Structural constituents of the ribosome” (GO:0003735) and its offspring terms (magenta); all other genes in “Translation” (GO:0006412) and its offspring terms (orange); all other genes (gray). Blue line shows a linear regression of all points ($R^2 = 0.1446$, $p < 2.2x10^{-16}$). Note that the axes were trimmed to (-3,3) for ease of display.
**(G-H)** Phosphorylation of the direct TOR substrate, S6K-pT449, in WT and *drmy1*. Representative images are shown in **(G)**. Top, Western blot against S6K-pT449. Middle, Western blot against total S6K protein. Bottom, Ponceau S staining as a loading control. **(H)** Quantification of the intensity of S6K-pT449 over Ponceau normalized by WT, in three experiments, shows that TOR activity decreased by half in *drmy1*. (mean ± SD; *, $p<0.05$).

**Figure 2. Defects in TOR activity, ribosome integrity, and translation cause variable sepal initiation.**

**(A-G)** Representative images of stage 5 buds in WT (A), *drmy1* (B), *ul4z* (C), *ul4y* (D), *ul18z* (E), *lst8-1-1* (F), and *spaghetti-1* (G). Tissue morphology is visualized by either propidium iodide (a cell wall-staining dye) or a plasma membrane marker. Arrowheads indicate sepal primordia that are variable in number, position, and size. Note that *ul4z* flowers always develop four sepal primordia, although of different sizes; *lst8-1-1* occasionally (4/41, 9.8%) develops buds with more than four sepal primordia. Scale bars, 25 μm.

**(H)** Quantification of sepal primordium number, comparing *ul4z* (n = 52 buds), *ul4y* (n = 53 buds), *ul18z* (n = 52 buds), *lst8-1-1* (n = 41 buds), and *spaghetti-1* (n = 84 buds) with WT (n = 51 buds). Asterisks indicate statistically significant ($p < 0.05$) differences from WT in Fisher's contingency table tests.

**(I)** Illustration of robust versus variable positioning of sepal primordia. Primordia are considered robustly positioned if they are evenly distributed around the edge of the bud. Within each bud, angles between adjacent primordia with respect to the center of the bud are measured, and coefficient of variation (CV) is calculated. A bud with robustly positioned primordia would have similar angular values and a low CV value. A bud with variably positioned primordia would have very different angular values and a high CV value.

**(J)** Quantification of variability in primordium positioning (CV) in the same buds as in (H), following illustration in (I). Asterisks indicate statistically significant ($p < 0.05$) differences from WT in Wilcoxon's rank sum tests.

**(K)** Representative images of buds from *in vitro*-cultured WT inflorescences treated with mock or 2 μM CHX for 9 days (see Material and Methods). Arrowheads indicate sepal primordia that are variable in number, position, and size. Scale bars, 25 μm.

**(L)** Representative images of buds from WT plants treated with mock or 2 nmol Torin2 for 15 days (see Material and Methods). Arrowheads indicate sepal primordia that are variable in number, position, and size. Scale bars, 25 μm.

**(M-N)** Quantification of variability in primordium number (M) and positional variability (N) similar to (H,J), comparing CHX-treated (n = 31 buds), CHX-mock (n = 42 buds), Torin2-treated (n = 51 buds) and Torin2-mock buds (n = 56 buds).

**Figure 3. TOR and ribosomal defects cause variability in the timing of sepal initiation.**
**(A-C)** 6h-interval live imaging of the sepal initiation process in WT (A) and *ul4y* (B), which is quantified in (C). n = 48 buds for WT; n = 40 buds for *ul4y*.
**(D-F)** 6h-interval live imaging of the sepal initiation process in buds from WT plants treated with mock or 2 nmol Torin2 bi-daily for 15 days, which is quantified in (F). n = 31 buds for mock; n = 15 buds for Torin2.
In **(A,B,D,E)**, top rows show the *35S::mCitrine-RCI2A* membrane marker, and bottom rows show Gaussian curvature heatmaps calculated from the same image stacks. Asterisks indicate sepal initiation events, defined as a dark red band (primordium with positive curvature) separated from the floral meristem by a dark blue band (boundary with negative curvature) in the Gaussian curvature heatmap. Scale bars, 25 μm.
In **(C,F)**, the amount of time between outer and inner sepal initiation (left) and between outer and lateral sepal initiation (right) were calculated for each bud, and summarized over all the buds. Asterisks indicate statistically significant ($p < 0.05$) differences in the distribution of relative initiation timing in Fisher's contingency table tests.

**Figure 4. Defects in TOR activity, ribosome integrity, and translation cause variability in auxin and cytokinin signaling.**

**(A-D)** The ribosomal mutant *ul4y* loses robustness in auxin and cytokinin signaling. (A) Representative images of late stage 2 buds of WT, *drmy1*, and *ul4y*, showing the auxin signaling reporter *DR5::3xVENUS-N7* in yellow, the cytokinin signaling reporter *TCS::GFP* in cyan, and both merged with Chlorophyll (in WT) or *UBQ10::mCherry-RCI2A* (in *drmy1* and *ul4y*) in magenta. (B) Quantification of TCS intensity (integrated density divided by area) from maximum intensity projection images, normalized to mean of WT. Shown are mean ± SD. Asterisks show statistically significant differences from WT in two-tailed Student's t-tests (*drmy1*, $p = 2.1 \times 10^{-6}$; *ul4y*, $p = 3.4 \times 10^{-5}$). (C) Circular histogram of DR5 distribution around the bud. Each bud was divided into 360 sectors of 1° each. Within each sector, DR5 signal measured in pixel intensity units (0-255 range) was summed. This sum was plotted along the x-axis starting from the sector at 1:30 position (between the incipient outer sepal and incipient lateral sepal on the right) going counterclockwise. I.e. in WT, the outer sepal is near 45°, the inner sepal near 225°, and the lateral sepals near 45° and 135° (vertical dotted lines). The mean was plotted as a solid line, and mean ± SD was plotted as a shaded area. (D) Circular histogram of TCS distribution around the bud. Sample size for (A-D): WT, n = 12 buds; *drmy1*, n = 15 buds; *ul4y*, n = 10 buds.

**(E-H)** 3 days of translation inhibition causes increased and diffuse cytokinin signaling, and diffuse auxin signaling. (E) Representative images of late stage 2 buds from dissected and cultured WT inflorescences treated with mock or 2 µM CHX for 3 days. Shown are *DR5::3xVENUS-N7* in yellow, *TCS::GFP* in cyan, and both merged with Chlorophyll in magenta. (F) Quantification of TCS intensity from maximum intensity projection images, normalized to mean of WT mock day 3. Shown are mean ± SD. Asterisk shows statistically significant difference in a two-tailed Student's t-test ($p = 2.0 \times 10^{-4}$). (G) Circular histogram of DR5 distribution around the bud. (H) Circular histogram of TCS distribution around the bud. Sample size for (E-H): WT mock day 3, n = 10 buds; WT CHX day 3, n = 12 buds.

**(I-L)** 6 days of TOR or translation inhibition causes increased and diffuse cytokinin signaling, and randomly positioned auxin signaling maxima. (I) Representative images of late stage 2 buds from dissected and cultured WT inflorescences treated with mock, 2 µM CHX, or 2 µM AZD for 6 days. Shown are *DR5::3xVENUS-N7* in yellow, *TCS::GFP* in cyan, and both merged with Chlorophyll in magenta. Arrowheads point to randomly positioned auxin maxima in buds of the CHX or AZD group. (J) Quantification of TCS intensity from maximum intensity projection images, normalized to mean of WT mock day 6. Shown are mean ± SD. Asterisks show statistically significant differences from mock in two-tailed Student's t-tests (CHX, $p = 1.0 \times 10^{-3}$; AZD, $p = 1.2 \times 10^{-4}$). (K) Circular histogram of DR5 distribution around the bud. (L) Circular histogram of TCS distribution around the bud. Sample size for (I-L): WT mock day 6, n = 12 buds; WT CHX day 6, n = 11 buds; WT AZD day 6, n = 10 buds. Scale bars in (A,E,I) represent 25 µm.

**Figure 5. Cytokinin signaling is required for variability in auxin signaling and sepal initiation under translation inhibition.**

**(A-D)** Cytokinin treatment makes auxin signaling diffuse. Shown are late stage 2 WT buds under mock (A,B) or 5 µM cytokinin (BAP) treatment (C,D) for 4 days. (A,C) Representative images of the auxin signaling reporter *DR5::3xVENUS-N7* in yellow, and *DR5* merged with Chlorophyll in magenta. (B,D) Circular histograms of the *DR5::3xVENUS-N7* signal, showing mean (solid line) and mean ± SD (shaded area). Arrows point to DR5 signal in variable positions. Sample size: WT Mock n = 10, WT BAP n = 10. Also see Zhu et al. (2020), Extended Data Figure 7e.

**(E-G)** Cytokinin signaling is required for variable sepal initiation in *drmy1*. (E) Representative images of stage 5 buds in WT, *drmy1*, *arr1,10,12*, *drmy1 arr1,10,12*, *wol*, and *drmy1 wol*. Arrowheads indicate initiated sepal primordia that are variable in number, position, and size. (F,G) Quantification of sepal primordium number (F) and positional variability (G), comparing WT (n = 58) with *drmy1* (n = 31), *arr1,10,12* (n = 24) with *drmy1 arr1,10,12* (n = 20), and *wol* (n = 36) with *drmy1 wol* (n = 39). Asterisks indicate statistically significant ($p < 0.05$) differences in Fisher's contingency table tests (F) and Wilcoxon's rank sum tests (G) respectively. ns indicates no significant difference.

**(H-K)** Cytokinin signaling is required for variable patterning of auxin signaling in *drmy1*. Shown are late stage 2 buds of WT vs *drmy1* (H,I), and *arr1,10,12* vs *drmy1 arr1,10,12* (J,K). (H,J) Representative images of the auxin signaling reporter *DR5::3xVENUS-N7* in yellow, and *DR5* merged with propidium iodide in magenta. Arrows point to diffuse DR5 signal in variable positions in the *drmy1* bud. Arrowheads show four robust DR5 maxima in *drmy1 arr1,10,12*. (I,K) Circular histograms of the *DR5::3xVENUS-N7* signal, showing mean (solid line) and mean ± SD (shaded area). For ease of visualization, circular histograms of *drmy1* and *drmy1 arr1,10,12* between 90 and 360 degrees are enlarged and shown as insets (y-axis range 0-0.4). Sample size: WT n = 19, *drmy1* n = 16, *arr1,10,12* n = 13, *drmy1 arr1,10,12* n = 9.

**(L-N)** Cytokinin signaling is required for variable sepal initiation under translation inhibition. (L) Representative images of stage 6 buds in WT, *arr1,10,12*, and *wol*, treated with Mock or 2 µM CHX for 10 days. Arrowheads indicate variable initiation of sepal primordia. (M,N) Quantification of sepal primordium number (M) and positional variability (N), comparing Mock and CHX within each genotype. Sample size: WT Mock n = 29, WT CHX n = 19, *arr1,10,12* Mock n = 18, *arr1,10,12* CHX n = 19, *wol* Mock n = 15, *wol* CHX n = 19. Asterisks indicate statistically significant ($p < 0.05$) differences in Fisher's contingency table tests (M) and Wilcoxon's rank sum tests (N) respectively. ns indicates no significant difference.

**(O-R)** Cytokinin signaling is required for diffuse auxin signaling under translation inhibition. Shown are late stage 2 buds of WT (O,P) and *arr1,10,12* (Q,R), treated with Mock or 2 µM CHX for 3 days. (O,Q) Representative images of the auxin signaling reporter *DR5::3xVENUS-N7* in yellow, and *DR5* merged with Chlorophyll in magenta. Arrows point to diffuse DR5 signal in variable positions in CHX-treated WT. Arrowheads show four robust DR5 maxima in CHX-treated *arr1,10,12*. (P,R) Circular histograms of the *DR5::3xVENUS-N7* signal, showing mean (solid line) and mean ± SD (shaded area). Sample size: WT Mock n = 17, WT CHX n = 18, *arr1,10,12* Mock n = 7, *arr1,10,12* CHX n = 7. Scale bars in (A,C,E,H,J,L,O,Q) represent 25 µm.

**Figure 6. Upregulation of cytokinin signaling is required to maintain translation and fitness in *drmy1*.**

**(A)** Puromycin labeling of WT seedlings with 4 h CHX pre-treatment (control), and three biological replicates each of WT and *arr1 35S::ARR1* seedlings with 4 h mock pre-treatment. All seedlings are 14 days old. RuBisCO large subunit in Ponceau S-stained membrane is shown as a loading control. Also see Karunadasa et al. (2020).

**(B,C)** Puromycin labeling of WT seedlings with 4 h CHX pre-treatment (control), and two biological replicates of WT, *drmy1*, *wol*, and *drmy1 wol* seedlings with 4 h mock pre-treatment. Seedlings are 8 days old in (B) and 14 days old in (C). RuBisCO large subunit in Ponceau S-stained membrane is shown as a loading control.

**(D)** Representative 14 days old seedling images of WT, *drmy1*, *wol*, and *drmy1 wol* used in (C). Notice that *drmy1 wol* is very small and pale. Scale bars, 5 mm.

**(E)** Representative aerial part images of 42 days old plants of WT, *drmy1*, *wol*, and *drmy1 wol*. Inset shows enlarged *drmy1 wol* plant; notice that it has a tiny rosette and inflorescence. Scale bars, 5 cm. See also Supplemental Figure 6F.

**(F)** Representative aerial part images of 74 days old plants of WT, *drmy1*, *arr1*,*10*,*12*, and *drmy1 arr1*,*10*,*12*. Inset shows enlarged *drmy1 arr1*,*10*,*12* plant; notice its pale leaves accumulating anthocyanin, and short inflorescence. Scale bars, 5 cm. See also Supplemental Figure 6E.

**(G)** Dissected siliques of *arr1,10,12* (left) and *drmy1 arr1,10,12* (right) showing developing seeds. Notice that while *arr1,10,12* occasionally have aborted seeds, all seeds in the *drmy1 arr1,10,12* silique were aborted. Scale bars, 0.2 mm.

**Figure 7. A-type ARR protein levels are sensitive to TOR and translation inhibition.**
**(A)** The hypothesis. A-type ARRs are rapidly synthesized and degraded to dampen cytokinin signaling. Translation inhibition causes inability to rapidly synthesize these proteins in response to cytokinin signaling, resulting in an upregulation of cytokinin signaling.
**(B)** Expression of A-type ARR genes in WT vs *drmy1* inflorescences (*ap1 cal AP1-GR*) measured in RNA-seq. Shown are the five A-type ARR genes with the highest expression, ranked by mean expression level in WT. Asterisk indicates statistically significant difference, while ns means no significant difference. P-values: ARR7, p = 0.807; ARR4, p = 0.611; ARR15, p = 0.532; ARR8, p = 0.0115; ARR9, p = 0.0416.
**(C)** A GFP-channel image of a stage 2 bud of GFP-nes (*pUBQ10::sfGFP-nes-UBQ3ter*). For this panel and (E-H), each image was brightened to reveal GFP distribution patterns. A square region taken from the image containing 5-10 cells is enlarged and shown on the top right. Within the enlargement, GFP intensity was quantified along the dotted line and plotted on the bottom right. X-axis, pixels (range 0-238). Y-axis, GFP intensity in gray value (smoothened by taking the average intensity of 11-pixel neighborhoods; range 90-210). Scale bars, 25 μm.
**(D)** Illustration of the Llama Tag system used in this study. Plants were co-transformed with *ARR7-llama* (*pARR7::ARR7-linker-llama-ARR7ter*) and *GFP-nes* (*pUBQ10::sfGFP-nes-UBQ3ter*). Without ARR7-llama, the GFP is localized in the cytosol. ARR7-llama is produced in the cytosol and translocates into the nucleus. When this happens, the Llama Tag capable of binding GFP drags GFP into the nucleus (note that from our observation it is excluded from the nucleolus). Therefore, at low ARR7-llama levels, GFP signal is mainly seen in the cytosol. At intermediate ARR7-llama levels, GFP is at comparable intensities between the cytosol and the nucleus, and no clear pattern can be seen. At high ARR7-llama levels, GFP is mainly seen in the nucleus.
**(E,F)** GFP channel images of stage 2 buds from two independent transgenic lines of *ARR7-llama GFP-nes*, 7-4 (E) and 7-6 (F), in WT (top) vs *drmy1* (bottom). Images are representative of n = 17 (line 7-4, WT), n = 40 (line 7-4, *drmy1*), n = 9 (line 7-6, WT), and n = 6 (line 7-6, *drmy1*) buds.
**(G)** GFP channel images of WT *ARR7-llama GFP-nes* buds treated with mock (top) or 2 μM CHX (bottom) for 24 hours. The mock image is representative of n = 20 buds (12 from line 7-4, 5 from line 7-6, and 3 from line 7-12). The CHX image is representative of n = 19 buds (11 from line 7-4, 5 from line 7-6, and 3 from line 7-12).
**(H)** GFP channel images of WT *ARR7-llama GFP-nes* buds treated with mock (top) or 2 μM AZD-8055 (bottom) for 72 hours. The mock image is representative of n = 13 buds (8 from line 7-4 and 5 from line 7-6). The AZD-8055 image is representative of n = 11 buds (8 from line 7-4 and 3 from line 7-6).
**(I-N)** *ARR7-llama* partially restores robustness in *drmy1* sepal primordia. (I-L) Representative stage 5 or 6 buds from WT (I), WT with the *ARR7-llama* and *GFP-nes* constructs (J), *drmy1* (K), and *drmy1* with these constructs (L). (M) Quantification of sepal primordium number. ns indicates no significance difference in a Fisher's exact test (WT vs *ARR7-llama*, p = 1; *drmy1* vs *drmy1 ARR7-llama*, p = 0.44). (N) Quantification of variability in sepal primordium position. Asterisk indicates statistically significant difference ($p = 5.7 \times 10^{-6}$), while ns indicates no statistically significant difference (p = 0.91). Data for WT and *drmy1* were reused from Figure 2H, 2J. Data for *ARR7-llama GFP-nes* and *drmy1 ARR7-llama GFP-nes* were pooled from line 7-4 and 7-6.

928 Sample size: WT n = 51, *ARR7-llama GFP-nes* n = 16, *drmy1* n = 67, *drmy1 ARR7-llama GFP-*
929 *nes* n = 20. Scale bars, 25 μm.
930 **(O)** Working model. In WT, DRMY1 maintains TOR activity and translation, which sustains the
931 rapid translation of A-type ARRs in response to cytokinin signaling. This suppresses excessive
932 cytokinin signaling, allowing auxin and cytokinin signaling to interact and form robust spatial
933 patterns. Robust patterning of auxin and cytokinin signaling gives rise to robustly numbered,
934 positioned, and sized sepal primordia. In *drmy1*, A-type ARR protein levels are reduced due to
935 insufficient TOR activity, ribosome content, and translation rate. Cytokinin signaling is
936 upregulated, which rescues the translation rate reduction in a homeostatic mechanism. This
937 upregulation of cytokinin signaling disrupts the robust spatial pattern of both cytokinin and auxin
938 signaling, which in turn causes variable sepal initiation.
939

## MATERIALS AND METHODS

### Plant material

Most Arabidopsis plants were in Col-0 background (WT). *ap1 cal 35S::AP1-GR* was in Ler background. *drmy1* (Col-0) was backcrossed to Ler twice and then crossed with *ap1 cal 35S::AP1-GR* to obtain *drmy1 ap1 cal 35S::AP1-GR*. R2D2 was originally in Col-Utrecht background and was backcrossed twice into WT (Col-0) and *drmy1* (Col-0). The following mutants and reporters were previously described: *drmy1-2*[26], *wol-1*[127], *spaghetti-1* (*tpr5-1*)[128], *ap1 cal 35S::AP1-GR* (Ler)[35,36], *arr1-1 35S::ARR1*[67], *DR5::3xVENUS-N7*[129], *TCS::GFP*[130], *pARF5::ER-EYFP-HDEL*[131], *pUS7Y-mDII-NtdTomato-pUS7Y-DII-N3xVENUS* (R2D2)[97], *35S::mCirtine-RCI2A*[26], *UBQ10::mCherry-RCI2A*[26]. The following mutants and reporter lines were obtained from Arabidopsis Biological Resource Center (ABRC): *ul4z* (SALK_130595), *ul4y* (SALK_029203), *ul18z* (SALK_089798), *arr1-3 arr10-5 arr12-1*[132] (CS39992), *lst8-1-1* (SALK_002459), *pARF3::N3xGFP*[133] (CS67072), *pARF6::N3xGFP*[133] (CS67078), *pARF8::N3xGFP*[133] (CS67082), *pARF10::N3xGFP*[133] (CS67086).

### Llama-tagged ARR7 construct

For the LlamaTag system, we first generated plasmid *pVV13* containing linker-llama. We amplified the LlamaTag (from a plasmid containing vhhGFP4[134]) and added a linker sequence of tccggagcagctgcggctgccgctgcggcagcggccactagt at its 5' end by two rounds of overlap PCRs. Primers for the first round were oVV64 and oVV53, and primers for the second round were oVV35 and oVV53. After the second round, we A-tailed the PCR product according to the Promega manufacturer's protocol. A-tailed product was ligated to the pGEMTeasy vector according to the Promega ligation protocol, to create the plasmid *pVV13*.

To make *pARR7::ARR7-llama*, a genomic fragment of *pARR7::ARR7* minus the stop codon and terminator was amplified from the Arabidopsis (Col-0) genome using the primers oSK197 and oSK198. The linker-llama fragment was PCR-amplified from *pVV13* using the primers oSK199 and oSK200. The *ARR7* stop codon, 3' UTR, and terminator was amplified from the Arabidopsis (Col-0) genome using the primers oSK201 and oSK202. *pMLBART* backbone was digested with NotI, and all fragments were assembled into *pMLBART* using NEBuilder according to the manufacturer's protocol.

To make *pUBQ10::sfGFP-NES:UBQ3ter*, sfGFP sequence was amplified from the *35S-sfGFP-nosT* plasmid[135] (Addgene # 80129) using primers UsfGM-F1 and UsfGnes-R1. The UBQ10 promoter was amplified from the *UPG* plasmid[136] (Addgene # 161003) using primers OutALFd and UsfGM-R1. The UBQ3 terminator was amplified from the *UPG* plasmid[136] (Addgene # 161003) using primers UsfGnes-F1 and OutALRb. Primer overhangs spanning the junction between sfGFP and the UBQ3 terminator contain the sequence of the mouse PKIα NES. *pCambia1300* backbone was digested with BamHI and KpnI, and all fragments were Gibson-assembled into the backbone. Sequences of primers, *pARR7::ARR7-llama*, and *pUBQ10::sfGFP-NES:UBQ3ter* can be found in Supplemental Dataset 5.

Col-0 plants were co-transformed with *pARR7::ARR7-llama* and *pUBQ10::sfGFP-NES:UBQ3ter*, and selected with Basta (for *pARR7::ARR7-llama*) + Hygromycin (for

*pUBQ10::sfGFP-NES:UBQ3ter*). Surviving T1 plants were screened for clear nuclear signal in the inflorescence, and 5 independent T1 plants were selected and crossed into *drmy1*. F2 plants from each line were again selected with Basta + Hygromycin and genotyped. One line showed co-segregation with the *DRMY1* locus. Two lines showed severe silencing in the F2 and could not be used. Two lines (7-4 and 7-6), though with minor silencing in F2, were used for imaging and image analysis. F3 plants of 7-4 and 7-6 had severe silencing, and therefore only F2 were imaged.

**Plant growth conditions**

For most experiments, seeds were sown in wetted Lamber Mix LM-111 soil and stratified at 4°C for 3-5 days. For experiments including *drmy1 wol* and *drmy1 arr1,10,12*, all seeds were sown onto ½ MS plates with 0.05% (w/v) MES, 1% (w/v) sucrose, 1.2% (w/v) agar, pH 5.7, and stratified at 4°C for a week. They were grown for 7-10 days before being transplanted to soil (for imaging of inflorescence or aerial part of the plant) or left on the plates until desired time of the experiment (for seedling imaging or puromycin labeling).

Most plants were grown under 16 h – 8 h light-dark cycles (fluorescent light, ~100 µmol $m^{-1}$ $s^{-1}$) at 22°C in a Percival walk-in growth chamber. We found that the *drmy1* phenotype is more pronounced in this condition than under continuous light. The *ap1 cal 35S::AP1-GR* and *drmy1 ap1 cal 35S::AP1-GR* plants were grown in soil under continuous light at 16°C to prevent premature floral induction.

**Flower staging**

Flower buds were staged as previously described[37]. Briefly, stage 1 is when the floral meristem emerges, but not yet separated, from the inflorescence meristem. Stage 2 is when the floral meristem separates from the inflorescence meristem but with no floral organs initiated. Stage 3 is when sepal primordia initiate. Stage 4 is when sepal primordia bend to cover part of the floral meristem. Stage 5 is when stamen primordia initiate. Stage 6 is when sepal primordia completely cover the floral meristem.

**RNA-seq data collection and analysis**

For RNA-seq in the inflorescence, bolting *ap1 cal 35S::AP1-GR* and *drmy1 ap1 cal 35S::AP1-GR* plants were induced daily with an aqueous solution containing 10 µM dexamethasone (Sigma-Aldrich), 0.01% (v/v) ethanol, and 0.015% (v/v) Silwet L-77 (Rosecare.com). When sepals initiated from the floral meristems, usually on the fourth day after three daily inductions, three inflorescence samples per genotype (including inflorescence meristems and buds under stage 6) were collected and immediately put into liquid nitrogen. RNA extraction, library preparation, RNA-seq, and data analysis for inflorescence samples were done as previously described[26] with a few changes. After read mapping, genes with at least two raw reads in at least two biological replicates in either WT or *drmy1* were kept for downstream analysis. For differentially expressed genes, we set a log2 fold change threshold of ±1 and a BH-adjusted p-value threshold of 0.05. For GO term enrichment, gene-GO mapping data was obtained from TAIR (https://www.arabidopsis.org /download_files/GO_and_PO_Annotations/Gene_Ontology_Annotations/ATH_GO_GOSLIM.txt)

. The R package "topGO"[137] (version 2.38.1) was used for the enrichment, with statistic "fisher", algorithm "weight01", annotation function "annFUN.gene2GO", and minimum node size 10. The results were ranked by their p-value, and the first 8 terms were plotted.

For RNA-seq in seedlings, WT and *drmy1* seedlings were grown to quiescence (7 days) in ½ MS liquid media as previously described[34]. After 7 days, the media was replaced with ½ MS liquid media containing 15 mM glucose and incubated for 24 hours to activate TOR. Seedlings were then incubated with or without AZD-8055 in addition to 15 mM glucose in ½ MS liquid media for 2 hours before collecting tissue. RNA was extracted from 100 mg pooled seedlings using the Spectrum Plant Total RNA Kit (Sigma). This RNA was used as a template for RNA-Seq library synthesis and sequencing, which was performed by Novogene. RNA-seq data for AZD-8055 treated WT and *drmy1* seedlings were preprocessed with fastp (v. 0.22.0) using default parameters. Preprocessed reads were then mapped to the TAIR10 reference genome using STAR (v. 2.7.10z_alpha_220314). Following alignment, BAM output files from STAR were used to generate feature counts for transcripts using subread-featureCounts (v. 2.0.3) and the Araport11 transcriptome. TPMs were generated using TPMCalculator (v. 0.0.3). Differential expression analysis was performed using feature count data and DESeq2 (v. 1.36.0).

A list of genes with uORFs based on gene models of the TAIR10 Arabidopsis genome assembly were downloaded from von Arnim et al.[62]. For each gene, within each genotype, protein-transcript ratio was calculated as the ratio between mean protein abundance and mean transcript TPM across all bio-reps in our proteomics and RNA-seq datasets, respectively. This was log2-transformed, and the difference between *drmy1* and WT was calculated. This was used as an indicator of translation rate difference between *drmy1* and WT, although we acknowledge that other factors such as protein stability may affect this number. This was plotted against the number of uORFs in each gene model (0, 1, or ≥ 2).

**Proteomics**

Five induced inflorescence samples of WT and *drmy1* in *ap1 cal AP1-GR* background were collected as described above. Samples were ground in liquid nitrogen. Total soluble proteins were extracted in ice-cold extraction buffer (50 mM PBS-HCl (pH 8.0) buffer with 150 mM NaCl, 2% NP-40, 1 mM PMSF, 1x Roche cOmplete protease inhibitor cocktail (Sigma 11697498001), and 1x Halt TM Phosphatase inhibitor cocktail (ThermoFisher 78420)) and filtered through Pierce™ Micro-Spin Columns (30 µm pore size; Thermo Scientific 89879). Extracts were RuBisCO-depleted using Seppro Bubisco Kit (Sigma SEP070-1KT), concentrated, denatured, reduced, cysteine blocked, trypsin-digested, and TMT 10-plex labeled. Then, mass spectrometry was done using an UltiMate 3000 RSLCnano / Orbitrap Fusion system (Thermo Scientific). Raw data was searched against the NCBI protein database using PD 2.3 (Thermo Scientific) with Sequest HT searching engine. Precursor-based protein identification and relative quantification was done using the standard processing workflow in PD 2.3, with an additional node of Minora Feature Detector. Proteins with at least 2 supporting peptides were kept for downstream analysis. For each protein, data was fit with an ANOVA model and a p-value was calculated. Proteins with a p-value < 0.05 were considered differentially accumulated in *drmy1*. GO term enrichment was done as above, using genes corresponding to the differentially accumulated proteins.

**Polysome extraction and profiling**

Three induced inflorescence samples of WT and *drmy1* in *ap1 cal AP1-GR* background were collected as described above, and polysomes were extracted as previously described[138]. Briefly, samples were ground in liquid nitrogen, mixed with an extraction buffer (0.2 M Tris pH 9.0, 0.2 M KCl, 0.025 M EGTA, 0.035 M $MgCl_2$, 1% (w/v) Brij-35, 1% (v/v) Triton X-100, 1% (v/v) Igepal CA-630, 1% (v/v) Tween-20, 1% (w/v) Sodium deoxycholate, 1% (v/v) Polyoxyethylene 10 tridecyl ether, 5 mM Dithiothreitol, 1 mM Phenylmethylsulfonyl fluoride, 100 µg/ml cycloheximide, 100 µg/ml chloramphenicol, 40 U/ml RNasin, 0.5 mg/ml Heparin), and let sit on ice for 10 min. Samples were centrifuged at 4°C 4,000 g for 5 min, supernatant was transferred to a new tube, centrifuged at 4°C 16,000 g for 15 min, and supernatant was filtered through Miracloth.

Polysome extracts were profiled as previously described[139]. Briefly, samples were loaded onto 15%-45% sucrose density gradients and centrifuged at 4°C 38,000 rpm in a SW41 rotor. Separated samples were fractionated at a rate of 0.375 mL/min in an Isco fractionation system, and absorbance at 254 nm was recorded.

**Puromycin labeling**

Puromycin labeling was done as previously described[39], with slight modifications.

In seedlings, when comparing WT and *drmy1*, in order to control for plant size, WT seedlings were grown for 8 days and *drmy1* seedlings were grown for 10 days (Figure 1E). When comparing WT, *drmy1*, *wol*, and *drmy1 wol*, we were unable to control for plant size because *drmy1 wol* seedlings were too small. We therefore controlled for plant age, and seedlings were grown to specified age (8 days for Figure 6B and 14 days for Figure 6C). Seedlings were harvested from plates and incubated with an incubation buffer (½ MS, 0.05% (w/v) MES, 1% (w/v) sucrose, 0.1% (v/v) Tween-20, 0.1% (v/v) DMSO, 1x Gamborg vitamin mix, pH 5.7), with or without 50 µM CHX, for 4 hours in an illuminated growth chamber. Then, the buffer was replaced with a fresh incubation buffer (which is same as above, but contains 50 µM puromycin (GoldBio P-600-100)), and incubation continued for another 45 min.

In inflorescences of WT and *drmy1* in *ap1 cal AP1-GR* background, inflorescences were DEX-induced as described above. Inflorescence samples were collected and put in an incubation buffer (½ MS, 1% (w/v) sucrose, 0.02% (v/v) Silwet L-77, 0.1% (v/v) DMSO, 50 µM puromycin, 1x Gamborg vitamin mix, pH 5.7), with or without 100 µM CHX. Samples were vacuum infiltrated for 15 minutes and then put on a rocking shaker in an illuminated growth chamber for 45 minutes.

In both cases, at the end of the incubation, samples were washed three times with water, blot dry, weighed, and frozen in liquid nitrogen. Soluble proteins were extracted as described above. Puromycin incorporated into the proteins were detected in a Western blot using a mouse-origin anti-puromycin monoclonal antibody (12D10, Sigma MABE343, lot # 3484967) and a goat-anti-mouse HRP-conjugated secondary antibody (Abcam ab6789, lot # 3436981). RuBisCO large subunit in Ponceau S-stained membrane was used as a loading control.

**TOR activity assay**

WT and *drmy1* seedlings were grown in a six-well plate containing ½ MS liquid media. After seven days, the media were replaced with half-strength MS liquid media plus 15 mM glucose and incubated for 24 hours. At least 120 quiescent seedlings per sample were collected and frozen in liquid nitrogen. Protein was then extracted from the plant tissue in 100 mM MOPS (pH 7.6), 100 mM NaCl, 5% SDS, 0.5% b-mercaptoethanol, 10% glycerin, 2 mM PMSF, and 1x PhosSTOP phosphatase inhibitor (Sigma). S6K-pT449 was detected by Western blot using a phosphospecific antibody (Abcam ab207399) and an HRP-conjugated goat anti-rabbit IgG secondary antibody (Jackson Immuno Research 111-035-003). Total S6K was detected using a custom monoclonal antibody described by Busche et al.[140]. Total protein visualized in Ponceau S-stained membrane was used as a loading control.

**Confocal microscopy**

Confocal imaging of reporter lines in the inflorescence were done as previously described[26]. Briefly, main inflorescences (not side branches) were cut and dissected with a Dumont tweezer (Electron Microscopy Sciences, style 5, no. 72701-D) to remove buds older than stage 9 or 10. The inflorescences were then inserted upright into a small petri dish (VWR, 60 x 15 mm) containing inflorescence culture medium (1/2 MS, 1% (w/v) sucrose, 1x Gamborg vitamin mixture, 0.1% (v/v) plant preservative mixture (Plant Cell Technology) 1% (w/v) agarose, pH 5.8), leaving most of the stem inside the medium and the buds outside. They were then further dissected to reveal stage 6 and younger buds, immersed with water, and imaged under a Zeiss710 upright confocal microscope with a 20x Plan-Apochromat water-dipping lens (1.0 NA). For live imaging experiments, inflorescence samples were put in a continuous-light growth chamber between time points. To prevent bacterial growth, samples were transferred onto fresh media every 2 to 3 days, and for live imaging experiments lasting longer than 6 days, once in the middle, plants were incubated with an aqueous solution of 100 µg/ml Carbenicillin (GoldBio, C-103-5, lot # 0129.091814A) for 30 minutes.

To visualize tissue morphology of inflorescence samples without a reporter, samples were stained for 5 minutes with an aqueous solution of 0.1 mg/ml propidium iodide (PI) and 0.1% (v/v) Tween-20, washed three times with water, and imaged.

The following laser and wavelength were used in confocal imaging. Chlorophyll, excitation 488 nm, emission 647-721 nm. PI, excitation 514 nm, emission 566-659 nm. mCherry, excitation 594 nm, emission 600-659 nm. tdTomato, excitation 561 nm, emission 566-595 nm. For EYFP/VENUS/mCitrine, in *35S::mCirtine-RCI2A*, excitation 514 nm, emission 519-580 nm; in *DR5::3xVENUS-N7*, excitation 514 nm, emission 519-569 nm; in *pARF5::ER-EYFP-HDEL*, excitation 514 nm, emission 519-550 nm; in *R2D2*, excitation 488 nm, emission 493-551 nm. For GFP/sfGFP, in *pARR7::ARR7-llama UBQ10::sfGFP-NES*, excitation 488 nm, emission 493-569 nm; in *pARF3::N3xGFP*, *pARF6::*N3xGFP, *pARF8::N3xGFP*, and *pARF10::N3xGFP*, excitation 488 nm, emission 493-564 nm; in *TCS::GFP*, excitation 488 nm, emission 493-513 nm.

**Visualization of tissue morphology**

For single-channel image stacks intended for the visualization of tissue morphology (*35S::mCitrine-RCI2A* or PI), stacks were 3D-rendered using the ZEN confocal software

(Processing -> 3D). Parameters were set to best visualize tissue morphology, typically, minimum 5-10, ramp 60-80, maximum 100. Buds were rotated to desired orientation, and screenshots were taken using the "Create Image" button. For fluorophores that are dimmer, less sharp, or have a noisy background (*UBQ10::mCherry-RCI2A* or Chlorophyll), stacks were converted from LSM to TIF using ImageJ[141,142], loaded into MorphoGraphX[143], and screenshots were taken using the built-in screenshot function in MorphoGraphX.

To aid visualizing tissue morphology and determine the timing of sepal initiation, each stack was fitted with a surface, and a Gaussian curvature heatmap was calculated from the surface (see below). We consider a sepal primordium as initiated when we see a dark red band of positive Gaussian curvature (primordium) separated from the center of the floral meristem by a dark blue band of negative Gaussian curvature (boundary)[26].

Gaussian curvature heatmaps were calculated as previously described[26], with slight modifications. Briefly, stacks underwent the following processes in MorphoGraphX: Gaussian blur (3 times; X/Y/Z sigma = 1 μm for the first 2 times, and 2 μm for the third time), edge detection (threshold = 2000-8000 depending on the brightness of the stack, multiplier = 2.0, adapt factor = 0.3, fill value = 30000), marching cube surface (cube size = 8 μm, threshold = 20000), subdivide mesh, smooth mesh (passes = 5), subdivide mesh, smooth mesh (passes = 5), project mesh curvature (type = Gaussian, neighborhood = 10 μm, autoscale = no, min curv = -0.0015, max curv = 0.0015). For ease of visualization, the lookup table "jet" was applied to the mesh.

**Quantification of sepal initiation robustness**

For sepal primordium number, screenshots were taken of stage 3-6 buds of indicated genotypes, in either ZEN or MorphoGraphX. The number of sepal primordia initiated were counted from these screenshots.

For variability in sepal primordium positioning, within each bud, an angular distance was measured between each pair of adjacent sepal primordia (with vertex at the center of the bud), using ImageJ. Note that the last pair was not measured – the angular distance was calculated as the sum of all other angular distances subtracted from 360°. A CV value (standard deviation divided by mean) was calculated from all the measured or calculated angular distances. Buds with sepal primordia evenly distributed around the bud periphery should have a small CV value, i.e. all angles are around 90° for four-sepal buds (or 72° for five-sepal buds, etc.). Buds whose sepal primordia distributed variably or randomly around the bud periphery will have widely varying angular distances between adjacent sepal primordia, and thus large CV values.

Relative sepal initiation timing was quantified as previously described[26]. Briefly, dissected inflorescence samples were live-imaged every 6 hours. A Gaussian curvature heatmap was generated for each sample at each time point and was used to determine the time point at which a sepal primordium initiates. A sepal primordium is considered initiated at time point Tn if it is absent at time point T(n-1) but becomes present at time point Tn. Within the same bud, we counted the number of time points between outer and inner sepal initiation, and between outer and lateral sepal initiation, and multiplied them by 6 hours to get the relative initiation timing of these sepals.

**Quantification of fluorescent reporters**

For *TCS::GFP*, *pARF3::N3xGFP*, *pARF5::ER-YFP-HDEL*, *pARF6::N3xGFP*, *pARF8::N3xGFP*, *pARF10::N3xGFP*, *pUS7Y::mDII-NtdTomato, pUS7Y::DII-N3xVENUS*, and *UBQ10::mCherry-RCI2A*, total signal (integrated density) was quantified from maximum intensity projection images using ImageJ[141,142]. Fluorescence intensity was measured in pixel intensity units (0-255 range). Signal intensity was calculated as total signal divided by area.

For both *TCS::GFP* and *DR5:3xVENUS-N7*, circular histogram analysis was done as previously described[26]. Briefly, individual buds were cropped out of image stacks, channels were split using FIJI and saved in TIF format, and TIF stacks were imported into MorphoGraphX. Signal from outside the buds (e.g. inflorescence meristem, parts of other buds within the same image) was manually removed using the Voxel Edit function. Buds were positioned so that the incipient sepal primordia are in the XY plane: the incipient outer sepal is at 45°, the incipient inner sepal and the inflorescence meristem are at 225°, and the incipient lateral sepals are at 135° and 315°, respectively. Fluorescence intensity was measured in pixel intensity units (0-255 range). A circular histogram of bin width 1° centered around the Z axis was exported for each replicate expressing DR5 and/or TCS. Multiple circular histograms of the same reporter and genotype were pooled and mean ± SD were plotted.

For GFP signal in plants carrying *pUBQ10::sfGFP-nes-UBQ3ter* and *pARR7::ARR7-linker-llama-ARR7ter* reporters, screenshots were taken in MorphoGraphX as described above. Screenshots were subtracted of a background determined using blank regions with no tissue, and brightened to the same level to reveal differences in GFP distribution patterns. A square region containing 5-10 cells were taken from each screenshot, and GFP intensity (in gray value ranging from 0 to 255) along a straight line of 239 pixels in length was quantified using ImageJ[141,142] (Analyze -> Plot profile). For ease of visualization, the curves were smoothed by taking the average of the gray value of 11 neighboring pixels (including itself) as the value of each pixel.

***In vitro* drug treatments on inflorescence samples**

For cycloheximide (CHX) treatment, a stock solution of 10 mM CHX was made from powder (Sigma C1988) in pH 4.0 water. The stock solution was filter-sterilized and stored in -20°C and replaced every six months to prevent degradation. The stock solution was added to an autoclaved and cooled (but not solidified) inflorescence culture medium (see above) to a final concentration of 2 µM. The medium was not pH-buffered. The medium was made at the beginning of each experiment and was stored at 4°C. After each imaging session (at day 3 and day 6), new medium was taken out of 4°C, warmed to room temperature, and inflorescence samples were transferred onto the new medium.

For AZD-8055 treatment, a stock solution of 16 mM AZD-8055 was prepared from powder (Cayman Chemical 16978) in DMSO within days of use, and stored in -80°C. The stock was serial-diluted with water to 2 mM, and added to autoclaved and cooled (but not solidified) inflorescence culture medium (see above) to a final concentration of 2 µM. For the mock medium, DMSO was added to the inflorescence culture medium to a final concentration of 0.0125% (v/v).

For 6-benzylaminopurine (BAP) treatment, a stock solution of 50 mM BAP was prepared from powder (Alfa Aesar A14678) in DMSO, and stored in -80°C. The stock was added to an

autoclaved and cooled (but not solidified) inflorescence culture medium (see above) to a final concentration of 5 μM. For the mock medium, DMSO was added to the inflorescence culture medium to a final concentration of 0.01% (v/v).

Inflorescences were dissected and inserted into regular inflorescence culture medium without drugs, and pre-treatment image stacks were captured. Then, they were transferred into specified treatment or mock media, and imaged at the specified time points.

**_In vivo_ Torin2 treatment**

Starting at 14 days after germination, twice each day for 15 days, 2 nmol of Torin2 (Cayman Chemical 14185) in 20 μl of aqueous solution containing 0.5% DMSO and 0.5% Tween-20 was applied to the center of the rosette using a pipette. For mock, 20 μl aqueous solution containing 0.5% DMSO and 0.5% Tween-20 was applied. At the end of the 15-day treatment period, inflorescences were dissected and put in the inflorescence culture medium for imaging.

To prevent Torin2 degradation, throughout the duration of this experiment, the Torin2 stock solution in DMSO was kept in -80°C and replaced each week, and the treatment and mock solutions were kept in 4°C and replaced each day.

**Imaging of whole plant, whole inflorescence, silique, and mature sepals**

For whole-plant imaging, aerial parts of the plants were removed from the pots, flattened, put on a dark cloth, and imaged with a cell phone (iPhone 12, iOS 16.2).

For whole-inflorescence imaging, inflorescences consisting of open flowers and unopened buds were removed from the plant and held with forceps. Images were taken under a Zeiss Stemi 2000-C Stereo Microscope with a cell phone (iPhone 12, iOS 16.2).

For silique imaging, siliques on inflorescences sufficiently distant from the shoot apex that were developed and started to ripen were picked with forceps, opened with a razor blade, and imaged under a Zeiss Stemi 2000-C Stereo Microscope with a cell phone (iPhone 12, iOS 16.2).

Mature sepal imaging was done as previously described[26,27]. Briefly, mature sepals from stage 15 flowers ($10^{th}$ to $25^{th}$ flower on the inflorescence) were dissected and sandwiched between two slides to flatten. Images were taken using a Canon Powershot A640 camera attached to a Zeiss Stemi 2000-C Stereo Microscope. Minor damages were manually fixed, and undesired objects such as pollen grains were manually removed from these images. Sepals with major damages were discarded. Then, a contour was extracted from each sepal using custom python scripts[27]. This gave us measurements such as length, width, area, etc. of each sepal. To measure between-flower variability of length, within each genotype and for each of outer, inner, and lateral positions, a CV (standard deviation divided by mean) of all sepals was calculated (for example, a CV of length of all outer sepals in WT). To determine statistical significance, genotypes were compared pairwise using permutation tests. To measure within-flower variability of length, a CV was calculated for all sepals within each flower (for example, a CV of length of outer, inner, and two lateral sepals in WT bud #10). For accurate calculation of CV, flowers with length data of at least four sepals were included in the analysis. To determine statistical significance, genotypes were compared pairwise using Wilcoxon rank sum tests.

**Cytokinin extraction and measurement**

Cytokinin extraction was based on a previously published protocol[144] with modifications. Briefly, five inflorescence samples of induced *ap1 cal 35S::AP1-GR*, and six inflorescence samples of induced *drmy1 ap1 cal 35S::AP1-GR* were collected as described above. Samples were ground in liquid nitrogen and twice extracted in methanol : water : formic acid (15:4:1). 200 pg of BAP per sample was added as an internal control. Extracts were centrifuged at 14,650 rpm in -4°C for 30 min, and supernatant was evaporated of methanol and reconstituted in 1% (v/v) acetic acid. Samples were passed through an Oasis MCX SPE column (Waters 186000252), washed with 1% acetic acid, washed with methanol, and eluted with 0.35 M ammonia in 70% methanol. Eluents were evaporated to complete dryness, reconstituted in 5% acetonitrile, and sent for LC-MS.

LC-MS was done as previously described[145], with modifications. Briefly, 1 µl of each sample was injected into a Thermo Fisher Scientific Vanquish Horizon UHPLC System coupled with a Thermo Q Exactive HF hybrid quadropole-orbitrap high-resolution mass spectrometer equipped with a HESI ion source. Samples were separated on a C18 ODS column (AQUITY UPLC BEH C18, 1.7 µm, 2.1 × 100 mm, Waters), at a flow rate of 0.3 ml/min, with linear gradients of solvent A (0.1% formic acid) and solvent B (0.1% formic acid in methanol) according to the following profile: 0 min, 99.0% A + 1.0% B; 4.0 min, 55.0% A + 45.0% B; 7 min, 30.0% A + 70.0% B; and then with isocratic conditions: 8 min, 1.0% A + 99.0% B; 12 min, 99.0% A + 1.0% B. Cytokinins were detected using the positive ion mode.

For tZ, tZR, iP, iPR, and the internal control BAP, peaks were identified from an external standard mix composed of 0.1 µg/ml each of BAP (Alfa Aesar A14678), tZ (Sigma Z0876), tZR (Sigma Z3541), iP (Cayman Chemical 17906), and iPR (Cayman chemical 20522) in 5% acetonitrile. For cZ and cZR, peaks were identified based on previously reported precursor m/z and retention time[146]. Using Xcalibur (Thermo Scientific), peak area was quantified for each cytokinin in each sample, normalized against the peak area of BAP (internal control) and sample fresh weight, and then normalized against the average abundance of tZ in WT samples.

**Software**

Image processing was done in ImageJ (version 2.9.0/1.53t, build a33148d777)[141,142] and MorphoGraphX (version 2.0, revision 1-294, CUDA version 11.40)[143].

Data processing was done in RStudio (R version 4.0.5 “Shake and Throw” (2021-03-31))[147]. Graphs were made using the package ggplot2 (version 3.3.3)[148]. Fisher’s contingency table tests were done using the function fisher.test in R. Wilcoxon rank sum tests were done using the function wilcox.test in R. Hypergeometric tests were done using the function phyper in R. Data fitting with ANOVA was done using the function aov in R.

Figures were assembled in Adobe Illustrator (version 25.4.1). An RGB color profile “Image P3” was used for all the figures.

## SUPPLEMENTAL INFORMATION TITLES AND LEGENDS

**Supplemental Figure 1. Evidence that the *drmy1* mutant has ribosomal and translation defects, associated with Figure 1.**

**(A)** The *drmy1* phenotype is reproduced in the *ap1 cal AP1-GR* system (Ler background). Shown are representative buds of *ap1 cal AP1-GR* (top row) *and drmy1 ap1 cal AP1-GR* (bottom row) at day 0 (before DEX induction), day 3 (after 3 DEX inductions, when tissue is collected for RNA, protein, or cytokinin extraction), and day 5 (after 5 DEX inductions). Arrowheads show sepal primordia that are of variable number, position, and sizes. Asterisks indicate periphery of the floral meristem that has limited or no sepal outgrowth in *drmy1 ap1 cal AP1-GR* compared with *ap1 cal AP1-GR*. Scale bars, 25 μm.

**(B)** Summary of the inflorescence RNA-seq and proteomics datasets. Shown are numbers of genes in each category. Down, downregulated in *drmy1*; NS, not significantly changed between *drmy1* and WT; Up, upregulated in *drmy1*; NA, not available. Note that in the combined dataset (gene-protein pairs), different genes encoding for the same protein were separately counted, so were different proteins encoded by the same gene. See also Supplemental Dataset 1.

**(C)** Violin and box plots of log2 fold change in RNA between *drmy1* and WT in induced *ap1 cal AP1-GR* inflorescence, for genes encoding ribosomal components (“Structural constituents of the ribosome” GO:0003735, and its offspring terms) and all other genes involved in translation (“Translation” GO:0006412, and its offspring terms). The following genes are labeled on the graph: *UL4Z* (AT3G09630), log2FC = -0.492; *UL4Y* (AT5G02870), log2FC = -0.509; *UL18Z* (AT3G25520), log2FC = -0.459. Note that the x-axis was trimmed to (-2,2) for ease of display.

**(D)** Violin and box plots of log2 fold change in protein level between *drmy1* and WT in induced *ap1 cal AP1-GR* inflorescence, for genes in the same categories as in (C). The following genes are labeled on the graph: *UL4Z* (AT3G09630), log2FC = 0.352; *UL4Y* (AT5G02870), log2FC = 0.811; *UL18Z* (AT3G25520), log2FC = 0.742.

**(E)** Coherent regulation of gene expression by *drmy1* and AZD-8055. Shown is a contingency table of genes downregulated (Down), not significantly changed (NS), and upregulated (Up) in *drmy1* vs WT (columns), and in AZD-8055-treated WT vs mock-treated WT (rows). Bold font shows the number of genes in each category, and gray font shows the expected number of genes if there were no correlation between two conditions (calculated as row margin × column margin / total number of genes). Categories where the number of genes is above expectation are highlighted blue, and categories where the number of genes is below expectation are highlighted red. Chi-square test $p < 2.2 \times 10^{-16}$.

**(F)** Gene ontology enrichment of genes coherently downregulated by both *drmy1* and AZD-8055. Shown are the top 8 terms and their enrichment p-values. A complete list can be found in Supplementary Dataset 3.

**(G-J)** Fluorescence of a constitutively expressed marker supports the hypothesis that *drmy1* has reduced translation rate. (G-I) are representative confocal images of *UBQ10::mCherry-RCI2A* in dissected inflorescences of WT (G), *drmy1* (H), and *ul4y* (I). Numbers show how the signal is divided based on the stage of floral meristem when quantified (IM+1, inflorescence meristem plus stage 1; 2, stage 2; 3, stage 3). Scale bars, 25μm. (J) shows quantification of signal intensity (i.e.

integrated density divided by area) in all images divided as in (G-I). Mean ± SD are shown. Data was fit using a two-way ANOVA model with genotype and stage as two additive factors. Asterisks show statistically significant pairwise contrasts between WT and *drmy1* ($p < 2x10^{-16}$) and between WT and *ul4y* ($p = 2.1x10^{-15}$). Sample sizes: WT IM+1, n = 30; *drmy1* IM+1, n = 22; *ul4y* IM+1, n = 18; WT stage 2, n = 99; *drmy1* stage 2, n = 100; *ul4y* stage 2, n = 52; WT stage 3, n = 39; *drmy1* stage 3, n = 27; *ul4y* stage 3, n = 26.

**Supplemental Figure 2. Ribosomal mutations enhance the *drmy1* phenotype, associated with Figure 2.**

**(A-H)** Examples of stage 5 buds from *drmy1* (A), *drmy1 ul4z* (B-D), *drmy1 ul4y* (E-F), and *drmy1 ul18z/+* (G-H). In (B,E,G) sepal primordia within each bud have bigger size differences than typical *drmy1* single mutant buds; asterisks show giant outer sepal primordia and brackets show bud peripheral regions with little or no primordium outgrowth. In (C,F,H), arrowheads show 6 sepal primordia within each bud, which does not occur in *drmy1*. In (D,H), asterisks show the presence of two outer sepal primordia within a bud, instead of one in *drmy1*. Scale bars, 25μm.

**(I-J)** Quantification of sepal primordium number (I) and positional variability (J), comparing each of *drmy1 ul4z* (n = 60), *drmy1 ul4y* (n = 61), and *drmy1 ul18z/+* (n = 69) with *drmy1* (n = 67). “ns” indicates no significant difference in Fisher’s contingency table tests (I) and Wilcoxon’s rank sum tests (J) respectively. Data of *drmy1* is reproduced from the same dataset presented in Figure 2.

**(K)** Dissected young silique of *drmy1 ul18z/+* mother plant. Arrowheads point to aborted ovules. Scale bar, 200 μm.

**Supplemental Figure 3. Sepal primordia in ribosome and TOR mutants catch up in growth to form uniformly sized mature sepals within the bud, associated with Figure 3.**

**(A-F)** Representative inflorescences images (left) of WT (A), *drmy1* (B), *ul4z* (C), *ul4y* (D), *ul18z* (E), and *lst8-1-1* (F), with boxed regions enlarged (right). Blue arrowheads show sepals of regular length, and red arrowheads show sepals shorter than others. Note that sepals in *drmy1* were unable to close due to unequal lengths, while sepals in *ul4z*, *ul4y*, and *ul18z*, and close like in WT. Sepals in *lst8-1-1* were unable to close although there is no apparent variation in length. Scale bars, 0.5 mm.

**(G-L)** Dissected sepals from a representative bud of WT (G), *drmy1* (H), *ul4z* (I), *ul4y* (J), *ul18z* (K), and two buds of *lst8-1-1* (L). Note that sepals in the *drmy1* bud are of different sizes. Sepals within each bud of *ul4z*, *ul4y*, *ul18z*, and *lst8-1-1* are of similar sizes, although there can be variation between different buds of the same genotype. O, outer sepal. I, inner sepal. L, lateral sepal. Scale bars, 200 μm.

**(M)** Quantification of between-flower variability of sepal length. Length was measured from all imaged outer sepals of each genotype, and coefficient of variation (CV) was calculated. A two-sided permutation test (100,000 permutations) for CV difference not equating to zero was done for each pair of genotypes, and results were represented by letters (left). Similar analysis was done for the inner sepal (middle), and the lateral sepal (right). Sample size: Outer sepal, WT n = 35, *drmy1* n = 43, *ul4z* n = 37, *ul4y* n = 42, *ul18z* n = 39, *lst8-1-1* n = 43. Inner sepal, WT n = 34, *drmy1* n = 46, *ul4z* n = 38, *ul4y* n = 44, *ul18z* n = 37, *lst8-1-1* n = 44. Lateral sepal, WT n = 65, *drmy1* n = 84, *ul4z* n = 81, *ul4y* n = 89, *ul18z* n = 76, *lst8-1-1* n = 82.

**(N)** Quantification of within-flower variability of length. Flowers with length data from at least four sepals were analyzed. A CV of length from all sepals within each flower was calculated, and mean ± SD was plotted, grouped by genotype. A Wilcoxon rank sum test was done for each pair of genotypes, and results were represented by letters. Sample size: WT n = 31 buds, *drmy1* n = 38 buds, *ul4z* n = 33 buds, *ul4y* n = 36 buds, *ul18z* n = 32 buds, *lst8-1-1* n = 39 buds.

**(O-Q)** Live imaging of sepal development from stage 3 to 6 in a bud each of WT, *drmy1*, and *ul4y*, showing chlorophyll or propidium iodide channel, and Gaussian curvature calculated from the surface. Note that both *drmy1* and *ul4y* have inner sepals that initiate late (day 2, asterisk). The *drmy1* inner sepal develops slowly, and leaves the bud open at day 3 (red arrowhead). The *ul4y* inner sepal catches up with the rest of the sepals and closes the bud (blue arrowhead). Scale bars, 25 μm.

**Supplemental Figure 4. Inhibition of TOR activity and translation causes auxin maxima formation at variable positions, correlated with variable positions of sepal primordia, associated with Figure 4.**

**(A-E)** Variable patterning of auxin signaling in *drmy1*, *ul4y*, and CHX-treated WT buds corresponds to variable sepal initiation. Shown are a representative bud each of the labeled genotype or treatment live-imaged over three or four days. In all but the last time point, in the top row is *DR5::3xVENUS-N7* (yellow), in the middle row is a composite of *DR5::3xVENUS-N7* (yellow) and Chlorophyll (magenta), and in the bottom row is Gaussian curvature calculated from a surface extracted from the Chlorophyll channel. In the last time point, propidium iodide is shown on the top, and Gaussian curvature calculated from a surface extracted from the propidium iodide channel is shown on the bottom. (A) In WT, four robustly positioned auxin maxima at day 1 correlates with four robustly positioned sepal primordia at day 4 (blue arrowheads). (B) In *drmy1*, at day 1 there are three robustly positioned auxin maxima (blue arrowheads). At day 2, a diffuse band of auxin signaling occurs in the adaxial periphery of the bud, joining with one of the lateral auxin maxima (red bracket). At day 3, this diffuse band splits into three auxin maxima (red arrowheads), making a total of 5. The maxima correlate with the five sepal primordia at day 4, three at robust positions (blue arrowheads) and two at irregular positions (red arrowheads). (C) In *ul4y*, at day 1 there are two auxin maxima at robust positions (blue arrowheads), one at robust lateral position but much weaker (red arrowhead), and a band of weak auxin signaling in the adaxial periphery of the bud (red bracket). At day 2, the weak auxin maxima at lateral position got stronger, and the weak band split into two auxin maxima on the adaxial side (red arrowheads). These five auxin maxima correspond to the five sepal primordia at day 3, three in robust positions (blue arrowheads) and two in irregular positions (red arrowheads). (D) In the WT bud treated with Mock, four robust auxin maxima at day 6 of the treatment corresponds to four robust sepal primordia seen at day 9 (blue arrowheads). (E) In the WT bud treated with CHX, at day 6 there are three stronger auxin maxima (blue arrowheads) and two weaker ones (red arrowheads), corresponding to three bigger primordium outgrowth regions (blue arrowheads) and two smaller ones (red arrowheads) at day 9. For ease of display, the DR5 channel in CHX-treated WT was brightened three times relative to mock. Scale bars, 25 μm.

**(F-I)** TOR inhibition using Torin2 causes increased cytokinin signaling, and occasional variability in both auxin and cytokinin signaling. (F) Representative images of late stage 2 buds from WT plants treated with mock or 2 nmol Torin2 for 15 days. Shown are *DR5::3xVENUS-N7* in yellow, *TCS::GFP* in cyan, and both merged with propidium iodide in magenta. Note that 3/16 (19%) buds had variable number and position of DR5 and TCS maxima, and 13/16 (81%) had robust DR5 and TCS maxima, although TCS intensity is higher in both cases compared with mock-treated buds. Scale bars, 25 μm. (G) Quantification of TCS intensity from maximum intensity projection images, normalized to the mean of WT mock. Shown are mean ± SD. Asterisk shows statistical significance in a two-tailed Student's t-test compared with WT mock ($p = 1.2x10^{-4}$). (H) Circular histograms of DR5 distribution around the bud (mean ± SD). (I) Circular histograms of TCS distribution around the bud (mean ± SD). For calculation of circular histograms, please see Figure 4 legends and Materials and Methods. Sample size: WT mock, n = 11 buds; WT Torin2, n = 16 buds.

**Supplemental Figure 5. Translation of uORF-containing ARFs is not universally downregulated in *drmy1*, associated with Figure 5.**

**(A)** *drmy1* has a lower protein-transcript ratio than WT for genes with at least 2 uORFs. 5,086 transcript-protein pairs in our dataset were grouped according to the maximum number of uORFs in all transcript isoforms (0, n = 3,485; 1, n = 874; ≥ 2, n = 724)[62]. For each pair, protein-transcript ratio was calculated, log-transformed, and the difference between *drmy1* and WT was plotted. A negative value means this gene has less protein per transcript in *drmy1* than WT, and could indicate reduced translation or protein stability. Medians for each group: 0 uORF, -0.00367; 1 uORF, -0.00808; ≥ 2 uORFs, -0.0243. Asterisk show statistically significant difference from Group 0 in a Wilcoxon rank sum test ($p = 3.167 \times 10^{-4}$), while ns means no significant difference from Group 0 ($p = 0.167$).

**(B-D)** There is no universal decrease in the expression of uORF-containing ARF reporters. (B) Transcript level of three activator *ARF*s (*ARF5*, *ARF6*, *ARF8*) and two repressor *ARF*s (*ARF3*, *ARF10*) in RNA-seq (n = 3 per genotype). Note that *ARF3*, *ARF5*, and *ARF6* contain uORFs before the main ORF, and *ARF8* and *ARF10* do not. Asterisks show statistically significant differences between WT and *drmy1*, and ns means no significance difference. p values: *ARF3*, p = 0.583; *ARF5*, p = 0.497; *ARF6*, p = 0.603; *ARF8*, p = 0.058; *ARF10* p = 0.019. (C) Transcriptional reporters for these ARFs (*pARF3::n3xGFP*, *pARF5::erYFP*, *pARF6::n3xGFP*, *pARF8::n3xGFP* and *pARF10::n3xGFP*) were imaged in WT and *drmy1*, and representative late stage 2 buds were shown (cyan, GFP or YFP; magenta, propidium iodide). Note that the *pARF3*, *pARF5*, and *pARF6* reporters contain the same uORFs as the genes, reflecting a combination of transcriptional and uORF regulations. Scale bars, 20 μm. (D) Quantification of GFP intensity. Sample size: *pARF3* WT, n = 22; *pARF3 drmy1*, n = 25; *pARF5* WT, n = 22; *pARF5 drmy1*, n = 22; *pARF6* WT, n = 19; *pARF6 drmy1*, n = 28; *pARF8* WT, n = 25; *pARF8 drmy1*, n = 31; *pARF10* WT, n = 20; *pARF10 drmy1*, n = 29. Asterisks show statistically significant differences between WT and *drmy1* in Wilcoxon rank sum tests, and ns means no significance difference. p values: *pARF3*, p = 0.3797; *pARF5*, $p = 6.22 \times 10^{-5}$; *pARF6*, $p = 2.868 \times 10^{-13}$; *pARF8*, p = 0.5127; *pARF10* $p = 7.073 \times 10^{-14}$.

**Supplemental Figure 6. Cytokinin signaling causes variability in mature sepal number and size in *drmy1*, associated with Figure 5.**

Shown are top-view inflorescence images of WT (A), *arr1,10,12* (B), *wol* (C), *drmy1* (D), *drmy1 arr1,10,12* (E), and *drmy1 wol* (F), with boxed areas of individual buds enlarged and shown on the right. In the enlarged views, blue arrowheads point to sepals of regular size, and red arrowheads point to sepals that are much smaller. Scale bars, 0.5 mm.

**Supplemental Figure 7. ARR7-llama partially restores robustness in mature sepal number and size, associated with Figure 7.**

**(A)** Cytokinin abundance does not significantly change in *drmy1*. Shown is mean ± SD of levels of trans-zeatin (tZ), cis-Zeatin (cZ), $N^6$-($\Delta^2$-Isopentenyl)adenine (iP), trans-Zeatin riboside (tZR), cis-Zeatin riboside (cZR), and $N^6$-($\Delta^2$-Isopentenyl)adenosine (iPR) quantified by LC-MS in induced WT and *drmy1* inflorescences of *ap1 cal AP1-GR* background. Levels are normalized to the mean tZ level in WT. Sample size: n = 5 for WT; n = 6 for *drmy1*. ns means no significant difference between WT and *drmy1* in a two-sided Wilcoxon rank sum test. P-values: tZ, p = 0.2468; cZ, p = 0.7922; iP, p = 0.2468; tZR, p = 0.1775; cZR, p = 0.6623; iPR, p = 0.6623.

**(B)** The *ARR7-llama* reporter responds to externally applied cytokinin. Shown are GFP channel images of stage 2 buds from *ARR7-llama GFP-nes* line 7-4 in WT, before (top) or after (bottom) 5 hours of 200 μM BAP treatment. Images are representative of n = 6 buds from line 7-4 and n = 3 buds from line 7-6.

**(C)** CHX treatment does not change the localization of GFP-nes. Shown are GFP channel images of stage 2 buds from *GFP-nes* in WT, treated with mock (top) or 2 μM CHX (bottom) for 24 hours. Images are representative of n = 10 buds (mock) and n = 9 buds (CHX).

**(D)** AZD-8055 treatment does not change the localization of GFP-nes. Shown are GFP channel images of stage 2 buds from *GFP-nes* in WT, treated with mock (top) or 2 μM AZD-8055 (bottom) for 72 hours. Images are representative of n = 10 buds (mock) and n = 11 buds (AZD-8055). For (B-D), each image was brightened to reveal patterns of GFP distribution. A square region taken from the image containing 5-10 cells is enlarged and shown on the top right. Within the enlargement, GFP intensity was quantified along the dotted line and plotted on the bottom right. X-axis, pixels (range 0-238). Y-axis, GFP intensity in gray value (smoothened by taking the average intensity of 11-pixel neighborhoods; range 90-175). Scale bars, 25 μm.

**(E-H)** The ARR7-llama construct partially rescues the mature sepal variability in *drmy1*. Shown are inflorescence images of WT (E), *ARR7-llama GFP-nes* (F), *drmy1* (G), and *drmy1 ARR7-llama GFP-nes* (H). The boxed regions were enlarged and shown on the right of each panel. Note that while *drmy1* buds have normal-sized (blue arrowheads) and smaller (red arrowheads) sepals, some buds in *drmy1 ARR7-llama GFP-nes* have robustly sized sepals (H, middle) while others still show variability (H, right). Scale bars, 0.5 mm.

**(I-J)** *drmy1* has decreased and disrupted pattern of DII degradation. (I) Representative late stage 2 buds of WT and *drmy1* showing *DII-n3xVENUS* (cyan), *mDII-ntdTomato* (magenta), and merge. For ease of display, the *VENUS* channel was brightened 3 times relative to the *tdTomato* channel. Scale bars, 25 μm. (J) Quantification of VENUS/tdTomato ratio using ImageJ. Note that a universal background of 6 gray value per pixel (determined in blank regions without tissue) were subtracted from each image before quantification. Sample size: WT, n = 8 buds; *drmy1*, n = 19 buds. Asterisk shows statistically significant difference in a Wilcoxon rank sum test (p = 0.01335).

**Supplemental Dataset 1. Inflorescence RNA-seq and proteomics.**

**Supplemental Dataset 2. Unprocessed ribosome profiles.**

**Supplemental Dataset 3. Seedling RNA-seq.**

**Supplemental Dataset 4. Data used in graphs.**

**Supplemental Dataset 5. DNA sequences.**

## REFERENCES


1. Kaneko, K. (2007). Evolution of robustness to noise and mutation in gene expression dynamics. PLoS One *2*, e434. 10.1371/journal.pone.0000434.
2. Lachowiec, J., Queitsch, C., and Kliebenstein, D.J. (2016). Molecular mechanisms governing differential robustness of development and environmental responses in plants. Ann. Bot. *117*, 795–809. 10.1093/aob/mcv151.
3. Waddington, C.H. (1942). Canalization of Development and the Inheritance of Acquired Characters. Nature *150*, 563–656.
4. Zabinsky, R.A., Mason, G.A., Queitsch, C., and Jarosz, D.F. (2019). It's not magic – Hsp90 and its effects on genetic and epigenetic variation. Semin. Cell Dev. Biol. *88*, 21–35. 10.1016/j.semcdb.2018.05.015.
5. Twitty, V.C., and Schwind, J.L. (1931). The growth of eyes and limbs transplanted heteroplastically between two species of <i>Amblystoma. J. Exp. Zool. *59*, 61–86. 10.1002/jez.1400590105.
6. Silber, S.J. (1976). Growth of Baby Kidneys Transplanted Into Adults. Arch. Surg. *111*, 75–77. 10.1001/archsurg.1976.01360190077014.
7. Summerbell, D., and Lewis, J.H. (1975). Time, place and positional value in the chick limb bud. J. Embryol. Exp. Morphol. *33*, 621–643. 10.1242/dev.33.3.621.
8. Parker, J., and Struhl, G. (2020). Control of *Drosophila* wing size by morphogen range and hormonal gating. Proc. Natl. Acad. Sci. U. S. A. *117*, 31935–31944. 10.1073/pnas.2018196117.
9. Garelli, A., Gontijo, A.M., Miguela, V., Caparros, E., and Dominguez, M. (2012). Imaginal discs secrete insulin-like peptide 8 to mediate plasticity of growth and maturation. Science *336*, 579–582. 10.1126/science.1216735.
10. Crickmore, M.A., and Mann, R.S. (2006). Hox control of organ size by regulation of morphogen production and mobility. Science *313*, 63–68. 10.1126/science.1128650.
11. Recasens-Alvarez, C., Ferreira, A., and Milán, M. (2017). JAK/STAT controls organ size and fate specification by regulating morphogen production and signalling. Nat. Commun. *8*, 10–12. 10.1038/ncomms13815.
12. Irish, V.F. (2008). The Arabidopsis petal: a model for plant organogenesis. Trends Plant Sci. *13*, 430–436. 10.1016/j.tplants.2008.05.006.
13. Fenster, C.B., Armbruster, W.S., Wilson, P., Dudash, M.R., and Thomson, J.D. (2004). Pollination syndromes and floral specialization. Annu. Rev. Ecol. Evol. Syst. *35*, 375–403. 10.1146/annurev.ecolsys.34.011802.132347.
14. King, S., Beck, F., and Lüttge, U. (2004). On the mystery of the golden angle in phyllotaxis. Plant, Cell Environ. *27*, 685–695. 10.1111/j.1365-3040.2004.01185.x.
15. Smith, R.S., Guyomarc'h, S., Mandel, T., Reinhardt, D., Kuhlemeier, C., and Prusinkiewicz, P. (2006). A plausible model of phyllotaxis. Proc. Natl. Acad. Sci. U. S. A. *103*, 1301–1306. 10.1073/pnas.0510457103.
16. Besnard, F., Refahi, Y., Morin, V., Marteaux, B., Brunoud, G., Chambrier, P., Rozier, F., Mirabet, V., Legrand, J., Lainé, S., et al. (2014). Cytokinin signalling inhibitory fields provide robustness to phyllotaxis. Nature *505*, 417–421. 10.1038/nature12791.
17. Queitsch, C., Sangster, T.A., and Lindquist, S. (2002). Hsp90 as a capacitor of phenotypic variation. Nature *417*, 618–624. 10.1038/nature749.
18. Rutherford, S.L., and Lindquist, S. (1998). Hsp90 as a capacitor for morphological evolution. Nature *396*, 336–342. 10.1038/24550.
19. Lehner, B., Crombie, C., Tischler, J., Fortunato, A., and Fraser, A.G. (2006). Systematic mapping of genetic interactions in *Caenorhabditis elegans* identifies common modifiers of diverse signaling pathways. Nat. Genet. *38*, 896–903. 10.1038/ng1844.
20. Levy, S.F., and Siegal, M.L. (2008). Network hubs buffer environmental variation in

*Saccharomyces cerevisiae*. PLoS Biol. *6*, 2588–2604. 10.1371/journal.pbio.0060264.

21. Folta, A., Severing, E.I., Krauskopf, J., van de Geest, H., Verver, J., Nap, J.P., and Mlynarova, L. (2014). Over-expression of Arabidopsis AtCHR23 chromatin remodeling ATPase results in increased variability of growth and gene expression. BMC Plant Biol. *14*, 76. 10.1186/1471-2229-14-76.
22. Marygold, S.J., Roote, J., Reuter, G., Lambertsson, A., Ashburner, M., Millburn, G.H., Harrison, P.M., Yu, Z., Kenmochi, N., Kaufman, T.C., et al. (2007). The ribosomal protein genes and Minute loci of *Drosophila melanogaster*. Genome Biol. *8*, R216. 10.1186/gb-2007-8-10-r216.
23. Hintze, M., Katsanos, D., Shahrezaei, V., and Barkoulas, M. (2021). Phenotypic Robustness of Epidermal Stem Cell Number in C. elegans Is Modulated by the Activity of the Conserved N-acetyltransferase nath-10/NAT10. Front. Cell Dev. Biol. *9*, 640856. 10.3389/fcell.2021.640856.
24. Wang, S., Kurepa, J., and Smalle, J.A. (2009). The *Arabidopsis* 26S proteasome subunit RPN1a is required for optimal plant growth and stress responses. Plant Cell Physiol. *50*, 1721–1725. 10.1093/pcp/pcp105.
25. Gallois, J.L., Guyon-Debast, A., Lecureuil, A., Vezon, D., Carpentier, V., Bonhomme, S., and Guerche, P. (2009). The *Arabidopsis* proteasome RPT5 subunits are essential for gametophyte development and show accession-dependent redundancy. Plant Cell *21*, 442–459. 10.1105/tpc.108.062372.
26. Zhu, M., Chen, W., Mirabet, V., Hong, L., Bovio, S., Strauss, S., Schwarz, E.M., Tsugawa, S., Wang, Z., Smith, R.S., et al. (2020). Robust organ size requires robust timing of initiation orchestrated by focused auxin and cytokinin signalling. Nat. Plants *6*, 686–698. 10.1038/s41477-020-0666-7.
27. Hong, L., Dumond, M., Tsugawa, S., Sapala, A., Routier-Kierzkowska, A.L., Zhou, Y., Chen, C., Kiss, A., Zhu, M., Hamant, O., et al. (2016). Variable Cell Growth Yields Reproducible Organ Development through Spatiotemporal Averaging. Dev. Cell *38*, 15–32. 10.1016/j.devcel.2016.06.016.
28. Roeder, A.H.K. (2021). Arabidopsis sepals: A model system for the emergent process of morphogenesis. Quant. Plant Biol. *2*. 10.1017/qpb.2021.12.
29. Trinh, D.-C., Martin, M., Bald, L., Maizel, A., Trehin, C., and Hamant, O. (2022). Paf1C denoises transcription and growth patterns to achieve organ shape reproducibility. bioRxiv, 2022.03.25.485770.
30. Jing, H., and Strader, L.C. (2019). Interplay of auxin and cytokinin in lateral root development. Int. J. Mol. Sci. *20*, 486. 10.3390/ijms20030486.
31. Hussain, S., Nanda, S., Zhang, J., Rehmani, M.I.A., Suleman, M., Li, G., and Hou, H. (2021). Auxin and Cytokinin Interplay during Leaf Morphogenesis and Phyllotaxy. Plants *10*, 1732. 10.3390/plants10081732.
32. Schaller, G.E., Bishopp, A., and Kieber, J.J. (2015). The yin-yang of hormones: Cytokinin and auxin interactions in plant development. Plant Cell *27*, 44–63. 10.1105/tpc.114.133595.
33. Ingargiola, C., Duarte, G.T., Robaglia, C., Leprince, A.S., and Meyer, C. (2020). The plant target of rapamycin: A conduc TOR of nutrition and metabolism in photosynthetic organisms. Genes (Basel). *11*, 1285. 10.3390/genes11111285.
34. Scarpin, M.R., Leiboff, S., and Brunkard, J.O. (2020). Parallel global profiling of plant tor dynamics reveals a conserved role for LARP1 in translation. eLife *9*, e58795. 10.7554/eLife.58795.
35. Yu, H., Ito, T., Wellmer, F., and Meyerowitz, E.M. (2004). Repression of AGAMOUS-LIKE 24 is a crucial step in promoting flower development. Nat. Genet. *36*, 157–161. 10.1038/ng1286.
36. Wellmer, F., Alves-Ferreira, M., Dubois, A., Riechmann, J.L., and Meyerowitz, E.M.

(2006). Genome-wide analysis of gene expression during early *Arabidopsis* flower development. PLoS Genet. *2*, 1012–1024. 10.1371/journal.pgen.0020117.

37. Smyth, D.R., Bowman, J.L., and Meyerowitz, E.M. (1990). Early flower development in Arabidopsis. Plant Cell *2*, 755–767. 10.1105/tpc.2.8.755.
38. Goodman, C.A., and Hornberger, T.A. (2013). Measuring protein synthesis with SUnSET: A valid alternative to traditional techniques? Exerc. Sport Sci. Rev. *41*, 107–115. 10.1097/JES.0b013e3182798a95.
39. Van Hoewyk, D. (2016). Use of the non-radioactive SUnSET method to detect decreased protein synthesis in proteasome inhibited Arabidopsis roots. Plant Methods *12*, 20. 10.1186/S13007-016-0120-Z.
40. Scarpin, M.R., Busche, M., Martinez, R.E., Harper, L.C., Reiser, L., Szakonyi, D., Merchante, C., Lan, T., Xiong, W., Mo, B., et al. (2023). An updated nomenclature for plant ribosomal protein genes. Plant Cell *35*, 640–643. 10.1093/plcell/koac333.
41. Schepetilnikov, M., and Ryabova, L.A. (2018). Recent discoveries on the role of tor (Target of rapamycin) signaling in translation in plants. Plant Physiol. *176*, 1095–1105. 10.1104/pp.17.01243.
42. Scarpin, M.R., Simmons, C.H., and Brunkard, J.O. (2022). Translating across kingdoms: target of rapamycin promotes protein synthesis through conserved and divergent pathways in plants. J. Exp. Bot. *73*, 7016–7025. 10.1093/jxb/erac267.
43. Brunkard, J.O. (2020). Exaptive Evolution of Target of Rapamycin Signaling in Multicellular Eukaryotes. Dev. Cell *54*, 142–155. 10.1016/j.devcel.2020.06.022.
44. Battaglioni, S., Benjamin, D., Wälchli, M., Maier, T., and Hall, M.N. (2022). mTOR substrate phosphorylation in growth control. Cell *185*, 1814–1836. 10.1016/j.cell.2022.04.013.
45. Valvezan, A.J., and Manning, B.D. (2019). Molecular logic of mTORC1 signalling as a metabolic rheostat. Nat. Metab. *1*, 321–333. 10.1038/s42255-019-0038-7.
46. Xiong, Y., McCormack, M., Li, L., Hall, Q., Xiang, C., and Sheen, J. (2013). Glucose-TOR signalling reprograms the transcriptome and activates meristems. Nature *496*, 181–186. 10.1038/nature12030.
47. Riegler, S., Servi, L., Scarpin, M.R., Godoy Herz, M.A., Kubaczka, M.G., Venhuizen, P., Meyer, C., Brunkard, J.O., Kalyna, M., Barta, A., et al. (2021). Light regulates alternative splicing outcomes via the TOR kinase pathway. Cell Rep. *36*, 109676. 10.1016/j.celrep.2021.109676.
48. Obomighie, I., Lapenas, K., Murphy, B.E., Bowles, A.M.C., Bechtold, U., and Prischi, F. (2021). The Role of Ribosomal Protein S6 Kinases in Plant Homeostasis. Front. Mol. Biosci. *8*, 636560. 10.3389/fmolb.2021.636560.
49. Xiong, Y., and Sheen, J. (2012). Rapamycin and glucose-target of rapamycin (TOR) protein signaling in plants. J. Biol. Chem. *287*, 2836–2842. 10.1074/jbc.M111.300749.
50. Moreau, M., Azzopardi, M., Clé ment, G., Dobrenel, T., Marchive, C., Renne, C., Martin-Magniette, M.L., Taconnat, L., Renou, J.P., Robaglia, C., et al. (2012). Mutations in the *Arabidopsis* homolog of LST8/GβL, a partner of the target of Rapamycin kinase, impair plant growth, flowering, and metabolic adaptation to long days. Plant Cell *24*, 463–481. 10.1105/tpc.111.091306.
51. Brunkard, J.O., Xu, M., Regina Scarpin, M., Chatterjee, S., Shemyakina, E.A., Goodman, H.M., and Zambryski, P. (2020). TOR dynamically regulates plant cell-cell transport. Proc. Natl. Acad. Sci. U. S. A. *117*, 5049–5058. 10.1073/pnas.1919196117.
52. Menand, B., Desnos, T., Nussaume, L., Bergert, F., Bouchez, D., Meyer, C., and Robaglia, C. (2002). Expression and disruption of the *Arabidopsis TOR* (target of rapamycin) gene. Proc. Natl. Acad. Sci. U. S. A. *99*, 6422–6427. 10.1073/pnas.092141899.
53. Zhao, Z., Andersen, S.U., Ljung, K., Dolezal, K., Miotk, A., Schultheiss, S.J., and

Lohmann, J.U. (2010). Hormonal control of the shoot stem-cell niche. Nature *465*, 1089–1092. 10.1038/nature09126.

54. Yoshida, S., Mandel, T., and Kuhlemeier, C. (2011). Stem cell activation by light guides plant organogenesis. Genes Dev. *25*, 1439–1450. 10.1101/gad.631211.
55. Du, F., Guan, C., and Jiao, Y. (2018). Molecular Mechanisms of Leaf Morphogenesis. Mol. Plant *11*, 1117–1134. 10.1016/j.molp.2018.06.006.
56. Taylor-Teeples, M., Lanctot, A., and Nemhauser, J.L. (2016). As above, so below: Auxin's role in lateral organ development. Dev. Biol. *419*, 156–164. 10.1016/j.ydbio.2016.03.020.
57. Rosado, A., Li, R., Van De Ven, W., Hsu, E., and Raikhel, N. V. (2012). *Arabidopsis* ribosomal proteins control developmental programs through translational regulation of auxin response factors. Proc. Natl. Acad. Sci. U. S. A. *109*, 19537–19544. 10.1073/pnas.1214774109.
58. Nishimura, T., Wada, T., Yamamoto, K.T., and Okada, K. (2005). The *Arabidopsis* STV1 protein, responsible for translation reinitiation, is required for auxin-mediated gynoecium patterning. Plant Cell *17*, 2940–2953. 10.1105/tpc.105.036533.
59. Zhou, F., Roy, B., and von Arnim, A.G. (2010). Translation reinitiation and development are compromised in similar ways by mutations in translation initiation factor eIF3h and the ribosomal protein RPL24. BMC Plant Biol. *10*, 193. 10.1186/1471-2229-10-193.
60. Cancé, C., Martin-Arevalillo, R., Boubekeur, K., and Dumas, R. (2022). Auxin response factors are keys to the many auxin doors. New Phytol. *235*, 402–419. 10.1111/nph.18159.
61. Kim, B.H., Cai, X., Vaughn, J.N., and Von Arnim, A.G. (2007). On the functions of the h subunit of eukaryotic initiation factor 3 in late stages of translation initiation. Genome Biol. *8*, R60. 10.1186/gb-2007-8-4-r60.
62. Von Arnim, A.G., Jia, Q., and Vaughn, J.N. (2014). Regulation of plant translation by upstream open reading frames. Plant Sci. *214*, 1–12. 10.1016/j.plantsci.2013.09.006.
63. Jones, B., Ljung, K., Gunnerås, S.A., Petersson, S. V., Tarkowski, P., Graham, N., May, S., Dolezal, K., and Sandberg, G. (2010). Cytokinin regulation of auxin synthesis in Arabidopsis involves a homeostatic feedback loop regulated via auxin and cytokinin signal transduction. Plant Cell *22*, 2956–2969. 10.1105/tpc.110.074856.
64. Marhavý, P., Duclercq, J., Weller, B., Feraru, E., Bielach, A., Offringa, R., Friml, J., Schwechheimer, C., Murphy, A., and Benková, E. (2014). Cytokinin controls polarity of PIN1-dependent Auxin transport during lateral root organogenesis. Curr. Biol. *24*, 1031–1037. 10.1016/j.cub.2014.04.002.
65. Růzička, K., Šimášková, M., Duclercq, J., Petrášek, J., Zažímalová, E., Simon, S., Friml, J., Van Montagu, M.C.E., and Benková, E. (2009). Cytokinin regulates root meristem activity via modulation of the polar auxin transport. Proc. Natl. Acad. Sci. U. S. A. *106*, 4284–4289. 10.1073/pnas.0900060106.
66. Müller, B., and Sheen, J. (2007). Advances in cytokinin signaling. Science *318*, 68–69. 10.1126/science.1145461.
67. Karunadasa, S.S., Kurepa, J., Shull, T.E., and Smalle, J.A. (2020). Cytokinin-induced protein synthesis suppresses growth and osmotic stress tolerance. New Phytol. *227*, 50–64. 10.1111/nph.16519.
68. Szweykowska, A., Gwoidi, E., and Spychala, M. (1980). The Cytokinin Control of Protein Synthesis in Plants. In Metabolism and Molecular Activities of Cytokinins, J. Guern and C. Peaud-Lenoel, eds. (Springer-Verlag Berlin Heidelberg), pp. 212–217. 10.1007/978-3-642-68035-9.
69. Woźny, A., and Gwóźdź, E.A. (1980). The effect of cytokinin on the polyribosome formation in cucumber cotyledons. Biochem. und Physiol. der Pflanz. *175*, 476–480. 10.1016/s0015-3796(80)80032-1.

70. Klyachko, N.L., Yakovleva, L.A., Shakirova, F.M., and Kulaeva, O.N. (1982). Cell-free translation of polyribosomes from detached pumpkin cotyledons: Effects of starvation and cytokinin. Biol. Plant. *24*, 374–380. 10.1007/BF02909106.
71. Short, K.C., Tepfer, D.A., and Fosket, D.E. (1974). Regulation of polyribosome formation and cell division in cultured soybean cells by cytokinin. J. Cell Sci. *15*, 75–87.
72. Brenner, W.G., and Schmülling, T. (2012). Transcript profiling of cytokinin action in *Arabidopsis* roots and shoots discovers largely similar but also organ-specific responses. BMC Plant Biol. *12*, 112. 10.1186/1471-2229-12-112.
73. Kiba, T., Naitou, T., Koizumi, N., Yamashino, T., Sakakibara, H., and Mizuno, T. (2005). Combinatorial microarray analysis revealing Arabidopsis genes implicated in cytokinin responses through the His→Asp phosphorelay circuitry. Plant Cell Physiol. *46*, 339–355. 10.1093/pcp/pci033.
74. Černý, M., Kuklová, A., Hoehenwarter, W., Fragner, L., Novák, O., Rotková, G., Jedelský, P.L., Žáková, K., Šmehilová, M., Strnad, M., et al. (2013). Proteome and metabolome profiling of cytokinin action in Arabidopsis identifying both distinct and similar responses to cytokinin down- and up-regulation. J. Exp. Bot. *64*, 4193–4206. 10.1093/jxb/ert227.
75. Cerný, M., Dycka, F., Bobál'Ová, J., and Brzobohatý, B. (2011). Early cytokinin response proteins and phosphoproteins of Arabidopsis thaliana identified by proteome and phosphoproteome profiling. J. Exp. Bot. *62*, 921–937. 10.1093/jxb/erq322.
76. Miyawaki, K., Tarkowski, P., Matsumoto-Kitano, M., Kato, T., Sato, S., Tarkowska, D., Tabata, S., Sandberg, G., and Kakimoto, T. (2006). Roles of Arabidopsis ATP/ADP isopentenyltransferases and tRNA isopentenyltransferases in cytokinin biosynthesis. Proc. Natl. Acad. Sci. U. S. A. *103*, 16598–16603. 10.1073/pnas.0603522103.
77. Ren, B., Liang, Y., Deng, Y., Chen, Q., Zhang, J., Yang, X., and Zuo, J. (2009). Genome-wide comparative analysis of type-A Arabidopsis response regulator genes by overexpression studies reveals their diverse roles and regulatory mechanisms in cytokinin signaling. Cell Res. *19*, 1178–1190. 10.1038/cr.2009.88.
78. Ferreira, F.J., and Kieber, J.J. (2005). Cytokinin signaling. Curr. Opin. Plant Biol. *8*, 518–525. 10.1016/j.pbi.2005.07.013.
79. Kakimoto, T. (2003). Perception and Signal Transduction of Cytokinins. Annu. Rev. Plant Biol. *54*, 605–627. 10.1146/annurev.arplant.54.031902.134802.
80. Jain, M., Tyagi, A.K., and Khurana, J.P. (2006). Molecular characterization and differential expression of cytokinin-responsive type-A response regulators in rice (*Oryza sativa*). BMC Plant Biol. *6*, 1. 10.1186/1471-2229-6-1.
81. To, J.P.C., Haberer, G., Ferreira, F.J., Deruère, J., Mason, M.G., Schaller, G.E., Alonso, J.M., Ecker, J.R., and Kieber, J.J. (2004). Type-A Arabidopsis response regulators are partially redundant negative regulators of cytokinin signaling. Plant Cell *16*, 658–671. 10.1105/tpc.018978.
82. Kiba, T., Yamada, H., Sato, S., Kato, T., Tabata, S., Yamashino, T., and Mizuno, T. (2003). The type-A response regulator, ARR15, acts as a negative regulator in the cytokinin-mediated signal transduction in *Arabidopsis thaliana*. Plant Cell Physiol. *44*, 868–874. 10.1093/pcp/pcg108.
83. To, J.P.C., Deruère, J., Maxwell, B.B., Morris, V.F., Hutchison, C.E., Ferreira, F.J., Schaller, G.E., and Kieber, J.J. (2007). Cytokinin regulates type-A Arabidopsis response regulator activity and protein stability via two-component phosphorelay. Plant Cell *19*, 3901–3914. 10.1105/tpc.107.052662.
84. Acheampong, A.K., Shanks, C., Cheng, C.Y., Eric Schaller, G., Dagdas, Y., and Kieber, J.J. (2020). EXO70D isoforms mediate selective autophagic degradation of type-A ARR proteins to regulate cytokinin sensitivity. Proc. Natl. Acad. Sci. U. S. A. *117*, 27034–27043. 10.1073/pnas.2013161117.
85. Bothma, J.P., Norstad, M.R., Alamos, S., and Garcia, H.G. (2018). LlamaTags: A

Versatile Tool to Image Transcription Factor Dynamics in Live Embryos. Cell *173*, 1810-1822.e16. 10.1016/j.cell.2018.03.069.

86. Imamura, A., Yoshino, Y., and Mizuno, T. (2001). Cellular Localization of the Signaling Components of Arabidopsis His-to-Asp Phosphorelay. Biosci. Biotechnol. Biochem. *65*, 2113–2117. 10.1271/bbb.65.2113.

87. Lee, D.J., Kim, S., Ha, Y.M., and Kim, J. (2008). Phosphorylation of Arabidopsis response regulator 7 (ARR7) at the putative phospho-accepting site is required for ARR7 to act as a negative regulator of cytokinin signaling. Planta *227*, 577–587. 10.1007/s00425-007-0640-x.

88. Buechel, S., Leibfried, A., To, J.P.C., Zhao, Z., Andersen, S.U., Kieber, J.J., and Lohmann, J.U. (2010). Role of A-type Arabidopsis Response Regulators in meristem maintenance and regeneration. Eur. J. Cell Biol. *89*, 279–284. 10.1016/j.ejcb.2009.11.016.

89. Xie, M., Chen, H., Huang, L., O'Neil, R.C., Shokhirev, M.N., and Ecker, J.R. (2018). A B-ARR-mediated cytokinin transcriptional network directs hormone cross-regulation and shoot development. Nat. Commun. *9*, 1604. 10.1038/s41467-018-03921-6.

90. Abel, S., Nguyen, M.D., and Theologis, A. (1995). The *PS-IAA4/5-like* Family of Early Auxin-inducible mRNAs in *Arabidopsis thaliana*. J. Mol. Biol. *251*, 533–549. 10.1006/jmbi.1995.0454.

91. Park, J.Y., Kim, H.J., and Kim, J. (2002). Mutation in domain II of IAA1 confers diverse auxin-related phenotypes and represses auxin-activated expression of Aux/IAA genes in steroid regulator-inducible system. Plant J. *32*, 669–683. 10.1046/j.1365-313X.2002.01459.x.

92. Abel, S., Oeller, P.W., and Theologis, A. (1994). Early auxin-induced genes encode short-lived nuclear proteins. Proc. Natl. Acad. Sci. U. S. A. *91*, 326–330. 10.1073/pnas.91.1.326.

93. Zenser, N., Ellsmore, A., Leasure, C., and Callis, J. (2001). Auxin modulates the degradation rate of Aux/IAA proteins. Proc. Natl. Acad. Sci. U. S. A. *98*, 11795–11800. 10.1073/pnas.211312798.

94. Worley, C.K., Zenser, N., Ramos, J., Rouse, D., Leyser, O., Theologis, A., and Callis, J. (2000). Degradation of Aux/IAA proteins is essential for normal auxin signalling. Plant J. *21*, 553–562. 10.1046/j.1365-313X.2000.00703.x.

95. Ramos, J.A., Zenser, N., Leyser, O., and Callis, J. (2001). Rapid degradation of auxin/indoleacetic acid proteins requires conserved amino acids of domain II and is proteasome dependent. Plant Cell *13*, 2349–2360. 10.1105/tpc.13.10.2349.

96. Figueiredo, M.R.A. de, and Strader, L.C. (2022). Intrinsic and extrinsic regulators of Aux/IAA protein degradation dynamics. Trends Biochem. Sci. *47*, 865–874. 10.1016/j.tibs.2022.06.004.

97. Liao, C.Y., Smet, W., Brunoud, G., Yoshida, S., Vernoux, T., and Weijers, D. (2015). Reporters for sensitive and quantitative measurement of auxin response. Nat. Methods *12*, 207–210. 10.1038/nmeth.3279.

98. Mills, E.W., and Green, R. (2017). Ribosomopathies: There's strength in numbers. Science *358*, eaan2755. 10.1126/science.aan2755.

99. Warren, A.J. (2018). Molecular basis of the human ribosomopathy Shwachman-Diamond syndrome. Adv. Biol. Regul. *67*, 109–127. 10.1016/j.jbior.2017.09.002.

100. Hawer, H., Mendelsohn, B.A., Mayer, K., Kung, A., Malhotra, A., Tuupanen, S., Schleit, J., Brinkmann, U., and Schaffrath, R. (2020). Diphthamide-deficiency syndrome: a novel human developmental disorder and ribosomopathy. Eur. J. Hum. Genet. *28*, 1497–1508. 10.1038/s41431-020-0668-y.

101. Armistead, J., Patel, N., Wu, X., Hemming, R., Chowdhury, B., Basra, G.S., Del Bigio, M.R., Ding, H., and Triggs-Raine, B. (2015). Growth arrest in the ribosomopathy, bowen-

conradi syndrome, is due to dramatically reduced cell proliferation and a defect in mitotic progression. Biochim. Biophys. Acta - Mol. Basis Dis. *1852*, 1029–1037. 10.1016/j.bbadis.2015.02.007.

102. Zhou, C., Zang, D., Jin, Y., Wu, H., Liu, Z., Du, J., and Zhang, J. (2011). Mutation in ribosomal protein L21 underlies hereditary hypotrichosis simplex. Hum. Mutat. *32*, 710–714. 10.1002/humu.21503.
103. Dixon, M.J. (1995). Treacher Collins syndrome. J. Med. Genet. *32*, 806–808. 10.1136/jmg.32.10.806.
104. Gazda, H.T., Sheen, M.R., Vlachos, A., Choesmel, V., O'Donohue, M.F., Schneider, H., Darras, N., Hasman, C., Sieff, C.A., Newburger, P.E., et al. (2008). Ribosomal Protein L5 and L11 Mutations Are Associated with Cleft Palate and Abnormal Thumbs in Diamond-Blackfan Anemia Patients. Am. J. Hum. Genet. *83*, 769–780. 10.1016/j.ajhg.2008.11.004.
105. Oliver, E.R., Saunders, T.L., Tarlé, S.A., and Glaser, T. (2004). Ribosomal protein L24 defect in belly spot and tail (*Bst*), a mouse *Minute*. Development *131*, 3907–3920. 10.1242/dev.01268.
106. McGowan, K.A., Li, J.Z., Park, C.Y., Beaudry, V., Tabor, H.K., Sabnis, A.J., Zhang, W., Fuchs, H., De Angelis, M.H., Myers, R.M., et al. (2008). Ribosomal mutations cause p53-mediated dark skin and pleiotropic effects. Nat. Genet. *40*, 963–970. 10.1038/ng.188.
107. Oristian, D.S., Slooíman, L.G., Zhou, X., Wang, L., Farach-Carson, M.C., and Kirn-Safran, C.B. (2009). Ribosomal protein L29/HIP deficiency delays osteogenesis and increases fragility of adult bone in mice. J. Orthop. Res. *27*, 28–35. 10.1002/jor.20706.
108. Uechi, T., Nakajima, Y., Nakao, A., Torihara, H., Chakraborty, A., Inoue, K., and Kenmochi, N. (2006). Ribosomal protein gene knockdown causes developmental defects in zebrafish. PLoS One *1*, e37. 10.1371/journal.pone.0000037.
109. Marygold, S.J., Coelho, C.M.A., and Leevers, S.J. (2005). Genetic analysis of RpL38 and RpL5, two minute genes located in the centric heterochromatin of chromosome 2 of *Drosophila melanogaster*. Genetics *169*, 683–695. 10.1534/genetics.104.034124.
110. Lee, C.C., Tsai, Y.T., Kao, C.W., Lee, L.W., Lai, H.J., Ma, T.H., Chang, Y.S., Yeh, N.H., and Lo, S.J. (2014). Mutation of a Nopp140 gene *dao-5* alters rDNA transcription and increases germ cell apoptosis in *C. elegans*. Cell Death Dis. *5*, e1158. 10.1038/cddis.2014.114.
111. Ito, T., Kim, G.T., and Shinozaki, K. (2000). Disruption of an Arabidopsis cytoplasmic ribosomal protein S13-homologous gene by transposon-mediated mutagenesis causes aberrant growth and development. Plant J. *22*, 257–264. 10.1046/j.1365-313X.2000.00728.x.
112. Horiguchi, G., Mollá-Morales, A., Pérez-Pérez, J.M., Kojima, K., Robles, P., Ponce, M.R., Micol, J.L., and Tsukaya, H. (2011). Differential contributions of ribosomal protein genes to *Arabidopsis thaliana* leaf development. Plant J. *65*, 724–736. 10.1111/j.1365-313X.2010.04457.x.
113. Zhao, H., Lü, S., Li, R., Chen, T., Zhang, H., Cui, P., Ding, F., Liu, P., Wang, G., Xia, Y., et al. (2015). The Arabidopsis gene *DIG6* encodes a large 60S subunit nuclear export GTPase 1 that is involved in ribosome biogenesis and affects multiple auxin-regulated development processes. J. Exp. Bot. *66*, 6863–6875. 10.1093/jxb/erv391.
114. Takagi, M., Absalon, M.J., McLure, K.G., and Kastan, M.B. (2005). Regulation of p53 translation and induction after DNA damage by ribosomal protein L26 and nucleolin. Cell *123*, 49–63. 10.1016/j.cell.2005.07.034.
115. Deisenroth, C., and Zhang, Y. (2010). Ribosome biogenesis surveillance: Probing the ribosomal protein-Mdm2-p53 pathway. Oncogene *29*, 4253–4260. 10.1038/onc.2010.189.
116. Warner, J.R., and McIntosh, K.B. (2009). How Common Are Extraribosomal Functions of Ribosomal Proteins? Mol. Cell *34*, 3–11. 10.1016/j.molcel.2009.03.006.

117. Dutt, S., Narla, A., Lin, K., Mullally, A., Abayasekara, N., Megerdichian, C., Wilson, F.H., Currie, T., Khanna-Gupta, A., Berliner, N., et al. (2011). Haploinsufficiency for ribosomal protein genes causes selective activation of p53 in human erythroid progenitor cells. Blood *117*, 2567–2576. 10.1182/blood-2010-07-295238.
118. Danilova, N., Sakamoto, K.M., and Lin, S. (2008). Ribosomal protein S19 deficiency in zebrafish leads to developmental abnormalities and defective erythropoiesis through activation of p53 protein family. Blood *112*, 5228–5237. 10.1182/blood-2008-01-132290.
119. Girardi, T., Vereecke, S., Sulima, S.O., Khan, Y., Fancello, L., Briggs, J.W., Schwab, C., De Beeck, J.O., Verbeeck, J., Royaert, J., et al. (2018). The T-cell leukemia-associated ribosomal RPL10 R98S mutation enhances JAK-STAT signaling. Leukemia *32*, 809–819. 10.1038/leu.2017.225.
120. Ludwig, L.S., Gazda, H.T., Eng, J.C., Eichhorn, S.W., Thiru, P., Ghazvinian, R., George, T.I., Gotlib, J.R., Beggs, A.H., Sieff, C.A., et al. (2014). Altered translation of GATA1 in Diamond-Blackfan anemia. Nat. Med. *20*, 748–753. 10.1038/nm.3557.
121. Khajuria, R.K., Munschauer, M., Ulirsch, J.C., Fiorini, C., Ludwig, L.S., McFarland, S.K., Abdulhay, N.J., Specht, H., Keshishian, H., Mani, D.R., et al. (2018). Ribosome Levels Selectively Regulate Translation and Lineage Commitment in Human Hematopoiesis. Cell *173*, 90-103.e19. 10.1016/j.cell.2018.02.036.
122. In, K., Zaini, M.A., Müller, C., Warren, A.J., Von Lindern, M., and Calkhoven, C.F. (2016). Shwachman-Bodian-Diamond syndrome (SBDS) protein deficiency impairs translation re-initiation from C/EBPα and C/EBPβ mRNAs. Nucleic Acids Res. *44*, 4134–4146. 10.1093/nar/gkw005.
123. Kondrashov, N., Pusic, A., Stumpf, C.R., Shimizu, K., Hsieh, A.C., Xue, S., Ishijima, J., Shiroishi, T., and Barna, M. (2011). Ribosome-mediated specificity in Hox mRNA translation and vertebrate tissue patterning. Cell *145*, 383–397. 10.1016/j.cell.2011.03.028.
124. Deliu, L.P., Turingan, M., Jadir, D., Lee, B., Ghosh, A., and Grewal, S.S. (2022). Serotonergic neuron ribosomal proteins regulate the neuroendocrine control of Drosophila development. PLoS Genet. *18*, e1010371. 10.1371/journal.pgen.1010371.
125. Adams, K.W., and Cooper, G.M. (2007). Rapid turnover of Mcl-1 couples translation to cell survival and apoptosis. J. Biol. Chem. *282*, 6192–6200. 10.1074/jbc.M610643200.
126. Truckenbrodt, S., Viplav, A., Jähne, S., Vogts, A., Denker, A., Wildhagen, H., Fornasiero, E.F., and Rizzoli, S.O. (2018). Newly produced synaptic vesicle proteins are preferentially used in synaptic transmission. EMBO J. *37*, e98044. 10.15252/embj.201798044.
127. Mähönen, A.P., Bonke, M., Kauppinen, L., Riikonen, M., Benfey, P.N., and Helariutta, Y. (2000). A novel two-component hybrid molecule regulates vascular morphogenesis of the Arabidopsis root. Genes Dev. *14*, 2938–2943. 10.1101/gad.189200.
128. Sotta, N., Shantikumar, L., Sakamoto, T., Matsunaga, S., and Fujiwara, T. (2016). TPR5 is involved in directional cell division and is essential for the maintenance of meristem cell organization in *Arabidopsis thaliana*. J. Exp. Bot. *67*, 2401–2411. 10.1093/jxb/erw043.
129. Heisler, M.G., Ohno, C., Das, P., Sieber, P., Reddy, G. V., Long, J.A., and Meyerowitz, E.M. (2005). Patterns of auxin transport and gene expression during primordium development revealed by live imaging of the Arabidopsis inflorescence meristem. Curr. Biol. *15*, 1899–1911. 10.1016/j.cub.2005.09.052.
130. Müller, B., and Sheen, J. (2008). Cytokinin and auxin interaction in root stem-cell specification during early embryogenesis. Nature *453*, 1094–1097. 10.1038/nature06943.
131. Brackmann, K., Qi, J., Gebert, M., Jouannet, V., Schlamp, T., Grünwald, K., Wallner, E.S., Novikova, D.D., Levitsky, V.G., Agustí, J., et al. (2018). Spatial specificity of auxin responses coordinates wood formation. Nat. Commun. *9*, 875. 10.1038/s41467-018-03256-2.
132. Argyros, R.D., Mathews, D.E., Chiang, Y.H., Palmer, C.M., Thibault, D.M., Etheridge, N.,

Argyros, D.A., Mason, M.G., Kieber, J.J., and Schallera, G.E. (2008). Type B response regulators of Arabidopsis play key roles in cytokinin signaling and plant development. Plant Cell *20*, 2102–2116. 10.1105/tpc.108.059584.

133. Rademacher, E.H., Möller, B., Lokerse, A.S., Llavata-Peris, C.I., Van Den Berg, W., and Weijers, D. (2011). A cellular expression map of the *Arabidopsis AUXIN RESPONSE FACTOR* gene family. Plant J. *68*, 597–606. 10.1111/j.1365-313X.2011.04710.x.
134. Saerens, D., Pellis, M., Loris, R., Pardon, E., Dumoulin, M., Matagne, A., Wyns, L., Muyldermans, S., and Conrath, K. (2005). Identification of a universal VHH framework to graft non-canonical antigen-binding loops of camel single-domain antibodies. J. Mol. Biol. *352*, 597–607. 10.1016/j.jmb.2005.07.038.
135. Fujii, Y., and Kodama, Y. (2015). *In planta* comparative analysis of improved green fluorescent proteins with reference to fluorescence intensity and bimolecular fluorescence complementation ability. Plant Biotechnol. *32*, 81–87. 10.5511/plantbiotechnology.15.0120a.
136. Alamos, S., Reimer, A., Niyogi, K.K., and Garcia, H.G. (2021). Quantitative imaging of RNA polymerase II activity in plants reveals the single-cell basis of tissue-wide transcriptional dynamics. Nat. Plants *7*, 1037–1049. 10.1038/s41477-021-00976-0.
137. Alexa, A., Rahnenführer, J., and Lengauer, T. (2006). Improved scoring of functional groups from gene expression data by decorrelating GO graph structure. Bioinformatics *22*, 1600–1607. 10.1093/bioinformatics/btl140.
138. Mustroph, A., Juntawong, P., and Bailey-Serres, J. (2009). Isolation of Plant Polysomal mRNA by Differential Centrifugation and Ribosome Immunopurification Methods. In Methods in molecular biology (vol. 553) (Humana Press, a part of Springer Science+Business Media, LLC), pp. 109–126. 10.1007/978-1-60327-563-7_6.
139. Gao, X., Wan, J., Liu, B., Ma, M., Shen, B., and Qian, S.B. (2015). Quantitative profiling of initiating ribosomes *in vivo*. Nat. Methods *12*, 147–153. 10.1038/nmeth.3208.
140. Busche, M., Regina Scarpin, M., Hnasko, R., and Brunkard, J.O. (2021). TOR coordinates nucleotide availability with ribosome biogenesis in plants. Plant Cell *33*, 1615–1632. 10.1093/plcell/koab043.
141. Schindelin, J., Rueden, C.T., Hiner, M.C., and Eliceiri, K.W. (2015). The ImageJ ecosystem: An open platform for biomedical image analysis. Mol. Reprod. Dev. *82*, 518–529. 10.1002/mrd.22489.
142. Schindelin, J., Arganda-Carreras, I., Frise, E., Kaynig, V., Longair, M., Pietzsch, T., Preibisch, S., Rueden, C., Saalfeld, S., Schmid, B., et al. (2012). Fiji: An open-source platform for biological-image analysis. Nat. Methods *9*, 676–682. 10.1038/nmeth.2019.
143. de Reuille, P.B., Routier-Kierzkowska, A.L., Kierzkowski, D., Bassel, G.W., Schüpbach, T., Tauriello, G., Bajpai, N., Strauss, S., Weber, A., Kiss, A., et al. (2015). MorphoGraphX: A platform for quantifying morphogenesis in 4D. eLife *4*, 1–20. 10.7554/eLife.05864.
144. Schäfer, M., Brütting, C., Baldwin, I.T., and Kallenbach, M. (2016). High-throughput quantification of more than 100 primary- and secondary-metabolites, and phytohormones by a single solid-phase extraction based sample preparation with analysis by UHPLC-HESI-MS/MS. Plant Methods *12*, 30. 10.1186/s13007-016-0130-x.
145. Kojima, M., Kamada-Nobusada, T., Komatsu, H., Takei, K., Kuroha, T., Mizutani, M., Ashikari, M., Ueguchi-Tanaka, M., Matsuoka, M., Suzuki, K., et al. (2009). Highly sensitive and high-throughput analysis of plant hormones using ms-probe modification and liquid chromatographytandem mass spectrometry: An application for hormone profiling in oryza sativa. Plant Cell Physiol. *50*, 1201–1214. 10.1093/pcp/pcp057.
146. Novák, O., Antoniadi, I., and Ljung, K. (2017). High-resolution cell-type specific analysis of cytokinins in sorted root cell populations of *Arabidopsis thaliana*. Methods Mol. Biol. *1497*, 231–248. 10.1007/978-1-4939-6469-7_1.

147. R Core Team (2021). R: A language and environment for statistical computing. R Foundation for Statistical Computing, Vienna, Austria. URL https://www.R-project.org/.
148. Wickham, H. (2009). ggplot2: Elegant Graphics for Data Analysis R. Gentleman, K. Hornik, and G. Parmigiani, eds. (Springer) 10.1007/978-0-387-98141-3.

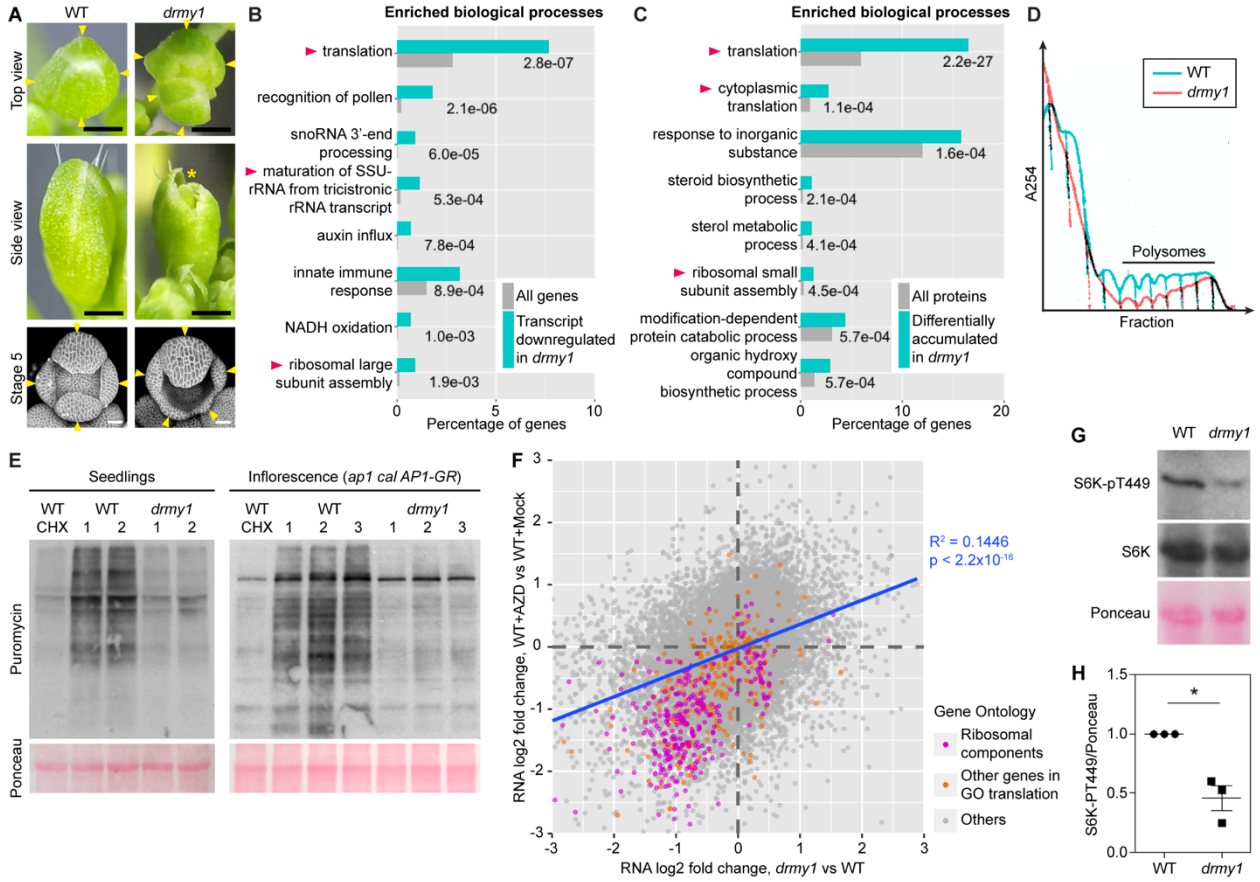


**Figure 1. *drmy1* has reduced ribosome abundance, translation rate, and TOR activity.**

**(A)** Top row, stage 12 buds of WT (left) and *drmy1* (right) viewed from the top. Arrowheads point to sepals. Note that the *drmy1* bud has 5 sepals of unequal size and unevenly spaced, exposing the stamens and carpels. Middle row, stage 12 buds of WT (left) and *drmy1* (right) viewed from the side. Asterisk shows the gap between sepals with petals and carpels exposed. Bottom row, stage 5 buds of WT (left) and *drmy1* (right) containing *35S::mCitrine-RCI2A* (plasma membrane marker). Arrowheads point to sepal primordia. Note that the *drmy1* bud has 5 sepal primordia of different sizes. Scale bars are 0.5 mm for stage 12 bud images and 25 µm for stage 5 bud images.

**(B-C)** Gene ontology (GO) enrichment of downregulated genes **(B)** and differentially accumulated proteins **(C)** in *drmy1* compared to WT, in the *ap1 cal AP1-GR* background. Shown are the top 8 GO terms and their enrichment p-values. A complete list can be found in Supplemental Dataset 1. Arrowheads highlight terms related to ribosome biogenesis or translation.

**(D)** Ribosome profiles of WT (blue) and *drmy1* (red) in the *ap1 cal AP1-GR* background, representative of 3 biological replicates each. Polysomal peaks are highlighted. All replicates can be found in Supplemental Dataset 2.

**(E)** Puromycin labeling of WT vs *drmy1*. Left, puromycin labeling in WT and *drmy1* seedlings. From left to right: WT pre-treated with CHX, two biological replicates of WT pre-treated with mock, and two biological replicates of *drmy1* pre-treated with mock. All groups were then treated with puromycin. For seedlings to match in size, WT seedlings were 8 days old and *drmy1* seedlings were 10 days old. Right, puromycin labeling in WT and *drmy1* inflorescences of induced *ap1 cal*

*AP1-GR* background. From left to right: WT co-treated with puromycin and CHX, three biological replicates of WT treated with puromycin, and three biological replicates of *drmy1* treated with puromycin. In both experiments, RuBisCO large subunit on Ponceau S-stained membrane is shown as a loading control (bottom).

**(F)** Coherent alteration of gene expression by *drmy1* and AZD-8055 TOR inhibitor treatment. Shown here is a scatterplot of RNA log 2 fold change in *drmy1* vs WT (x-axis), and WT+AZD vs WT+Mock (y-axis), in 7-day-old seedlings. Genes are color-coded based on the following categories: genes in "Structural constituents of the ribosome" (GO:0003735) and its offspring terms (magenta); all other genes in "Translation" (GO:0006412) and its offspring terms (orange); all other genes (gray). Blue line shows a linear regression of all points ($R^2 = 0.1446$, $p < 2.2x10^{-16}$). Note that the axes were trimmed to (-3,3) for ease of display.

**(G-H)** Phosphorylation of the direct TOR substrate, S6K-pT449, in WT and *drmy1*. Representative images are shown in **(G)**. Top, Western blot against S6K-pT449. Middle, Western blot against total S6K protein. Bottom, Ponceau S staining as a loading control. **(H)** Quantification of the intensity of S6K-pT449 over Ponceau normalized by WT, in three experiments, shows that TOR activity decreased by half in *drmy1*. (mean ± SD; *, $p<0.05$).

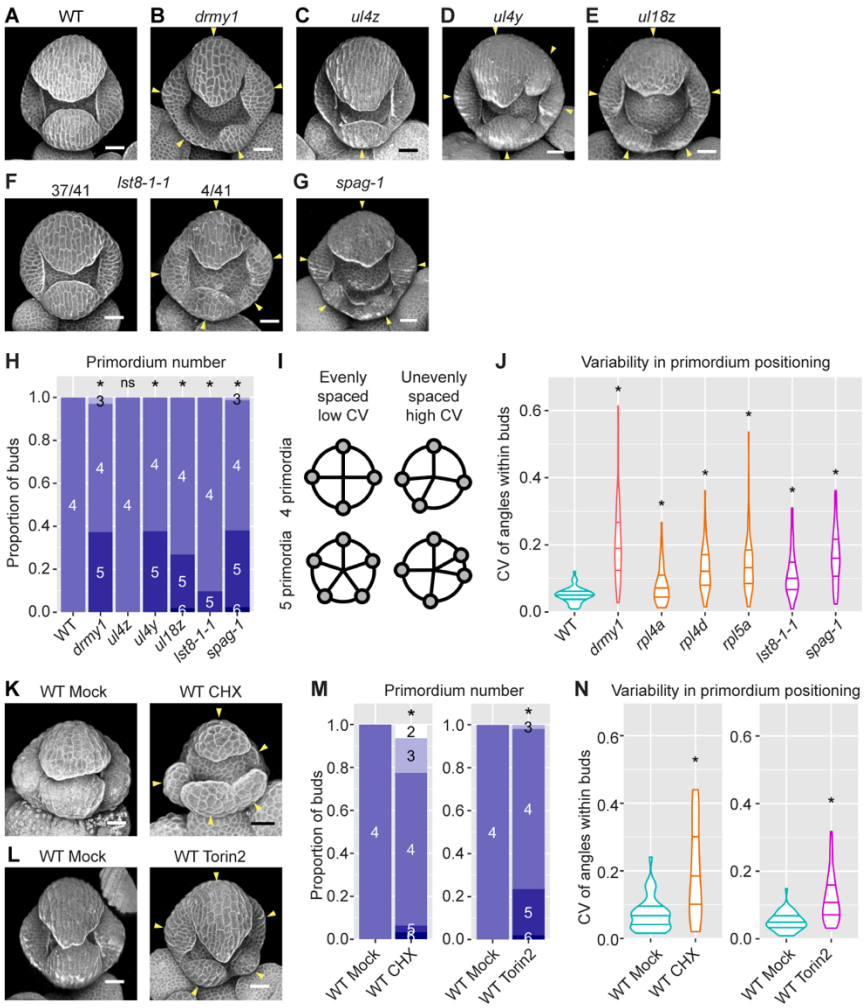


**Figure 2. Defects in TOR activity, ribosome integrity, and translation cause variable sepal initiation.**

**(A-G)** Representative images of stage 5 buds in WT (A), *drmy1* (B), *ul4z* (C), *ul4y* (D), *ul18z* (E), *lst8-1-1* (F), and *spaghetti-1* (G). Tissue morphology is visualized by either propidium iodide (a cell wall-staining dye) or a plasma membrane marker. Arrowheads indicate sepal primordia that are variable in number, position, and size. Note that *ul4z* flowers always develop four sepal primordia, although of different sizes; *lst8-1-1* occasionally (4/41, 9.8%) develops buds with more than four sepal primordia. Scale bars, 25 μm.

**(H)** Quantification of sepal primordium number, comparing *drmy1* (n = 67 buds), *ul4z* (n = 52 buds), *ul4y* (n = 53 buds), *ul18z* (n = 52 buds), *lst8-1-1* (n = 41 buds), and *spaghetti-1* (n = 84 buds) with WT (n = 51 buds). Asterisks indicate statistically significant ($p < 0.05$) differences from WT in Fisher's contingency table tests.

**(I)** Illustration of robust versus variable positioning of sepal primordia. Primordia are considered robustly positioned if they are evenly distributed around the edge of the bud. Within each bud, angles between adjacent primordia with respect to the center of the bud are measured, and coefficient of variation (CV) is calculated. A bud with robustly positioned primordia would have

similar angular values and a low CV value. A bud with variably positioned primordia would have very different angular values and a high CV value.
**(J)** Quantification of variability in primordium positioning (CV) in the same buds as in (H), following illustration in (I). Asterisks indicate statistically significant ($p < 0.05$) differences from WT in Wilcoxon's rank sum tests.
**(K)** Representative images of buds from *in vitro*-cultured WT inflorescences treated with mock or 2 μM CHX for 9-10 days (see Material and Methods). Arrowheads indicate sepal primordia that are variable in number, position, and size. Scale bars, 25 μm.
**(L)** Representative images of buds from WT plants treated with mock or 2 nmol Torin2 for 15 days (see Material and Methods). Arrowheads indicate sepal primordia that are variable in number, position, and size. Scale bars, 25 μm.
**(M-N)** Quantification of variability in primordium number (M) and positional variability (N) similar to (H,J), comparing CHX-treated (n = 31 buds), CHX-mock (n = 42 buds), Torin2-treated (n = 51 buds) and Torin2-mock buds (n = 56 buds).

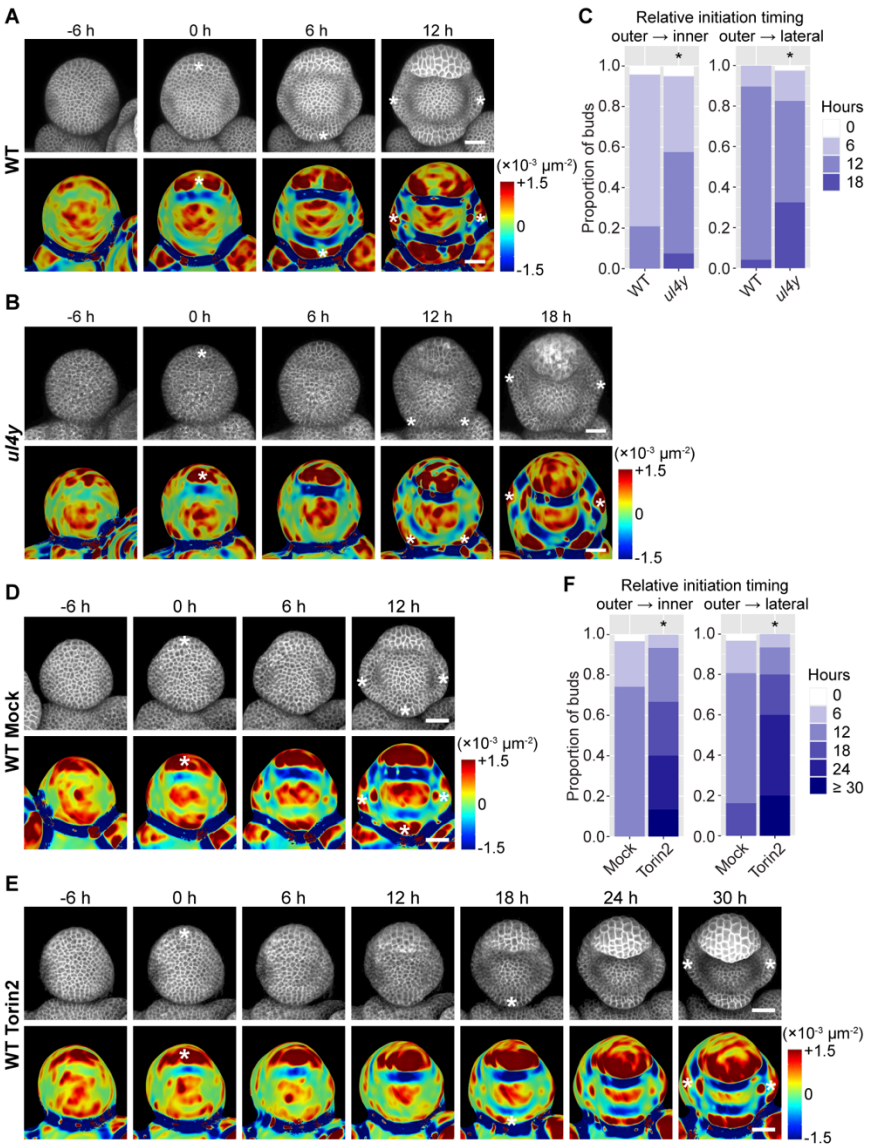


**Figure 3. TOR and ribosomal defects cause variability in the timing of sepal initiation.**

**(A-C)** 6h-interval live imaging of the sepal initiation process in WT (A) and *ul4y* (B), which is quantified in (C). n = 48 buds for WT; n = 40 buds for *ul4y*.

**(D-F)** 6h-interval live imaging of the sepal initiation process in buds from WT plants treated with mock or 2 nmol Torin2 bi-daily for 15 days, which is quantified in (F). n = 31 buds for mock; n = 15 buds for Torin2.

In **(A,B,D,E)**, top rows show the *35S::mCitrine-RCI2A* membrane marker, and bottom rows show Gaussian curvature heatmaps calculated from the same image stacks. Asterisks indicate sepal initiation events, defined as a dark red band (primordium with positive curvature) separated from the floral meristem by a dark blue band (boundary with negative curvature) in the Gaussian curvature heatmap. Scale bars, 25 μm.

In **(C,F)**, the amount of time between outer and inner sepal initiation (left) and between outer and lateral sepal initiation (right) were calculated for each bud, and summarized over all the buds.

Asterisks indicate statistically significant ($p < 0.05$) differences in the distribution of relative initiation timing in Fisher's contingency table tests.

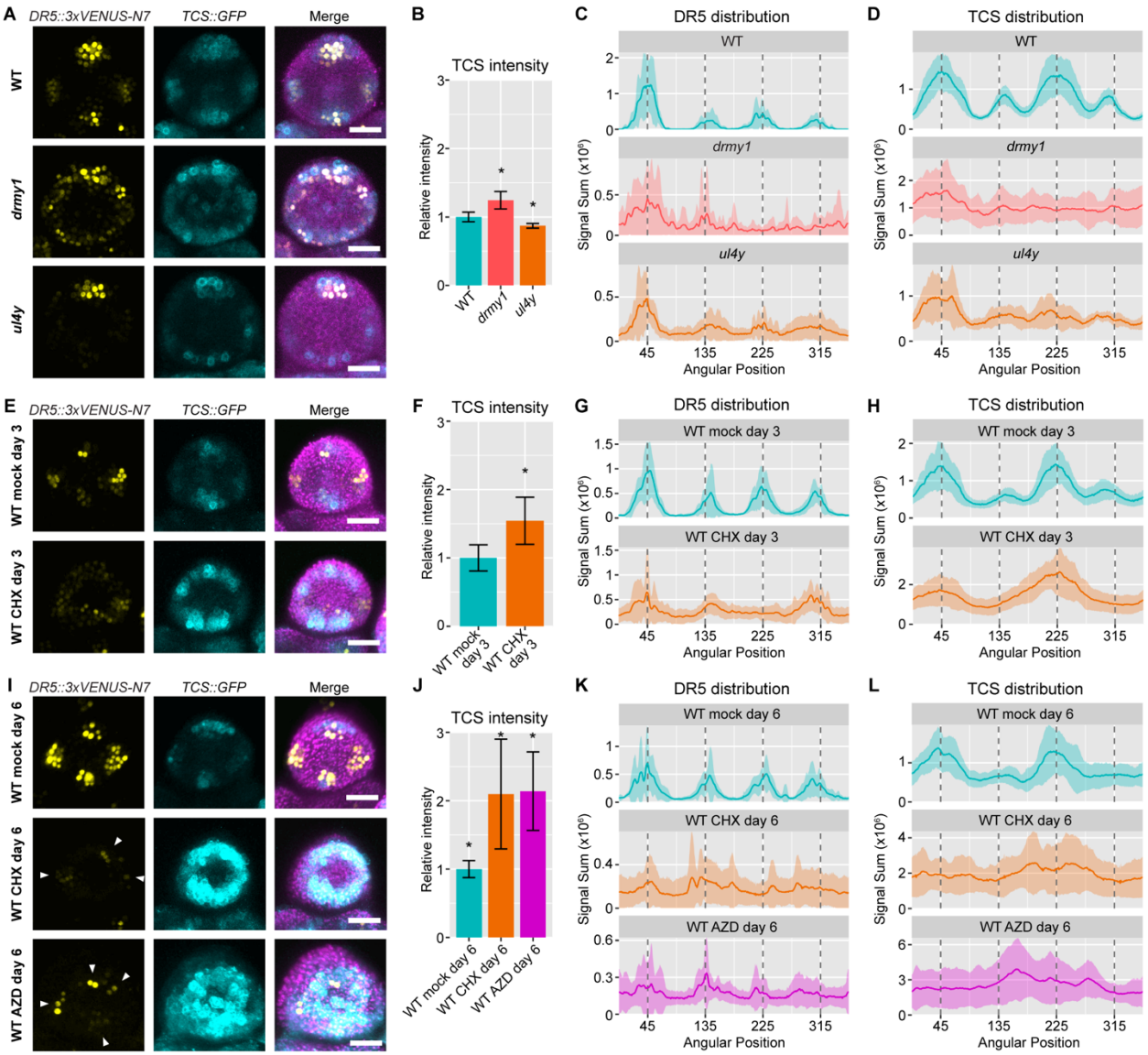


**Figure 4. Defects in TOR activity, ribosome integrity, and translation cause variability in auxin and cytokinin signaling.**

**(A-D)** The ribosomal mutant *ul4y* loses robustness in auxin and cytokinin signaling. (A) Representative images of late stage 2 buds of WT, *drmy1*, and *ul4y*, showing the auxin signaling reporter *DR5::3xVENUS-N7* in yellow, the cytokinin signaling reporter *TCS::GFP* in cyan, and both merged with Chlorophyll (in WT) or *UBQ10::mCherry-RCI2A* (in *drmy1* and *ul4y*) in magenta. (B) Quantification of TCS intensity (integrated density divided by area) from maximum intensity projection images, normalized to mean of WT. Shown are mean ± SD. Asterisks show statistically significant differences from WT in two-tailed Student's t-tests (*drmy1*, p = $2.1 \times 10^{-6}$; *ul4y*, p = $3.4 \times 10^{-5}$). (C) Circular histogram of DR5 distribution around the bud. Each bud was divided into 360 sectors of 1° each. Within each sector, DR5 signal measured in pixel intensity units (0-255 range) was summed. This sum was plotted along the x-axis starting from the sector at 1:30 position (between the incipient outer sepal and incipient lateral sepal on the right) going

counterclockwise. I.e. in WT, the outer sepal is near 45°, the inner sepal near 225°, and the lateral sepals near 45° and 135° (vertical dotted lines). The mean was plotted as a solid line, and mean ± SD was plotted as a shaded area. (D) Circular histogram of TCS distribution around the bud. Sample size for (A-D): WT, n = 12 buds; *drmy1*, n = 15 buds; *ul4y*, n = 10 buds.

**(E-H)** 3 days of translation inhibition causes increased and diffuse cytokinin signaling, and diffuse auxin signaling. (E) Representative images of late stage 2 buds from dissected and cultured WT inflorescences treated with mock or 2 µM CHX for 3 days. Shown are *DR5::3xVENUS-N7* in yellow, *TCS::GFP* in cyan, and both merged with Chlorophyll in magenta. (F) Quantification of TCS intensity from maximum intensity projection images, normalized to mean of WT mock day 3. Shown are mean ± SD. Asterisk shows statistically significant difference in a two-tailed Student's t-test ($p = 2.0x10^{-4}$). (G) Circular histogram of DR5 distribution around the bud. (H) Circular histogram of TCS distribution around the bud. Sample size for (E-H): WT mock day 3, n = 10 buds; WT CHX day 3, n = 12 buds.

**(I-L)** 6 days of TOR or translation inhibition causes increased and diffuse cytokinin signaling, and randomly positioned auxin signaling maxima. (I) Representative images of late stage 2 buds from dissected and cultured WT inflorescences treated with mock, 2 µM CHX, or 2 µM AZD for 6 days. Shown are *DR5::3xVENUS-N7* in yellow, *TCS::GFP* in cyan, and both merged with Chlorophyll in magenta. Arrowheads point to randomly positioned auxin maxima in buds of the CHX or AZD group. (J) Quantification of TCS intensity from maximum intensity projection images, normalized to mean of WT mock day 6. Shown are mean ± SD. Asterisks show statistically significant differences from mock in two-tailed Student's t-tests (CHX, $p = 1.0x10^{-3}$; AZD, $p = 1.2x10^{-4}$). (K) Circular histogram of DR5 distribution around the bud. (L) Circular histogram of TCS distribution around the bud. Sample size for (I-L): WT mock day 6, n = 12 buds; WT CHX day 6, n = 11 buds; WT AZD day 6, n = 10 buds. Scale bars in (A,E,I) represent 25 µm.

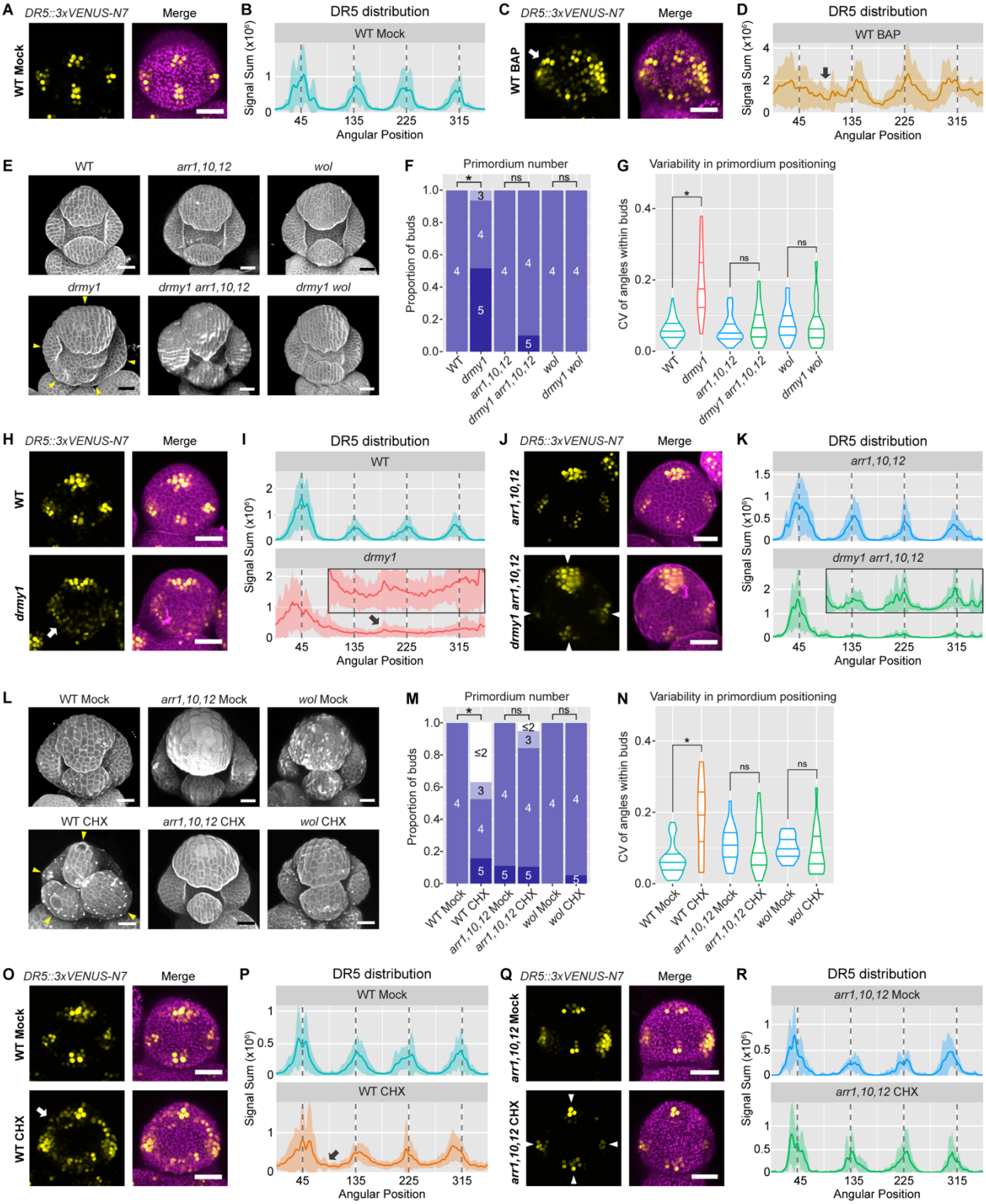


**Figure 5. Cytokinin signaling is required for variability in auxin signaling and sepal initiation under translation inhibition.**

**(A-D)** Cytokinin treatment makes auxin signaling diffuse. Shown are late stage 2 WT buds under mock (A,B) or 5 µM cytokinin (BAP) treatment (C,D) for 4 days. (A,C) Representative images of

the auxin signaling reporter *DR5::3xVENUS-N7* in yellow, and *DR5* merged with Chlorophyll in magenta. (B,D) Circular histograms of the *DR5::3xVENUS-N7* signal, showing mean (solid line) and mean ± SD (shaded area). Arrows point to DR5 signal in variable positions. Sample size: WT Mock n = 10, WT BAP n = 10. Also see Zhu et al. (2020), Extended Data Figure 7e.

**(E-G)** Cytokinin signaling is required for variable sepal initiation in *drmy1*. (E) Representative images of stage 5 buds in WT, *drmy1*, *arr1,10,12*, *drmy1 arr1,10,12*, *wol*, and *drmy1 wol*. Arrowheads indicate initiated sepal primordia that are variable in number, position, and size. (F,G) Quantification of sepal primordium number (F) and positional variability (G), comparing WT (n = 58) with *drmy1* (n = 31), *arr1,10,12* (n = 24) with *drmy1 arr1,10,12* (n = 20), and *wol* (n = 36) with *drmy1 wol* (n = 39). Asterisks indicate statistically significant ($p < 0.05$) differences in Fisher's contingency table tests (F) and Wilcoxon's rank sum tests (G) respectively. ns indicates no significant difference.

**(H-K)** Cytokinin signaling is required for variable patterning of auxin signaling in *drmy1*. Shown are late stage 2 buds of WT vs *drmy1* (H,I), and *arr1,10,12* vs *drmy1 arr1,10,12* (J,K). (H,J) Representative images of the auxin signaling reporter *DR5::3xVENUS-N7* in yellow, and *DR5* merged with propidium iodide in magenta. Arrows point to diffuse DR5 signal in variable positions in the *drmy1* bud. Arrowheads show four robust DR5 maxima in *drmy1 arr1,10,12*. (I,K) Circular histograms of the *DR5::3xVENUS-N7* signal, showing mean (solid line) and mean ± SD (shaded area). For ease of visualization, circular histograms of *drmy1* and *drmy1 arr1,10,12* between 90 and 360 degrees are enlarged and shown as insets (y-axis range 0-0.4). Sample size: WT n = 19, *drmy1* n = 16, *arr1,10,12* n = 13, *drmy1 arr1,10,12* n = 9.

**(L-N)** Cytokinin signaling is required for variable sepal initiation under translation inhibition. (L) Representative images of stage 6 buds in WT, *arr1,10,12*, and *wol*, treated with Mock or 2 μM CHX for 10 days. Arrowheads indicate variable initiation of sepal primordia. (M,N) Quantification of sepal primordium number (M) and positional variability (N), comparing Mock and CHX within each genotype. Sample size: WT Mock n = 29, WT CHX n = 19, *arr1,10,12* Mock n = 18, *arr1,10,12* CHX n = 19, *wol* Mock n = 15, *wol* CHX n = 19. Asterisks indicate statistically significant ($p < 0.05$) differences in Fisher's contingency table tests (M) and Wilcoxon's rank sum tests (N) respectively. ns indicates no significant difference.

**(O-R)** Cytokinin signaling is required for diffuse auxin signaling under translation inhibition. Shown are late stage 2 buds of WT (O,P) and *arr1,10,12* (Q,R), treated with Mock or 2 μM CHX for 3 days. (O,Q) Representative images of the auxin signaling reporter *DR5::3xVENUS-N7* in yellow, and *DR5* merged with Chlorophyll in magenta. Arrows point to diffuse DR5 signal in variable positions in CHX-treated WT. Arrowheads show four robust DR5 maxima in CHX-treated *arr1,10,12*. (P,R) Circular histograms of the *DR5::3xVENUS-N7* signal, showing mean (solid line) and mean ± SD (shaded area). Sample size: WT Mock n = 17, WT CHX n = 18, *arr1,10,12* Mock n = 7, *arr1,10,12* CHX n = 7. Scale bars in (A,C,E,H,J,L,O,Q) represent 25 μm.

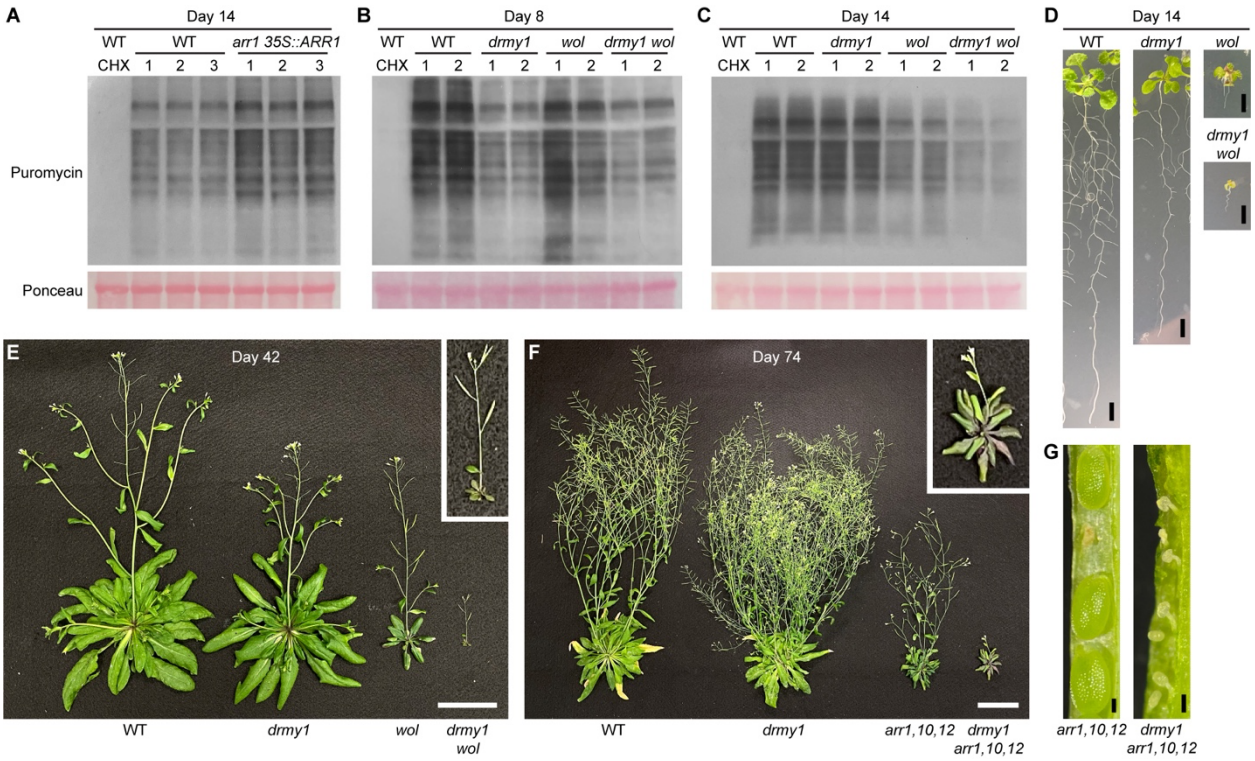


**Figure 6. Upregulation of cytokinin signaling is required to maintain translation and fitness in *drmy1*.**

**(A)** Puromycin labeling of WT seedlings with 4 h CHX pre-treatment (control), and three biological replicates each of WT and *arr1 35S::ARR1* seedlings with 4 h mock pre-treatment. All seedlings are 14 days old. RuBisCO large subunit in Ponceau S-stained membrane is shown as a loading control. Also see Karunadasa et al. (2020).

**(B,C)** Puromycin labeling of WT seedlings with 4 h CHX pre-treatment (control), and two biological replicates of WT, *drmy1*, *wol*, and *drmy1 wol* seedlings with 4 h mock pre-treatment. Seedlings are 8 days old in (B) and 14 days old in (C). RuBisCO large subunit in Ponceau S-stained membrane is shown as a loading control.

**(D)** Representative 14 days old seedling images of WT, *drmy1*, *wol*, and *drmy1 wol* used in (C). Notice that *drmy1 wol* is very small and pale. Scale bars, 5 mm.

**(E)** Representative aerial part images of 42 days old plants of WT, *drmy1*, *wol*, and *drmy1 wol*. Inset shows enlarged *drmy1 wol* plant; notice that it has a tiny rosette and inflorescence. Scale bars, 5 cm. See also Supplemental Figure 6F.

**(F)** Representative aerial part images of 74 days old plants of WT, *drmy1*, *arr1*,*10*,*12*, and *drmy1 arr1*,*10*,*12*. Inset shows enlarged *drmy1 arr1*,*10*,*12* plant; notice its pale leaves accumulating anthocyanin, and short inflorescence. Scale bars, 5 cm. See also Supplemental Figure 6E.

**(G)** Dissected siliques of *arr1,10,12* (left) and *drmy1 arr1,10,12* (right) showing developing seeds. Notice that while *arr1,10,12* occasionally have aborted seeds, all seeds in the *drmy1 arr1,10,12* silique were aborted. Scale bars, 0.2 mm.

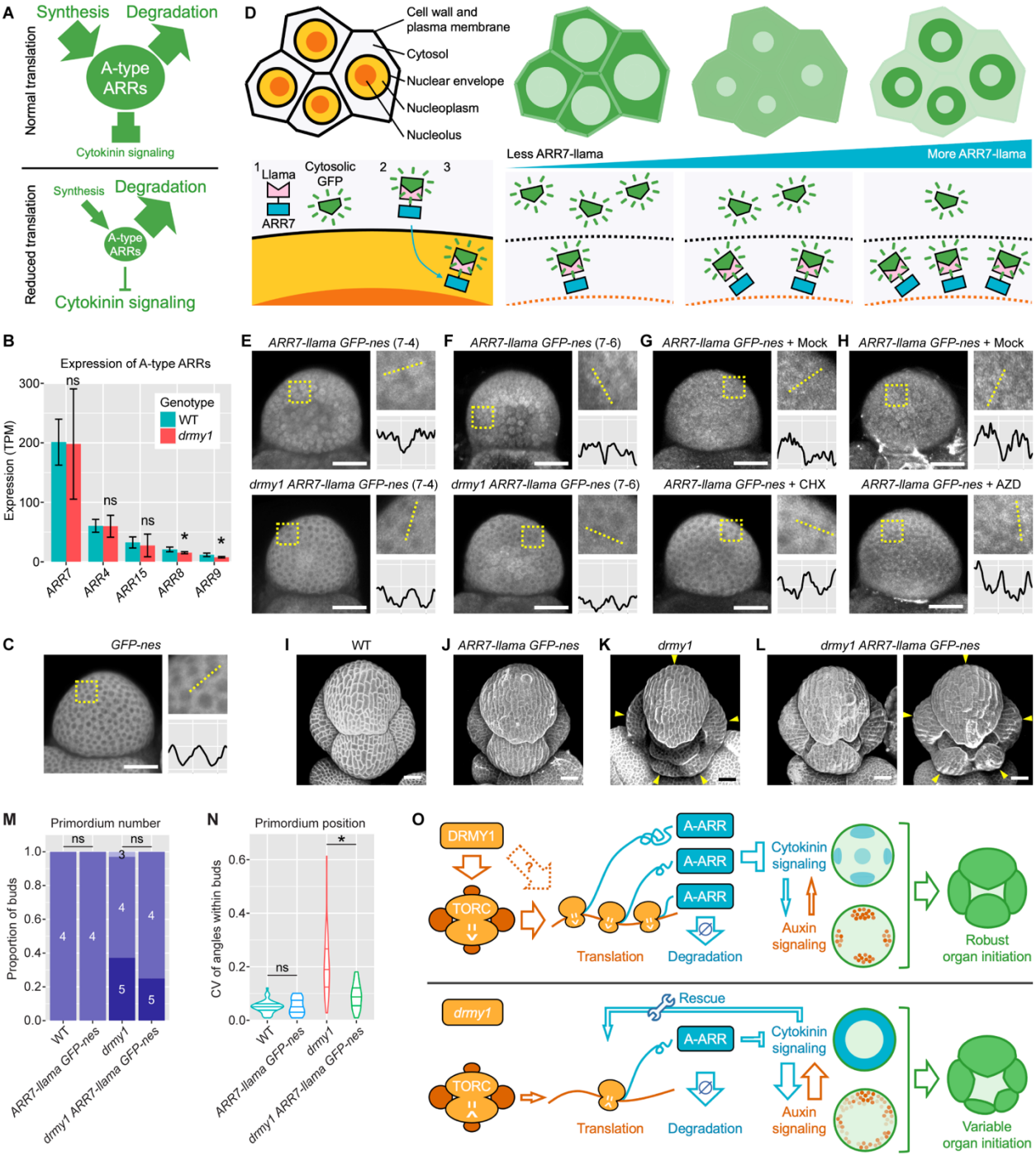


**Figure 7. A-type ARR protein levels are sensitive to TOR and translation inhibition.**

**(A)** The hypothesis. A-type ARRs are rapidly synthesized and degraded to dampen cytokinin signaling. Translation inhibition causes inability to rapidly synthesize these proteins in response to cytokinin signaling, resulting in an upregulation of cytokinin signaling.

**(B)** Expression of A-type ARR genes in WT vs *drmy1* inflorescences (*ap1 cal AP1-GR*) measured in RNA-seq. Shown are the five A-type ARR genes with the highest expression, ranked by mean expression level in WT. Asterisk indicates statistically significant difference, while ns means no

significant difference. P-values: ARR7, p = 0.807; ARR4, p = 0.611; ARR15, p = 0.532; ARR8, p = 0.0115; ARR9, p = 0.0416.

**(C)** A GFP-channel image of a stage 2 bud of GFP-nes (*pUBQ10::sfGFP-nes-UBQ3ter*). For this panel and (E-H), each image was brightened to reveal GFP distribution patterns. A square region taken from the image containing 5-10 cells is enlarged and shown on the top right. Within the enlargement, GFP intensity was quantified along the dotted line and plotted on the bottom right. X-axis, pixels (range 0-238). Y-axis, GFP intensity in gray value (smoothened by taking the average intensity of 11-pixel neighborhoods; range 90-210). Scale bars, 25 μm.

**(D)** Illustration of the Llama Tag system used in this study. Plants were co-transformed with *ARR7-llama* (*pARR7::ARR7-linker-llama-ARR7ter*) and *GFP-nes* (*pUBQ10::sfGFP-nes-UBQ3ter*). Without ARR7-llama, the GFP is localized in the cytosol. ARR7-llama is produced in the cytosol and translocates into the nucleus. When this happens, the Llama Tag capable of binding GFP drags GFP into the nucleus (note that from our observation it is excluded from the nucleolus). Therefore, at low ARR7-llama levels, GFP signal is mainly seen in the cytosol. At intermediate ARR7-llama levels, GFP is at comparable intensities between the cytosol and the nucleus, and no clear pattern can be seen. At high ARR7-llama levels, GFP is mainly seen in the nucleus.

**(E,F)** GFP channel images of stage 2 buds from two independent transgenic lines of *ARR7-llama GFP-nes*, 7-4 (E) and 7-6 (F), in WT (top) vs *drmy1* (bottom). Images are representative of n = 17 (line 7-4, WT), n = 40 (line 7-4, *drmy1*), n = 9 (line 7-6, WT), and n = 6 (line 7-6, *drmy1*) buds.

**(G)** GFP channel images of WT *ARR7-llama GFP-nes* buds treated with mock (top) or 2 μM CHX (bottom) for 24 hours. The mock image is representative of n = 20 buds (12 from line 7-4, 5 from line 7-6, and 3 from line 7-12). The CHX image is representative of n = 19 buds (11 from line 7-4, 5 from line 7-6, and 3 from line 7-12).

**(H)** GFP channel images of WT *ARR7-llama GFP-nes* buds treated with mock (top) or 2 μM AZD-8055 (bottom) for 72 hours. The mock image is representative of n = 13 buds (8 from line 7-4 and 5 from line 7-6). The AZD-8055 image is representative of n = 11 buds (8 from line 7-4 and 3 from line 7-6).

**(I-N)** *ARR7-llama* partially restores robustness in *drmy1* sepal primordia. (I-L) Representative stage 5 or 6 buds from WT (I), WT with the *ARR7-llama* and *GFP-nes* constructs (J), *drmy1* (K), and *drmy1* with these constructs (L). (M) Quantification of sepal primordium number. ns indicates no significance difference in a Fisher's exact test (WT vs *ARR7-llama*, p = 1; *drmy1* vs *drmy1 ARR7-llama*, p = 0.44). (N) Quantification of variability in sepal primordium position. Asterisk indicates statistically significant difference ($p = 5.7 \times 10^{-6}$), while ns indicates no statistically significant difference (p = 0.91). Data for WT and *drmy1* were reused from Figure 2H, 2J. Data for *ARR7-llama GFP-nes* and *drmy1 ARR7-llama GFP-nes* were pooled from line 7-4 and 7-6. Sample size: WT n = 51, *ARR7-llama GFP-nes* n = 16, *drmy1* n = 67, *drmy1 ARR7-llama GFP-nes* n = 20. Scale bars, 25 μm.

**(O)** Working model. In WT, DRMY1 maintains TOR activity and translation, which sustains the rapid translation of A-type ARRs in response to cytokinin signaling. This suppresses excessive cytokinin signaling, allowing auxin and cytokinin signaling to interact and form robust spatial patterns. Robust patterning of auxin and cytokinin signaling gives rise to robustly numbered, positioned, and sized sepal primordia. In *drmy1*, A-type ARR protein levels are reduced due to

insufficient TOR activity, ribosome content, and translation rate. Cytokinin signaling is upregulated, which rescues the translation rate reduction in a homeostatic mechanism. This upregulation of cytokinin signaling disrupts the robust spatial pattern of both cytokinin and auxin signaling, which in turn causes variable sepal initiation.